Functional characterization of the *Ustilago maydis* virulence gene *scp2*

DISSERTATION

zur
Erlangung des Doktorgrades
der Naturwissenschaften
(Dr. rer. nat.)

dem Fachbereich Biologie
der Philipps-Universität Marburg
vorgelegt von

Sina Krombach
aus Betzdorf

Marburg/Lahn im Oktober 2016

Die Untersuchungen zur vorliegenden Arbeit wurden von Oktober 2012 bis Oktober 2016 am Max-Planck-Institut für Terrestrische Mikrobiologie unter der Leitung von Frau Prof. Dr. Regine Kahmann in der Abteilung Organismische Interaktionen durchgeführt.

Vom Fachbereich Biologie der Philipps-Universität Marburg
als Dissertation angenommen am: _____

Erstgutachter/in: Frau Prof. Dr. Regine Kahmann
Zweitgutachter/in: Herr Prof. Dr. Michael Bölker

Tag der mündlichen Prüfung am: _____

Erklärung

Ich erkläre, dass ich meine Dissertation

„ Functional characterization of the *Ustilago maydis* virulence gene *scp2* “

selbstständig, ohne unerlaubte Hilfe angefertigt und mich dabei keiner anderen als der von mir ausdrücklich bezeichneten Quellen und Hilfsmittel bedient habe.

Die Dissertation wurde in der jetzigen oder einer ähnlichen Form noch bei keiner anderen Hochschule eingereicht und hat noch keinen sonstigen Prüfungszwecken gedient.

(Ort / Datum)	(Sina Krombach)

Dedicated to my family and friends

Table of Contents

Abbreviations

Amp	Ampicillin
bp(s)	base pair(s)
BSA	bovine serum albumin
BIC	biotrophic interfacial complex
cbx/CB	carboxin
cDNA	complementary DNA
CM	complete medium
CSA	colony secretion assay
C-terminal	carboxy-terminal
CW	calcofluor white
Δ	deletion/delta
DNA	desoxyribonucleic acid
DIC	differential interface contrast
DMSO	dimethyl sulphoxide
dpi	days post infection
DTT	dithiothreitol
ECM	extracellular matrix
ER	Endoplasmic Reticulum
f	forward (hybridizes with the antisense strand)
f. c.	final concentration
Fig.	figure
GAPDH	glyceraldehyde 3-phosphate dehydrogenase
GFP	green fluorescent protein
glc	glucose
h	hour(s)
H_2O_{bid}	double distilled water
H_2O_2	hydrogen peroxide
HA	hemagglutinin
hpi	hours post infection
HFA	hydroxy fatty acids
HY	hygromycin
i.e.	*id est* (it is)
ip	gene encoding an iron-sulphur protein
IPTG	isopropyl β-D-1-thiogalactopyranoside
kb	kilobase pair(s)
kDa	kilodalton(s)
M	molar
min	minute(s)
ml	milliliter
mM	millimolar
mRNA	messenger RNA
NA	nourseothricin
NE	geneticin
N-terminal	amino terminal
OD_{600}	optical density at 600 nm
ORF	open reading frame
PAGE	polyacrylamide gel electrophoresis
PCR	polymerase chain reaction
PH	phleomycin
PI	propidium iodid
ppi	peptidyl-prolyl isomerase gene
PTS1	peroxisomal targeting signal type 1
qPCR	quantitative real time PCR
r	reverse (hybridizes with the sense-strand)
RNA	ribonucleic acid
RT	room temperature
s	second(s)
SDS	sodium dodecyl sulfate
SP	signal peptide
Tab.	table
TEMED	tetramethylethylenediamine
Tris	trishydroxymethyl-aminomethane
U	unit (enzyme activity)
UV	ultraviolet radiation
rpm	rounds per minute
WGA	wheat germ agglutinin
WT	wildtyp
YNB	yeast nitrogen base
µg	microgram
µl	microliter
µm	micrometer
µM	micromolar

Summary

The causative agent of the corn smut disease *Ustilago maydis* infects its host plant *Zea mays* by specialized infection structures, so-called appressoria, which are formed upon perception of chemical and physical stimuli on the leave surface. During the colonization process *U. maydis* secretes effector proteins that help to establish a biotrophic interaction. These effector proteins harbor an N-terminal hydrophobic secretion signal that targets them to the classical secretory pathway. In recent years, however, the existence of unconventionally secreted proteins has been uncovered which reach the extracellular space independently of the classical ER-Golgi system. In the present study the non-specific lipid transfer protein Scp2 (sterol carrier protein 2) of *U. maydis* was analyzed, which was identified as a putative candidate for unconventional protein secretion. Scp2 lacks a classical N-terminal signal peptide but exhibits a peroxisomal targeting signal (PTS1).

A quantitative real-time PCR approach revealed that *scp2* is up-regulated during early stages of plant colonization. Microscopic analyses demonstrated that the ability of *scp2* deletion strains to form appressoria on artificial surfaces was significantly decreased. Furthermore, deletion of *scp2* caused a virulence defect that appeared to result from a reduced efficiency of plant cuticle penetration. These defects are unlikely to result from deficiency in peroxisomal β-oxidation. In contrast to *scp2* deletion strains, the infection of maize plants with a strain overexpressing *scp2* under the *cmu1* promoter triggered strong plant defense reactions. Two Scp2 paralogs were shown to localize in peroxisomes but deletion of the respective genes revealed no effect on *U. maydis* virulence. With the help of colony secretion assays it was demonstrated that small amounts of Scp2 are unconventionally secreted. The export of Scp2 via the classical ER-Golgi route, however, could not complement the virulence phenotype of the *scp2* mutant strain, suggesting that the virulence defect is unconnected to the extracellular population of the protein.

Surprisingly, peroxisomes and lipid droplets in the *scp2* deletion strains displayed an altered distribution during filamentation on parafilm and on the plant surface. Based on these results, it is proposed that Scp2 affects appressorium development by influencing the distribution of peroxisomes and lipid droplets and thus constitutes a novel player in plant surface penetration.

Zusammenfassung

Der Maisbeulenbranderreger *Ustilago maydis* infiziert seine Wirtspflanze *Zea mays* mithilfe spezialisierter Infektionsstrukturen, sogenannter Appressorien. Die Ausbildung von Appressorien wird durch die Wahrnehmung chemischer und physikalischer Stimuli auf der Blattoberfläche induziert. Im Verlauf der Kolonisierung sekretiert *U. maydis* Effektor-Proteine die zur Etablierung der biotrophen Interaktion beitragen. Diese Effektoren besitzen ein N-terminales hydrophobes Sekretionssignal, welches den Transport über den klassischen Sekretionsweg vermittelt. In den vergangenen Jahren wurde jedoch eine Vielzahl unkonventionell sekretierter Proteine identifiziert, die den Extrazellularraum unabhängig vom ER-Golgi-System erreichen. In der vorliegenden Studie wurde das unspezifische Lipid-Transfer Protein Scp2 (*sterol carrier protein 2*) von *U. maydis* analysiert, welches als potentieller Kandidat für unkonventionelle Proteinsekretion identifiziert wurde. Scp2 besitzt kein N-terminales Signalpeptid, verfügt jedoch über eine peroxisomale Zielsteuerungssequenz (PTS1). Quantitative Echtzeit-PCR zeigte eine Induktion der *scp2*-Expression in frühen Stadien der Pflanzen-Kolonisierung. Mikroskopische Untersuchungen ergaben, dass *scp2* Deletionsstämme eine stark eingeschränkte Fähigkeit zur Appressorienbildung auf künstlichen Oberflächen aufweisen. Des Weiteren führte die Deletion von *scp2* zu einem Virulenzdefekt, der auf eine reduzierte Penetration der pflanzlichen Cuticula zurückgeführt werden konnte. Die beobachteten Defekte wurden dabei vermutlich nicht durch eine gestörte peroxisomale β-Oxidation verursacht. Im Gegensatz zu *scp2*-Deletionsstämmen führte die Infektion von Maispflanzen mit Stämmen, die *scp2* unter dem *cmu1* Promoter überexprimierten, zu starken Pflanzenabwehrreaktionen. Zwei weitere Scp2-ähnliche Proteine konnten in Peroxisomen nachgewiesen werden, doch die Deletion der beiden Gene hatte keinen Einfluss auf die Virulenz von *U. maydis*. Mithilfe von Koloniesekretions-Analysen konnte bestätigt werden, dass Scp2 in geringen Mengen unkonventionell sekretiert wird. Der Export von Scp2 über die klassische ER-Golgi-Route führte jedoch nicht zu einer Komplementation des Virulenz-Phänotyps eines *scp2*-Deletionsstammes, was vermuten lässt, dass der Virulenzdefekt nicht in Verbindung mit der extrazellulären Population des Proteins steht. Erstaunlicherweise wiesen *scp2*-Deletionsstämme eine veränderte Verteilung von Peroxisomen und Lipidtropfen in Filamenten auf Parafilm und auf der Pflanzenoberfläche auf. Daher wird vermutet, dass Scp2 an der Appressorienbildung beteiligt ist, indem es die Verteilung von Peroxisomen und Lipidtropfen beeinflusst. Scp2 könnte somit einen neuen Faktor für die Penetration der Pflanzenoberfläche darstellen.

1. Introduction

Approximately 10 to 16 % of global crop production is annually lost to plant diseases caused by different pests (Bebber *et al.*, 2013). Besides ectoparasites like insects, a multitude of organisms is able to infect plants including bacteria, oomycetes, viruses and fungi. A molecular understanding of the interaction between plant pathogens and their respective hosts is important to develop new methods for crop protection. In this context, model systems are of major importance since they allow functional studies on the pathogen as well as on the plant side. A well-established model system for plant disease is the interaction between the biotrophic smut fungus *Ustilago maydis* and its host plant *Zea mays* (maize).

1.1 The *U. maydis* and *Z. mays* pathosystem

Z. mays belongs to the family of Gramineae (Poaceae), commonly referred to as grasses (Strable and Scanlon, 2009). Among other cereals, maize is one of the most comprehensive studied model systems for genetic, cytogenetic and genomic research (Strable and Scanlon, 2009).
The facultative biotrophic pathogen *U. maydis* belongs to the order of Basidiomycota and infects maize and its wild ancestor teosinte which is native to Mexico and Central America (Fukunaga *et al.*, 2005). *U. maydis* is the causative agent of corn smut disease that is characterized by the formation of large tumors which can form on all aerial parts of the plant. The smut disease was named after the dark pigmented teliospores that are released from tumors and give the plant a burned appearance (Kahmann *et al.*, 2000). Smuts commonly infect grasses including economically important species such as maize, sorghum, sugar cane, wheat and barley (Brefort *et al.*, 2009). As biotrophic pathogens, these fungi depend on living plant tissue. This is in contrast to necrotrophic fungi that kill their host plant during the colonization process. *U. maydis* infections accounted worldwide for about 11 % of global corn losses due to fungal and oomycete diseases in the years 2009 and 2010 (Fisher *et al.*, 2012). In contrast, the soybean rust *Phakopsora pachyrhizi* caused an average of 45 % of the global soybean yield losses that were caused by fungal and oomycete diseases making *U. maydis* one of the economically less threatening pathogens (Fisher *et al.*, 2012). Nevertheless, *U. maydis* has been established as an excellent model system to understand the molecular basis of plant infection mechanisms and disease (Basse and Steinberg, 2004). Compared to other plant pathogenic fungi *U. maydis* has a relatively small genome of only 20.5 mega base pairs which was found to encode approximately 6,900 proteins (Kämper *et al.*, 2006; PEDANT 3 database

(http://pedant.gsf.de/)). *U. maydis* is accessible for molecular manipulations and its disease cycle can be completed within three weeks under greenhouse conditions (Donaldson *et al.*, 2013). Reverse genetic approaches like conventional gene replacement or genome editing using the CRISPR-Cas system, a large set of fluorescent proteins and the availability of many cell biological approaches contributed to making *U. maydis* a model organism (Steinberg and Perez-Martin, 2008; Brachmann *et al.*, 2004; Schuster *et al.*, 2016). Further, the fungus can be cultivated in liquid culture or on solid medium and cryoconservation allows the storage of *U. maydis* strains over a period of several years. Infection assays of maize seedlings or floral tissue with fungal cells can be easily performed under controlled greenhouse or phytochamber conditions and the evaluation of fungal induced disease symptoms is feasible starting six days after infection (Brefort *et al.*, 2009).

1.2 The *U. maydis* life cycle

One of the first descriptions of the *U. maydis* life cycle was performed in 1883 by the botanist and mycologist Julius Oscar Brefeld (Brefeld, 1883). During its life cycle the dimorphic fungus undergoes a transition from saprophytically growing yeast-like sporidia (Fig. 1 A) to an infectious dikaryotic filament that is formed when two compatible haploid cells fuse (Fig. 1 B and C). The fusion process and the subsequent pathogenic development is controlled by a tetrapolar mating system that comprises two unlinked mating loci: the biallelic *a* locus and the multiallelic *b* locus. The *a* locus encodes for a pheromone/pheromone receptor system which is responsible for the recognition and fusion of compatible haploid sporidia (Bölker *et al.*, 1992). The initiation of sexual and pathogenic development is mediated by the *b* mating type locus that encodes for the homeodomain transcription factors bE and bW that are able to dimerize when derived from different alleles (Kämper *et al.*, 1995). The active *b* heterodimer is a transcriptional master regulator that affects genes involved in cell cycle control and cell division and has been shown to be essential for establishing the biotrophic interaction with the plant (Brachmann *et al.*, 2001). The ability of the active *b* heterodimer to initiate pathogenic development allowed the generation of the haploid solopathogenic strain SG200 that encodes compatible *bE1* and *bW2* alleles and is therefore able to infect plants without a compatible mating partner (Kämper *et al.*, 2006). On the leaf surface the dikaryotic filament extends by polarized growth, with the cytoplasm migrating towards the growing tip while older parts of the filament are separated by the regular insertion of septa (Fig. 1 D) (Steinberg *et al.*, 1998). During this stage of development the fungal cell cycle is arrested in the G2 phase (García-Muse *et al.*, 2003). Upon the perception of plant derived physical and chemical stimuli *U. maydis*

forms specialized infection structures termed appressoria (Fig. 1 E). These appressoria are non-melanized and penetration of the plant cuticle is presumably mediated by the secretion of lytic enzymes that loosen the cell wall and permit access to lower plant tissue (Mendoza-Mendoza *et al.*, 2009; Schirawski *et al.*, 2005; Lanver *et al.*, 2014). During the penetration process *U. maydis* becomes surrounded by the plant plasma membrane that encloses the fungal hyphae like a glove (Fig. 1 F) (Snetselaar, 1993; Döhlemann *et al.*, 2009). Between the fungal cell wall and the plant plasma membrane a biotrophic interaction zone is established. Upon invasion of the epidermal layer the cell cycle arrest is abrogated and *U. maydis* proceeds to colonize the mesophyll and the vascular bundles by inter- and intracellularly branching hyphae (Snetselaar, 1994). This stage of infection is characterized by strong proliferation of the dikaryotic filaments and the formation of clamp-like structures that coordinate the distribution of nuclei between hyphal cells (Fig. 1 G) (Scherer *et al.*, 2006).

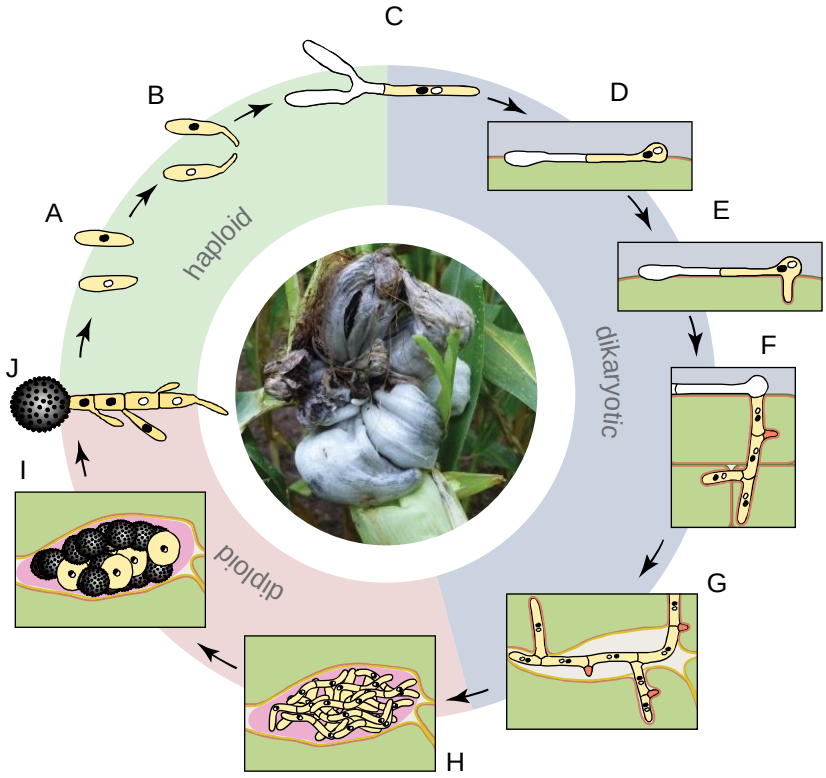

Fig. 1: Schematic representation of the *U. maydis* life cycle. The biphasic life cycle is characterized by the transition through different morphological and nuclear states and can be subdivided into a saprophytic (A-C) and a biotrophic phase (D-J). The photograph displays an *U. maydis* infected corncob (picture: modified from S. Reißmann, unpublished; photograph: S. Krombach).

Tumor formation is initiated approximately five to six days after infection by the development of hyphal aggregates embedded in a mucilaginous matrix in which the dikaryotic nuclei fuse (Fig. 1 H) (Banuett and Herskowitz, 1996; Tollot *et al.*, 2016). Nine to twelve days after infection the diploid hyphae start to fragment and release individual cells which start to round

and to develop into dark pigmented teliospores. When the tumors dry up and rupture the enclosed spores are released and spread by wind and rain (Fig. 1 I) (Banuett and Herskowitz, 1996). Under favorable conditions the spores germinate, undergo meiosis and develop a promycelium from which haploid sporidia bud off (Fig. 1 J) (Kahmann *et al.*, 2000).

1.3 Secreted *U. maydis* effectors

In order to establish a biotrophic interaction with its host plant *U. maydis* depends on effector proteins that grant protection from plant defense responses and prime host cells for the fungal invasion. *U. maydis* contains 467 secreted proteins of which 203 do not harbor a conserved protein domain (G. Schweizer, M. Schuster, unpublished). Approximately 19 % of the genes that encode secreted proteins were shown to be arranged in gene clusters which are distributed throughout the genome and comprise 3-26 genes (Kämper *et al.*, 2006).

Effectors can be subdivided into apoplastic and cytoplasmic effectors (Djamei and Kahmann, 2012). Apoplastic effectors are secreted into the biotrophic interaction zone between the fungal cell wall and the plant plasma membrane. In contrast, cytoplasmic effectors traverse the apoplastic space and are taken up by the plant cell. The mechanisms by which the effector proteins translocate into the plant cell are poorly understood and the existence of potential uptake motifs of fungal and oomycete effectors are still under debate (Petre and Kamoun, 2014). Several apoplastic and cytoplasmic *U. maydis* effectors have been studied during the past years in terms of their localization and their function during pathogenic development.

Pep1 is an apoplastic effector protein that functions in suppressing the early immune responses of maize. Deletion mutants of *pep1* elicit strong plant defense responses and pathogenic development is blocked immediately upon penetration of the epidermal layer. Pep1 inhibits the secreted maize peroxidase POX12 and thus blocks the peroxidase driven oxidative burst (Hemetsberger *et al.*, 2012). The effector protein Pit2 is secreted into the biotrophic interaction zone. While *pit2* deletion mutants are still able to invade the plant tissue, tumor induction is severely attenuated. Pit2 has been shown to act as an inhibitor of apoplastic maize cysteine proteases involved in salicylic-acid-associated plant defenses (Müller *et al.*, 2013).

The *U. maydis* chorismate mutase Cmu1 is a cytoplasmic effector that translocates into the plant cytosol were it counteracts salicylic acid-induced immune responses (Djamei *et al.*, 2011). Salicylic acid is a plant hormone that has been shown to be involved in the defense against biotrophic pathogens (Glazebrook, 2005). Cmu1 is predicted to reroute the flow of chorismate, thereby restricting the available substrate for salicylic acid biosynthesis. Importantly, Cmu1 can spread from cell to cell which is thought to prime the surrounding tissue for the upcoming fungal

infection (Djamei *et al.*, 2011). A second *U. maydis* effector that translocates into the plant cytoplasm and presumably manipulates plant metabolic pathways is Tin2. Deletion mutants of *tin2* induce attenuated virulence symptoms and infected leaves do not produce anthocyanin, a red pigment that typically accumulates in the infected plant tissue (Tanaka *et al.*, 2014; Banuett and Herskowitz, 1996). Tin2 interacts with and stabilizes the maize protein kinase ZmTTK1 which has been proposed to control the biosynthesis of anthocyanin. The stabilization of ZmTTK1 supposedly induces the production of anthocyanin which in turn lowers the availability of pre-cursors needed for the lignification of plant cell walls. The absence of lignification allows *U. maydis* a more efficient colonization of the plant tissue (Brefort *et al.*, 2014; Tanaka *et al.*, 2014).

Some of the secreted *U. maydis* effectors have been shown to be expressed and to function in an organ specific manner (Skibbe *et al.*, 2010). The protein See1 is translocated to the maize cytoplasm and into the nucleus where it reactivates the DNA synthesis in vegetative tissue which is needed as a prerequisite for the formation of tumors in maize leaves. In contrast, tumor formation in floral tissue, which is actively dividing, was shown to be independent of See1, underlining that this effector is needed only during leaf infection (Redkar *et al.*, 2015).

1.4 Unconventional protein secretion

Effectors have been typically defined as proteins that are externalized by signal peptide-mediated secretion directing them from the endoplasmic reticulum (ER) through the Golgi apparatus to their final extracellular destination. However, there are also secreted proteins that do not contain a classical signal peptide but which reach the extracellular space ER and/or Golgi independent via unconventional secretion mechanisms (Chua *et al.*, 2012). Over the past years several different mechanisms of leaderless secretion have been described (Rabouille *et al.*, 2012). Many of these proteins have been shown to be involved in cellular processes like cell survival, immune surveillance and tissue organization, underlining the significance of unconventionally secreted proteins (Rabouille *et al.*, 2012). To identify such proteins an algorithm has been developed that allows the prediction of unconventional secreted proteins (SecretomeP). The prognosis is based on sequence-derived features such as putative posttranslational modifications and structure, degradation signals, composition, size and charge (Bendtsen *et al.*, 2004). Unconventional secretion mechanisms have further been shown to be insensitive to the treatment with Brefeldin A (BFA). BFA is a fungal toxin that blocks the COPI-mediated retrograde transport from the Golgi to the ER which in turn causes an impairment of the COPII-dependent anterograde trafficking of proteins determined for classical

secretion and hence should not affect unconventional secretion pathways (Grieve and Rabouille, 2011). Many leaderless proteins are secreted in exceptionally small amounts and their secretion often occurs in a cell type specific and signal dependent manner making their analysis a challenging task (Malhotra, 2013).

In recent years, a multitude of proteins was identified in animals, bacteria, oomycetes, fungi and plants that are non-conventionally secreted (Rabouille *et al.*, 2012; Liu *et al.*, 2014; Ding *et al.*, 2014). Generally, unconventional secretion can be subdivided into vesicular and non-vesicular export mechanisms. Non-vesicular mechanisms include protein export via self-sustained secretion as it was shown for the signaling molecule fibroblast growth factor 2 (FGF2) (Nickel, 2011). The mechanism is driven by the phosphatidylinositol 4,5-bisphosphate dependent oligomerization of FGF2 and the formation of a transient lipidic pore in the plasma membrane. Binding to extracellular heparan sulfate proteoglycans is assumed to cause the disintegration of the lipidic pore and to promote the secretion of FGF2 to the extracellular space (Steringer *et al.*, 2012). Non-vesicular secretion of the yeast a-factor mating pheromone is mediated by the ATP-binding cassette transporter Ste6 which is located in the plasma membrane (McGrath and Varshavsky, 1989).

In contrast to these non-vesicular export mechanisms at least two secretion modes have been proposed that rely on intracellular membranous structures. The vesicle based pathways of the proteins AcbA/Acb1 and CFTR both depend on the Golgi reassembly stacking protein (GRASP) which is usually located in close proximity to ER exit sites and the early Golgi compartments (Curwin and Brouwers, 2016; Prydz *et al.*, 2013).

The acyl-CoA binding protein AcbA is needed as a precursor protein to trigger sporulation within fruiting bodies of the social amoeba *Dictyostelium discoideum* (Anjard and Loomis, 2005). The unconventional secretion of the AcbA yeast ortholog Acb1 is mediated by a novel compartment for unconventional protein secretion (CUPS) which seems to predominantly consist of secretory and endosomal membranes (Bruns *et al.*, 2011). Upon starvation, the GRASP protein Grh1 translocates from the ER exit site and Golgi membranes to immature CUPS, a membrane cluster that resembles the mammalian intermediate compartment. These immature CUPS are engulfed by a saccular structure leading to the formation of stable CUPS which were found to contain Acb1. These CUPS mediate the transport to the plasma membrane were their contents are released into the extracellular space (Fig. 2 (1)). The capturing of Acb1 by CUPS and the mechanism of protein externalization, however, remains elusive (Curwin and Brouwers, 2016).

Another route of unconventional secretion has been defined as Golgi bypass in which transmembrane proteins are transported from the ER to the plasma membrane without entering the Golgi apparatus. A prominent example for Golgi bypass is the cystic fibrosis transmembrane conductance regulator (CFTR). Gene mutations of CFTR can cause a range of epithelial disorders including cystic fibrosis since only negligible amount of the mutated CFTR version reach the plasma membrane. Induction of ER stress results in the activation of an unconventional GRASP-dependent secretion pathway that allows the mutated CFTR to enter the intermediate compartment between ER and Golgi (Gee *et al.*, 2011; Marie *et al.*, 2009). From there, CFTR seems to bypass the Golgi cisternae via an endosomal intermediate which facilitate the transport to the trans-Golgi network (TNG) and to the plasma membrane (Prydz *et al.*, 2013; Grieve and Rabouille, 2011).

Besides the described mechanisms several other pathways exist that facilitate the unconventional secretion of proteins such as the incorporation into microvesicles which bud outward from the plasma membrane, the uptake into the internal vesicles of multivesicular bodies (MVBs), which are subsequently released as exosomes or the export via secretory lysosomes (Fig. 2) (Prydz *et al.*, 2013).

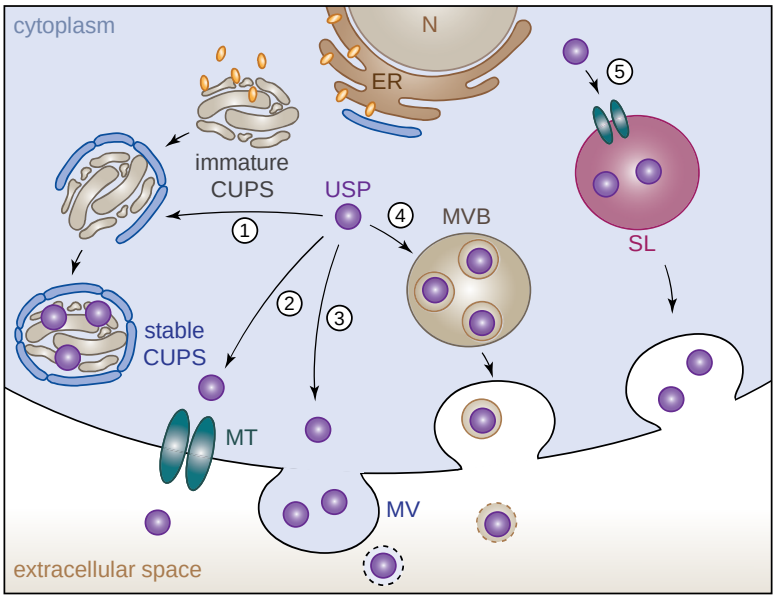

Fig. 2: Proposed mechanisms of unconventional protein secretion. To simplify the model, Golgi bypass of proteins containing a signal peptide such as CFTR were excluded. Unconventional secretion mechanisms can be subdivided into vesicular (1, 3, 4 and 5) and non-vesicular mechanisms (2). 1. Externalization of cytoplasmic proteins via CUPS. 2. Direct membrane translocation of cytoplasmic proteins by membrane transporters or by self-sustained insertion into the plasma membrane. 3. Translocation of proteins by microvesicles that bud from the plasma membrane which results in the formation of exosomes. 4. Capturing of cytoplasmic proteins by inwards budding endosomes which leads to the biosynthesis of MVBs. These MVBs can fuse with the plasma membrane and release the cargo proteins as exosomes. 5. Protein secretion of cytoplasmic proteins by secretory lysosomes. N: nucleus, ER: endoplasmic reticulum, SL: secretory lysosomes, MVB: multivesicular body, USP: unconventional secreted protein, CUPS: compartment of unconventional protein secretion, MT: membrane transporter, MV: microvesicle (picture modified from Nickel and Rabouille, 2009; Curwin and Brouwers, 2016).

In the recent years it became evident that unconventional secretion also has a major impact on the virulence of filamentous pathogens. In *Phytophthora sojae* and *Verticillium dahliae* unconventional mechanisms have been shown to mediate the secretion of the two leaderless effector proteins PsIsc1 and VdIsc1, respectively, which are required for full virulence. The two isochorismatases translocate to the plant cytoplasm and are, like the *U. maydis* effector Cmu1, involved in the suppression of the salicylate-mediated innate plant immunity (Liu *et al.*, 2014). These findings underline that defining effector proteins by the presence of a classical secretion signal is not sufficient anymore to establish a comprehensive picture of the fungal effector inventory that mediates infection and interaction with the host.

1.5 Peroxisomes

Peroxisomes are multifunctional single-membrane organelles present in all major groups of eukaryotes (Gabaldón, 2010). The spherical organelles range in diameter from 0.1 to 1.0 µm and are thought to originate *de novo* from the ER or to be generated by division from pre-existing peroxisomes (Titorenko and Rachubinski, 2001; Schrader *et al.*, 2016). The assembly of peroxisomal membranes, peroxisome proliferation and inheritance and the import of matrix proteins are controlled by so-called peroxins (Titorenko and Rachubinski, 2001). External stimuli such as fatty acids can affect peroxisome biogenesis and degradation and thus allow the rapid adaptation to environmental requirements (Schrader *et al.*, 2016). The name peroxisome originated from the presence of oxidases and catalases within the peroxisomal matrix that catalyse the generation and decomposition of hydrogen peroxide, respectively (de Duve, 1969). In recent years, however, it has been shown that peroxisomal metabolic functions extend far beyond the production and degradation of hydrogen peroxide. Peroxisomes contribute to the degradation of fatty acids by fatty acid β-oxidation, are involved in certain steps of the glyoxylate cycle, the metabolism of cholesterol, the biosynthesis of β-lactam antibiotics and they allow certain yeast species to use methanol as sole carbon source (Brown and Baker, 2008). The enzymatic composition of peroxisomes can differ substantially between organisms or different cell types and is strongly influenced by environmental conditions (Titorenko and Rachubinski, 2001). Glyoxysomes of plants, for instance, are specialized peroxisomes that mainly harbor enzymes of the glyoxylate cycle. Trypanosomatides like Leishmania and Trypanosoma ssp. possess a particular class of peroxisomes named glycosomes in which 90 % of the protein content consists of glycolytic enzymes (Michels *et al.*, 2006).

Peroxisomes are generally distributed equally throughout the cell. In *U. maydis*, the intracellular transport of peroxisomes, lipid droplets and the ER relies on the transient binding to early

endosomes which display motor protein dependent motility along microtubules (Guimaraes *et al.*, 2015). In *Aspergillus nidulans* the transport of peroxisomes has been shown to be mediated by the endosome-associated linker protein PxdA which tethers early endosomes and peroxisomes by interacting with yet unknown components on each organelle. The deletion of PxdA caused the accumulation of peroxisomes in the hyphal tip without affecting the distribution of early endosomes (Salogiannis *et al.*, 2016).

Interestingly, peroxisomes interact with a multitude of other cellular organelles such as the ER, mitochondria, chloroplasts, lysosomes, lipid droplets and with themselves (Shai *et al.*, 2016). These interactions promote peroxisome maturation and proliferation, peroxisome inheritance as well as the transport and exchange of proteins, molecules and metabolites between the different organelles (Shai *et al.*, 2016). In contrast to chloroplasts and mitochondria, peroxisomes do not contain their own genome or an independent protein synthesis machinery. Therefore, peroxisomal proteins are encoded in the nucleus of the cell and protein synthesis is mostly mediated by polysomes in the cytoplasm (Titorenko and Rachubinski, 2001). Two peroxisomal targeting sequences are responsible for the import of cytosolic proteins into the peroxisomal matrix or membrane (Erdmann, 2016). The peroxisomal targeting signal 1 (PTS1) is located at the C-terminus of the respective proteins and is composed of the tripeptide SKL or conserved variants (S/A/C)-(K/R/H)-(L/M). The second peroxisomal import signal PTS2 consists of a nonapeptide (R/K)-(L/V/I/Q)-XX-(L/V/I/H)-(L/S/G/A)-X-(H/Q)-(L/A) located in proximity to the N-terminus of the respective proteins (Ast *et al.*, 2013; Meinecke *et al.*, 2016). Two cargo receptors cycle between cytosol and peroxisomal membrane to facilitate the import of proteins into peroxisomes. PTS1-containing proteins are recognized by the peroxin Pex5 while proteins containing a PTS2 import signal are recognized by the peroxine Pex7 (Girzalsky *et al.*, 2010). Proteins destined for the peroxisome are bound by the respective receptors in the cytosol and translocate to the peroxisomal membrane. After import of the protein-receptor complex the cargo receptor is recycled from the peroxisomal matrix either for the degradation in proteasomes or for another round of protein import (Erdmann, 2016). Peroxisomes allow the translocation of folded and even oligomeric proteins which is exploited by proteins without a PTS targeting sequence that can reach the peroxisomal lumen independently of Pex5 or Pex7 by piggy-backing on PTS-containing proteins (Meinecke *et al.*, 2016).

1.6 Peroxisomes and pathogenicity

Several diseases and malfunctions can be attributed to defects in peroxisomes. In mammals, mutations in genes encoding different peroxins have been shown to cause a variety of

peroxisomal disorders which either affect specific metabolic pathways or cause a generalized defect in the assembly of peroxisomes (Wanders, 2014). A rare genetic disease that is based on a peroxisomal biogenesis disorders is the Zellweger syndrome (ZS). ZS patient cells lack morphologically identifiable peroxisomes which can lead to severe developmental defects of the brain and death in early infancy (Erdmann, 2016; Steinberg *et al.*, 2006).

In plant pathogenic fungi several peroxisomal functions have been determined to be essential for the infection of the respective host. Peroxisomal fatty acid β-oxidation mediates the break-down of fatty acids that is driven by a set of four major enzymes: Acyl-CoA oxidase, 2-enoyl-CoA hydratese, 3-hydroxacyl-CoA dehydrogenase and the 3-ketoacyl-CoA thiolase (Wanders, 2014). In each round of β-oxidation two carbons are released from the oxidized fatty acid as an acetyl-CoA unit that serves as a substrate for the glyoxylate cycle or the citric acid cycle. In *Magnaporthe grisea*, defects in peroxisomal β-oxidation abolish its ability to grow on fatty acids as the sole carbon source and have been shown to diminish appressorium-mediated plant infection (Wang *et al.*, 2007). Besides the enzymes for fatty acid β-oxidation several enzymes of the glyoxylate cycle are located within peroxisomes. The glyoxylate cycle mediates the conversion of two acetyl-CoA units to C4-precursors that can replenish the TCA cycle or function as precursors for amino acid or carbohydrate biosynthesis and thus allow growth on fatty acids, ethanol or acetate as a sole carbon source (Kunze *et al.*, 2006). In *Magnaporthe grisea* gene disruptions in glyoxylate cycle key enzymes like isocitrate lyase (ICL) have been shown to delay germination, infection related development and cuticle penetration (Wang *et al.*, 2003). Pexophagy is the selective degradation of peroxisomes by autophagy that contributes to the regulation of their abundance within the cell (Oku and Sakai, 2016). The deletion of essential pexophagy mediators can cause defects in appressorium formation and plant cuticle penetration as it has been shown for *Colletotrichum orbiculare*, the causative agent of anthracnose disease (Asakura *et al.*, 2009). In Pezizomycotina peroxisome derived woronin bodies plug the septal pore upon hyphal lysis to prevent excessive cytoplasmic loss (Maruyama and Kitamoto, 2013). Woronin bodies are required for appressorium development and function and are crucial for the survival during host plant infection (Soundararajan *et al.*, 2004).

These examples document the importance of peroxisomes for fungal growth, survival and pathogenic development.

1.7 Sterol carrier proteins

Sterol carrier protein 2 is a ubiquitous protein domain present in mammals, insects, plants, bacteria, archaea and fungi (Edqvist and Blomqvist, 2006). The majority of Scp2 proteins

contains a PTS1 sequence that targets them to the peroxisomal matrix. However, two Scp2 proteins in A*edes aegypti* lack peroxisomal localization and are mostly present in the cytoplasm (Lan and Massey, 2004). Scp2, also called non-specific lipid transfer protein, binds a variety of lipids such as fatty acids, fatty acyl-CoAs, phospholipids, sterols and bile salts. The conformation of Scp2 proteins in different organisms is highly conserved and generally consists of a five-stranded β-sheet and five α-helices which form a hydrophobic cavity that allows the loose accommodation of a lipidic ligand (De Berti *et al.*, 2013).

Numerous intracellular processes have been shown to be influenced by Scp2 including cholesterol uptake and secretion, intracellular lipid trafficking and signaling (Gallegos *et al.*, 2001; Stolowich *et al.*, 2002). Scp2 can function as part of a multidomain protein or as a standalone protein with an individual function (De Berti *et al.*, 2013). Well known examples of Scp2 as part of a multi domain protein is the mammalian SCPX protein consisting of a thiolase and a Scp2 domain or the multifunctional β-oxidation enzyme MFE-2 which contains a dehydrogenase and a hydratase domain in addition to Scp2 (Leenders *et al.*, 1996; Lensink *et al.*, 2002). Several functions have been ascribed to SCPX and MFE-2 but the association with additional domains turned out to be a challenging feature for elucidating a Scp2-specific function (Schroeder *et al.*, 2007; Baes *et al.*, 2000).

Single domain Scp2 proteins have been identified in the yellow fever mosquito *A. aegypti* where deletion of *scp2* leads to alterations of cholesterol and fatty acid uptake (Blitzer *et al.*, 2005). Further standalone Scp2 proteins were identified in plants like *Arabidopsis thaliana* where a mutation caused alterations in seed morphology, compromised germination and delayed seedling establishment (Zheng *et al.*, 2008). Although structural information has been obtained for the *Thermus thermophilus* Scp2 the biological function of bacterial and archaeal Scp2s still remains elusive (Goroncy *et al.*, 2010).

In fungi Scp2 domains are found in multidomain proteins but have also been frequently identified as standalone proteins (Edqvist and Blomqvist, 2006). Interestingly, while Scp2 has been described in a variety of eukaryotes no such protein has been detected in the baker's yeast *S. cerevisiae* and the fission yeast *S. pombe* (Edqvist and Blomqvist, 2006). The first crystal structure of a fungal Scp2 was reported by De Berti *et al*. in 2013 for the yeast *Yarrowia lipolytica*. Even though several studies addressed the YLScp2 biophysical properties, localization and its ability to bind and transfer fatty acids no distinct biological function could be attributed to the protein until today.

The *U. maydis* genome encodes three single domain sterol-binding proteins namely UMAG_01850 (Um01850), UMAG_11277 (Um11277) and UMAG_11938 (Scp2) (Edqvist and Blomqvist, 2006; PEDANT 3 database (http://pedant.gsf.de/)).

The *U. maydis* Scp2 protein exhibits a predicted molecular weight of 13.49 kDa and bioinformatic analyses using the SignalP 4.1 server revealed that Scp2 does not encode for a hydrophobic secretion sequence (http://www.cbs.dtu.dk/services/SignalP/). The C-terminus of Scp2, however, harbors a peroxisomal targeting sequence, in form of the tripeptide AKL that facilitates the translocation of the protein from the cytosol to peroxisomes (http://mendel.imp.ac.at/mendeljsp/sat/pts1/PTS1predictor.jsp). Previous work showed that the deletion of *scp2* in *U. maydis* causes a virulence defect characterized by a significant reduction of tumor formation (S. Reißmann, personal communication). Mutation of the PTS1 sequence abolished peroxisomal localization causing Scp2 to reside in the cytosol. The cytoplasmic version of Scp2 could not complement the *scp2* deletion mutant phenotype indicating that peroxisomal localization might be important for the virulence related function of Scp2 (S. Krombach and S. Reißmann, unpublished). A sequence based analysis using the SecretomeP server classified Scp2 as a potential candidate for unconventional secretion (http://www.cbs.dtu.dk/services/SecretomeP/). Moreover, Scp2 was detected in the isolated apoplastic fluid of infected maize leaves, in culture supernatants of *b*-induced filaments as well as in colony secretion assays (T. Brefort, M. Mann, K. Schipper, unpublished; F. Bochen, S. Krombach and S. Reißmann, unpublished).

1.8 Aims and objectives of this study

The aim of the present study is the analysis of the *U. maydis* protein Scp2 with respect to its intracellular and putative extracellular function. The potential leaderless secretion of Scp2 will be explored in particular with respect to its contribution to virulence. A comprehensive phenotypical characterization of *scp2* deletion strains will be performed in order to elucidate a biological role of Scp2 during pathogenic development. The evaluation of binding specificities could thereby offer insights into the Scp2 function on a molecular level. Beyond the analysis of Scp2, the two remaining sterol carrier proteins present in the *U. maydis* genome will be analyzed with respect to their impact on virulence and to uncover potential redundant functions.

2. Results

2.1 The impact of Scp2 on the pathogenic development of *U. maydis*

Previous experiments showed that deletion of the *scp2* gene in the solopathogenic *U. maydis* strain SG200 causes a decrease in virulence (S. Reißmann, F. Ahrens and S. Kreibich, unpublished). SG200 is a genetically modified haploid strain that carries the genetic information of both mating type loci and therefore does not require cell fusion events to induce filament formation and infection (Kämper *et al.*, 2006). In the following paragraphs, growth rates, the ability to mate and the virulence of *scp2* deletion strains was analyzed using either existing mutants in SG200 or newly generated mutants in the wild type strains FB1 and FB2.

2.1.1 The role of Scp2 during saprophytic growth

Previous work indicated that deletion of *scp2* in SG200 does not lead to a significant growth defect when using colony size as an indicator (F. Bochen, personal communication). To detect minor differences in saprophytic proliferation, growth curves were generated using SG200, SG200Δscp2 as well as the respective complementation strain SG200Δscp2-c.

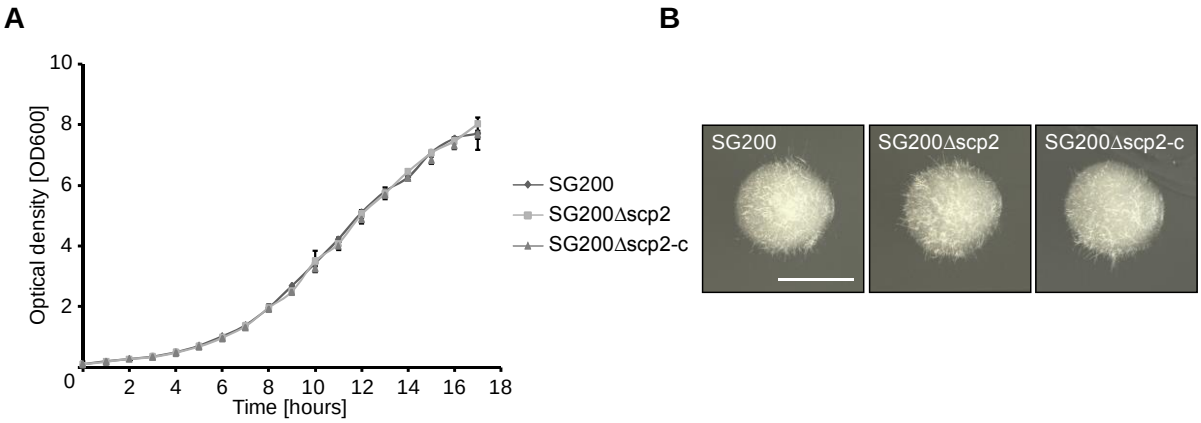

Fig. 3: Saprophytic growth of SG200, SG200Δscp2 and the complementation strain SG200Δscp2-c. (A) The growth curve was generated by growing the respective strains in $YEPS_{light}$ complete medium starting with an optical density (OD_{600}) of 0.1. Growth was recorded over a period of 17 hours. For each strain the OD_{600} of three independent replicates was measured. Error bars indicate the ± standard deviation between the three replicates. (B) For the analysis of colony morphology, the respective strains were singled out on CM-glc solid medium. The plates were incubated at 28 °C for two days. Pictures of single colonies were taken with a binocular microscope. The scale bar equals 500 µm.

In comparison to SG200, no significant differences of saprophytic growth rates could be observed for SG200Δscp2 (Fig. 3 A). Furthermore, after singling the strains out on defined complete medium (CM-glc) the analysis of colony morphology did not reveal differences with respect to size or filamentation between SG200, SG200Δscp2 and SG200Δscp2-c (Fig. 3 B).

These results rule out that a reduced growth rate of *scp2* deletion strains causes the virulence phenotype observed in plant infections.

2.1.2 Scp2 is not involved in mating

In further experiments the ability of *scp2* deletion mutants to form dikaryotic hyphae after successful mating with a respective mating partner was analyzed. On charcoal-supplemented solid medium *U. maydis* forms dikaryotic filaments after successful fusion with a compatible mating partner. These filaments have a white appearance due to empty sections in older parts of the developing hyphae (Day and Anagnostakis, 1971). To analyze mating, mixtures of compatible FB1 and FB2 strains and the respective *scp2* deletion strains were spotted on PD charcoal plates. After 24 hours, wild type and s*cp2* deletion strain crossings formed white fuzzy colonies (Fig. 4). These results show, that *scp2* mutants are not affected in mating and the development of dikaryotic filaments.

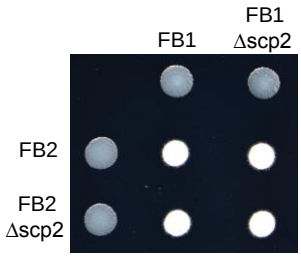

Fig. 4: Mating of FB1Δscp2 and FB2Δscp2 on PD-charcoal plates. Indicated haploid *U. maydis* strains were spotted on PD charcoal plates either alone or in a 1:1 mixture of compatible mating partners. The plates were incubated at room temperature for two days. White colonies indicate the development of dikaryotic hyphae after successful mating.

2.1.3 Pathogenicity of *U. maydis scp2* deletion mutants is reduced

To evaluate the impact of Scp2 on virulence, FB1Δscp2 and FB2Δscp2 were analyzed in plant infection experiments. As already observed for infections with SG200Δscp2, mixtures of FB1Δscp2 with FB2Δscp2 showed a significant reduction of virulence in comparison to the mixture of FB1 and FB2. Particularly, the amount of dead plants was strongly reduced when *scp2* mutants were crossed (Fig. 5 A and B). Interestingly, the whole range of disease symptoms was observed in *scp2* deletion strain crossings although the frequency by which the respective symptoms appeared was significantly decreased. These results show that the *scp2* deletion phenotype observed in SG200 also manifests in crossings of FB1 and FB2 wild type strains determining Scp2 as a pathogenicity factor in *U. maydis*.

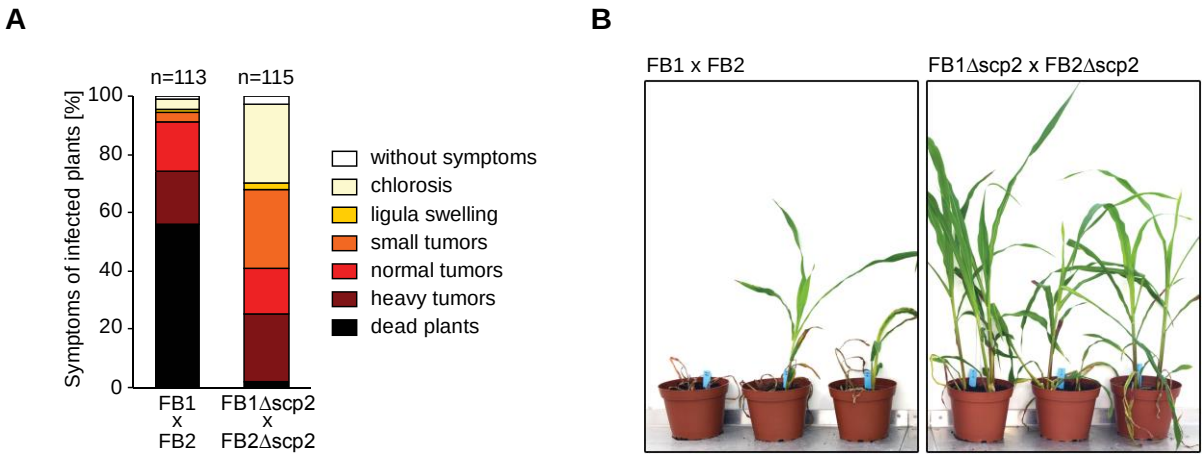

Fig. 5: Virulence of compatible haploid strains carrying deletions of *scp2*. (A) Mixtures (1:1) of the indicated FB1 and FB2 derivatives were injected into seven day old maize seedlings (Early Golden Bantam; EGB). Infection symptom development was quantified twelve days post infection. The respective symptom categories are depicted on the right hand side of the diagram. For the virulence assay average values of three independent replicates were taken. The total number of infected plants (n) is depicted above each column. (B) Maize plants infected with FB1 x FB2 or FB1Δscp2 x FB2Δscp2 were photographed 12 days after infection.

2.2 *Scp2* is upregulated in early and late stages of plant colonization

To narrow down at which stage of plant colonization Scp2 might be required and to determine relative gene expression of *scp2* during different stages of pathogenic development quantitative real time polymerase chain reaction (qPCR) was conducted. To this end, RNA was isolated from saprophytically growing cells as well as from SG200 infected plant material 20 hours (hpi), 2, 4 and 12 days (dpi) after maize seedling infection. Plants infected with water were used for normalization (mock). The isolated RNA was reverse transcribed into cDNA and used as a template for the amplification process. The constitutively expressed *U. maydis* gene *ppi* encoding a peptidylprolyl isomerase (*um03726*) served as a reference gene (Bohlmann, 1996). The qPCR results showed a 16-fold increase of *scp2* expression during appressorium formation and penetration at 20 hpi (Fig. 6). The expression dropped significantly at 2 dpi and increased again at later stages of biotrophic development starting at 4 dpi (Fig. 6).

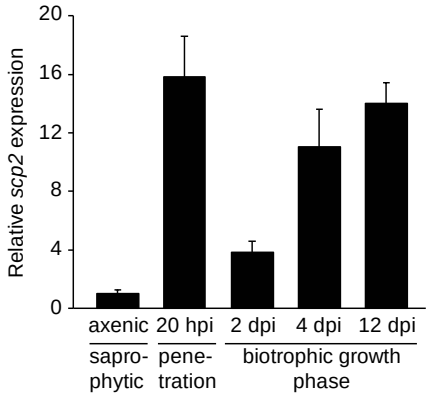

Fig. 6: Relative expression of *scp2* during biotrophic development. Relative expression of *scp2* was determined proportional to the constitutively expressed *ppi* gene. RNA samples of SG200 were extracted from exponentially growing cells cultivated in $YEPS_{light}$ medium and from SG200 infected maize plants 20 hpi, 2, 4 and 12 dpi. Extracted RNA samples were reverse transcribed into cDNA. Average values of three biological replicates are shown with error bars indicating the ± standard deviation. Values were normalized to *scp2* expression in axenic culture which was set to value 1. The different stages of biotrophic interaction are indicated below the graph.

2.3 Two paralogs of *scp2* are present in the *U. maydis* genome

As *scp2* deletion strains are still able to cause disease symptoms albeit reduced when compared with wild type strains, additional putative sterol carrier proteins encoded in the *U. maydis* genome were analyzed with respect to their contribution to *U. maydis* virulence. A database search on the "PEDANT 3" database (http://pedant.gsf.de/) revealed two paralogs of Scp2, namely UMAG_01850 (Um01850) and UMAG_11277 (Um11277). Amino acid alignments using the "t-coffee" alignment tool (http://www.ebi.ac.uk/Tools/msa/tcoffee/) showed that Scp2 shares an amino acid sequence identity of 38.5 % and 28.1 % with its two paralogs, respectively. RNAseq data revealed that *um01850* and *um11277* have expression patterns similar to *scp2*. Expression of the paralogs during growth in axenic culture, however, was about 18-fold and 5-fold lower than the expression of *scp2*, respectively (D. Lanver, personal communication).

By using the "PTS1 predictor" tool (http://mendel.imp.ac.at/mendeljsp/sat/pts1/PTS1 predictor.jsp) that recognizes potential peroxisomal targeting signals type 1 Scp2 (score: 13.810) and Um01850 (score: 10.004) were predicted to be targeted to peroxisomes while Um11277 peroxisomal targeting was classified as "twilight zone" (score: -9.285). Proteins with scores above 0 are considered to be targeted to peroxisomes. Scores ranging from 0 - (-10) are considered as twilight zone, i.e. unreliable PTS1 prediction and proteins with a sequence score below -10 are classified as proteins that are not predicted to be targeted to peroxisomes (Neuberger *et al.*, 2003).

2.3.1 Um01850 and Um11277 are targeted to peroxisomes

Colocalization experiments were performed to determine in which cellular compartment Um01850 and Um11277 reside. To this end, N-terminal GFP-fusions were generated for Um01850 and Um11277 (GFP-01850 and GFP-11277). The respective constructs were integrated into the *ip* locus of the peroxisomal marker strain AB31Pex (kindly provided by J. Freitag). The *U. maydis* strain AB31Pex is a FB2 derivative in which the *b*-genes are regulated by the arabinose-inducible *crg* promoter (Brachmann *et al.*, 2001). In addition, AB31Pex expresses a mCherry protein that is fused to a peroxisomal targeting signal (mCherry-PTS1). Since expression profiles had indicated low expression levels for both *scp2* paralogs in axenic culture, *gfp-01850* and *gfp-11277* fusion constructs were expressed under the control of the endogenous *scp2* promoter. To determine the subcellular localization of the two fluorescently labeled proteins, exponentially growing cells of AB31PexGFP-01850 and AB31PexGFP-11277 were analyzed by fluorescence microscopy. Colocalization of GFP-01850 and GFP-11277 fusion proteins with the peroxisomal marker mCherry-PTS1 revealed peroxisomal localization of both Um01850 and Um11277 (Fig. 7).

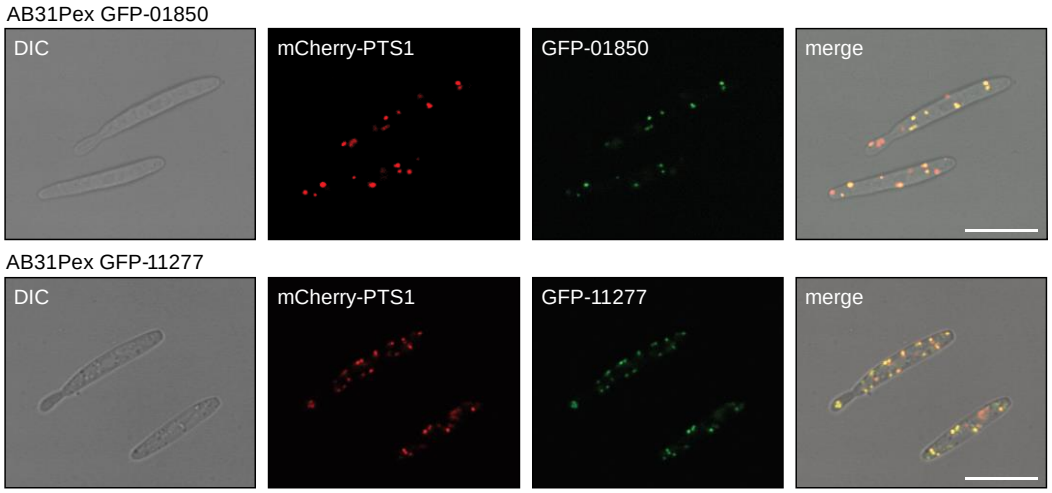

Fig. 7: Cellular localization of GFP-01850 and GFP-11277 fusion proteins. Exponentially growing sporidia of AB31PexGFP-01850 and AB31PexGFP-11277 were analyzed using fluorescence microscopy. Red fluorescence displays localization of the peroxisomal marker protein mCherry-PTS1, green fluorescence displays localization of GFP-01850 or GFP-11277, respectively. The merge channel indicates colocalization of GFP-01850 and GFP-11277 with peroxisomes. Scale bars equal 10 µm.

2.3.2 Deletion of *um01850* and *um11277* does not affect virulence

To determine the impact of *um01850* and *um11277* on virulence of the solopathogenic strain, SG200 deletion strains were generated carrying single gene deletions of the two Scp2 paralogs (SG200Δ01850 and SG200Δ11277). The influence of the deletions on *U. maydis* pathogenicity was examined in plant infection experiments. Both single deletion strains showed symptom development comparable to that of the SG200 progenitor strain (Fig. 8 A and B).

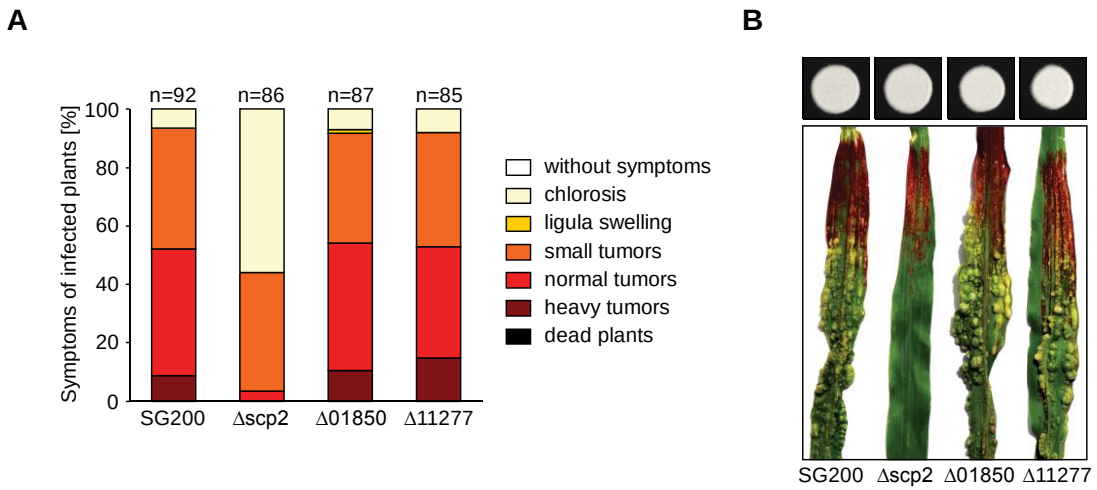

Fig. 8: Virulence of *um01850* and *um11277* mutants. (A) Infection symptoms on maize seedlings infected with SG200 and the single gene deletion strains SG200Δscp2, SG200Δ01850 and SG200Δ11277, respectively. Infection symptoms were evaluated twelve days post infection. The respective symptom categories are depicted on the right hand side of the diagram. For the virulence assay average values of three independent infections were taken. The total number of infected plants (n) is depicted above each column. (B) Filamentous growth of the respective strains on charcoal plates (top panel). Pictures of representative leaves from plant infections (lower panel).

2.3.3 Deletion of *scp2* and its two paralogs has no additive effect on virulence

To investigate whether Scp2, Um01850 and Um11277 might have partially redundant functions a triple mutant strain SG200Δscp2Δ01850Δ11277 (SG200ΔΔΔ) was generated. Three independent triple deletion mutants where analyzed in plant infection experiments of which one is depicted in Fig. 9. All three independent mutants resembled the *scp2* single deletion strain in strength of induced virulence symptoms, indicating no redundant function between Scp2 and its paralogs. Furthermore, the virulence defect observed for SG200ΔΔΔ could be fully complemented by inserting the *scp2* gene into the *ip* locus of the SG200ΔΔΔ genome in single copy (SG200ΔΔΔ-c) (Fig. 9 A and B). Filamentation of SG200ΔΔΔ on charcoal plates was slightly delayed (not shown). However, no difference in filamentation was visible after two days of incubation (Fig. 9 B). In conclusion, the infection experiments showed that *um01850* and *um11277* do not exhibit a virulence related function. Further, the three proteins do not seem to have redundant functions.

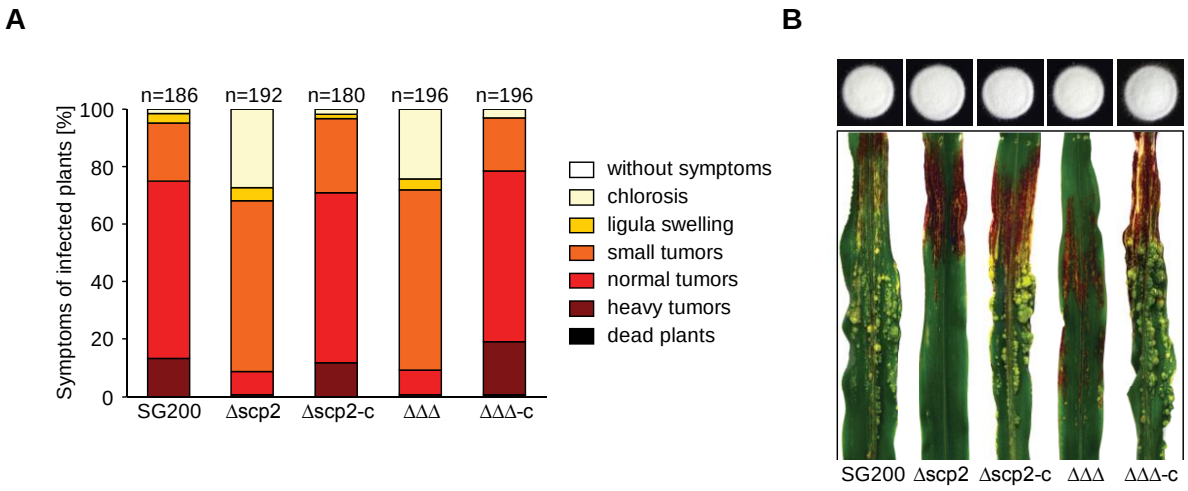

Fig. 9: Virulence of the triple deletion strain SG200Δscp2Δ01850Δ11277 (SG200ΔΔΔ). (A) Infection symptoms on maize seedlings infected with SG200, SG200Δscp2, the complementation strain SG200Δscp2-c, the triple deletion strain SG200ΔΔΔ and the respective complementation strain SG200ΔΔΔ-c. Infection symptoms were evaluated twelve days post infection. The respective symptom categories are depicted on the right hand side of the diagram. For the virulence assay average values of four independent infections were taken. The total number of plants (n) is depicted above each column. (B) Filamentous growth of the respective strains on charcoal plates (top panel). Pictures of representative leaves from plant infections (lower panel).

2.3.4 Scp2 and its two paralogs are not involved in peroxisomal β-oxidation

One of the main tasks of peroxisomes in eukaryotic cells is the breakdown of very long chain fatty acids in order to obtain acetyl-CoA in a process called peroxisomal β-oxidation (Wanders *et al.*, 2016). It is known that defects in this important process lead to a reduction of virulence in *U. maydis* and several other plant pathogenic fungi like *Magnaporthe oryzae* or *Colletotrichum orbiculare* (Ramos-Pamplona and Naqvi, 2006; Klose and Kronstad, 2006; Asakura *et al.*, 2012). All three putative sterol carrier proteins of *U. maydis* Scp2, Um01850 and Um11277 localize in peroxisomes and are predicted to be involved in fatty acids binding and transport (PEDANT 3 database (http://pedant.gsf.de/)). Hence, peroxisomal β-oxidation was assayed in the three single deletion strains as well as in the triple deletion strain to reveal a possible impairment by using fatty acid growth assays. For this, *U. maydis* was grown on solid medium supplemented with fatty acids ranging from 16 to 18 in carbon chain length (saturated and unsaturated) as the only available carbon source. *U. maydis* is able to utilize fatty acids as an energy source as long as peroxisomal β-oxidation is functional (Klose and Kronstad, 2006). The peroxisome deficient mutant SG200Δpex6 was used as a negative control. This strain lacks the peroxisomal biogenesis factor 6 causing *U. maydis* to produce "peroxisomal ghosts" that are not able to metabolize fatty acids via peroxisomal β-oxidation (Freitag *et al.*, 2012).

As expected, the *pex6* deletion strain was unable to grow on oleic and linoleic acid and was strongly reduced in growth on palmitic and stearic acid (Freitag *et al.*, 2012) (Fig. 10). SG200 and derivatives lacking either *scp2*, *um01850*, *um11277* or all three putative sterol carrier

proteins showed comparable growth on all plates containing fatty acids as sole carbon source (Fig. 10). This shows that peroxisomal β-oxidation of long-chain fatty acids is independent of Scp2, Um01850 and Um11277 function.

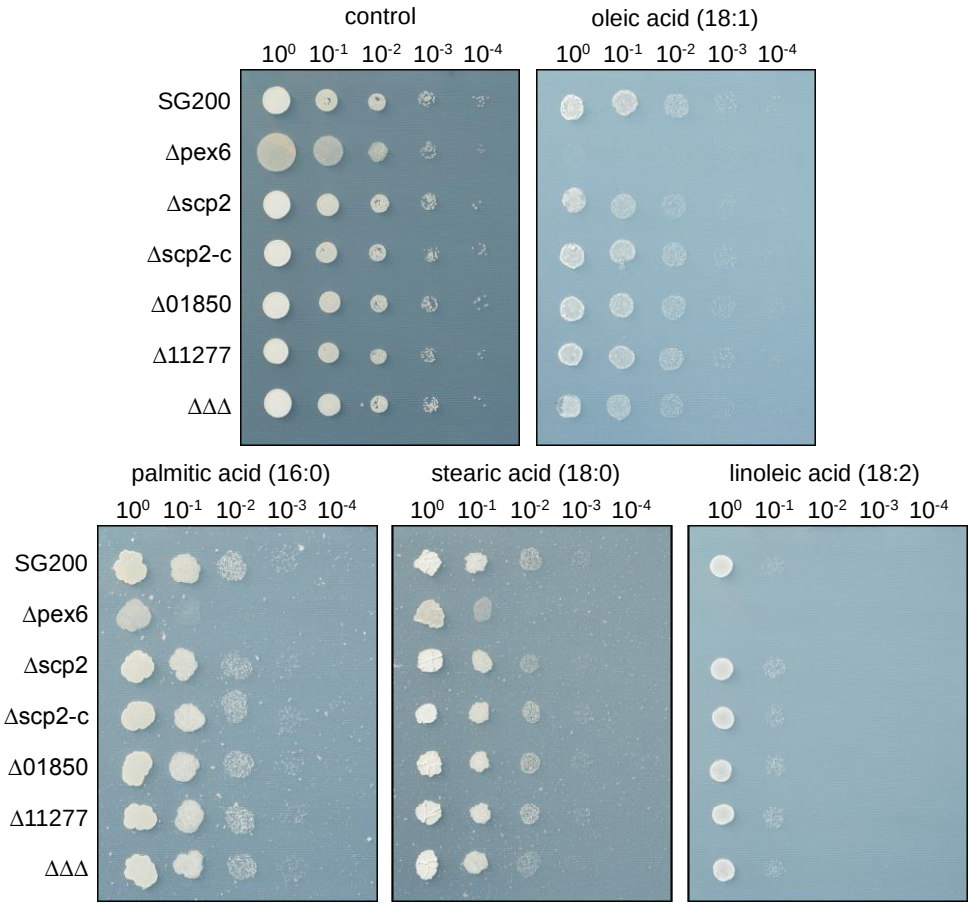

Fig. 10: Growth assays on different fatty acid substrates. YNB medium without amino acids was supplemented with glucose (control), oleic acid, palmitic acid, stearic acid or linoleic acid to assay functional peroxisomal β-oxidation. Exponentially growing cultures of the indicated SG200 derivatives were washed in water and optical densities were adjusted to 1. Serial dilutions were spotted on the respective media. Plates were sealed with parafilm and incubated for two days at 28 °C.

2.4 Overexpression of *scp2* under the *cmu1* promoter causes a strong virulence defect

In order to characterize the biological function of a protein, overexpression of the respective gene can offer valuable clues. Therefore, *scp2* was overexpressed by generating a strain carrying a multiple integration event (m) of the complementation construct in the *ip* locus of the SG200 genome (SG200Δscp2-c #10 and SG200Δscp2-c #13). Protein levels of Scp2 were determined in lysates from saprophytically growing cells using western blot analysis and a Scp2 peptide-specific antibody to proof successful overexpression of *scp2* in the respective strains (Fig. 11 A). In comparison to SG200 and the complementation strain carrying a single integration of the complementation construct (SG200Δscp2-c) plant infection experiments

using the two generated strains with multiple integrations showed that overexpression of *scp2* had no negative effect on *U. maydis* virulence (Fig. 11 B).

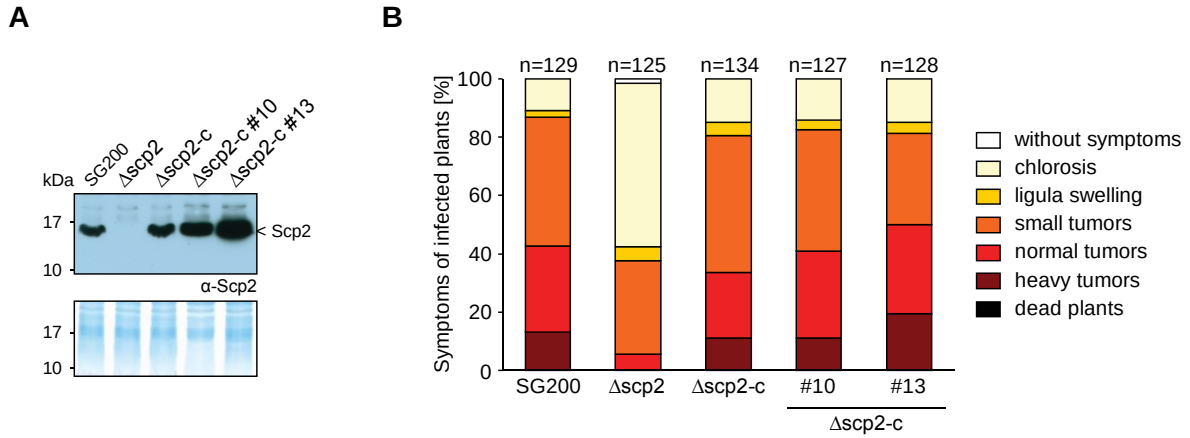

Fig. 11: Virulence of SG200 derivatives overexpressing *scp2*. (A) Scp2 protein levels in cell lysates of sporidia. Protein extracts were generated from exponentially growing cells of the indicated strains. Protein quantities in each extract were determined by Bradford protein assays. 10 µg of total protein was loaded and separated by SDS-PAGE. Western blot analysis was used to determine Scp2 levels for each strain using an anti-Scp2 peptide-specific antibody (top panel). An InstantBlue stained polyacrylamide gel served as a loading control to ensure that equal protein quantities were used for the western blot analysis (lower panel). (B) Infection symptoms on maize seedlings infected with SG200, the deletion strain SG200Δscp2, the complementation strain SG200Δscp2-c carrying a single integration of the *scp2* complementation construct and the two independent mutant strains SG200Δscp2-c #10 and SG200Δscp2-c #13 carrying a multiple integration of the *scp2* complementation construct. Infection symptoms were evaluated twelve days post infection. The respective symptom categories are depicted on the right hand side of the diagram. For the virulence assay average values of four independent replicates were taken. The total number of plants (n) is depicted above each column.

To produce Scp2 at even higher protein levels and to assay the importance of the *scp2* gene expression pattern during plant infection, *scp2* was expressed under the strong *cmu1* promoter. Cmu1 is a chorismate mutase involved in the metabolic priming of the host plant during colonization and was shown to be one of the most highly expressed effector genes in *U. maydis* (Djamei *et al.*, 2011). The *scp2* and the *cmu1* promoter show an opposing expression pattern. While *scp2* expression is induced 20 hpi and downregulated at 2 dpi the expression of *scp2* under control of the *cmu1* promoter would result in a strong constitutive overexpression during plant colonization (D. Lanver, personal communication).

The generated *scp2* overexpression strains (SG200P_{cmu1}-Scp2 and SG200Δscp2P_{cmu1}-Scp2) were analyzed in plant infection experiments. The overexpression of *scp2* under control of the *cmu1* promoter caused a severe reduction of virulence when integrated into the *ip* locus of SG200 and SG200Δscp2 (Fig. 12 A). This dominant negative effect caused a significantly stronger attenuation of virulence than what was observed for *scp2* deletion strains. In addition, hardly any anthocyanin production could be detected in plants infected with SG200P_{cmu1}-Scp2 and SG200Δscp2P_{cmu1}-Scp2 (Fig. 12 B and C). Close-up views from SG200P_{cmu1}-Scp2 infected leaves revealed a high amount of chlorotic lesions throughout the entire leaf, indicating plant

defense reactions (Fig. 12 C and D). The obtained results raised the question whether the observed virulence defect was caused by overloading the peroxisomes due to the strong overexpression of Scp2. To test this hypothesis a construct expressing peroxisomal mCherry was put under the control of the *cmu1* promoter and multiple copies were inserted into the SG200 genome (SG200P_{cmu1}-mCherry$_{pex}$). Quantification of disease symptoms showed that the overexpression of peroxisomal mCherry did not lower virulence significantly (Fig. 12 A). In addition, none of the overexpression strains analyzed showed defects in filament formation on PD-charcoal plates (Fig. 12 B). These results could suggest that not only the level of Scp2 protein but also the timing of *scp2* expression might be a crucial during pathogenic development of *U. maydis*.

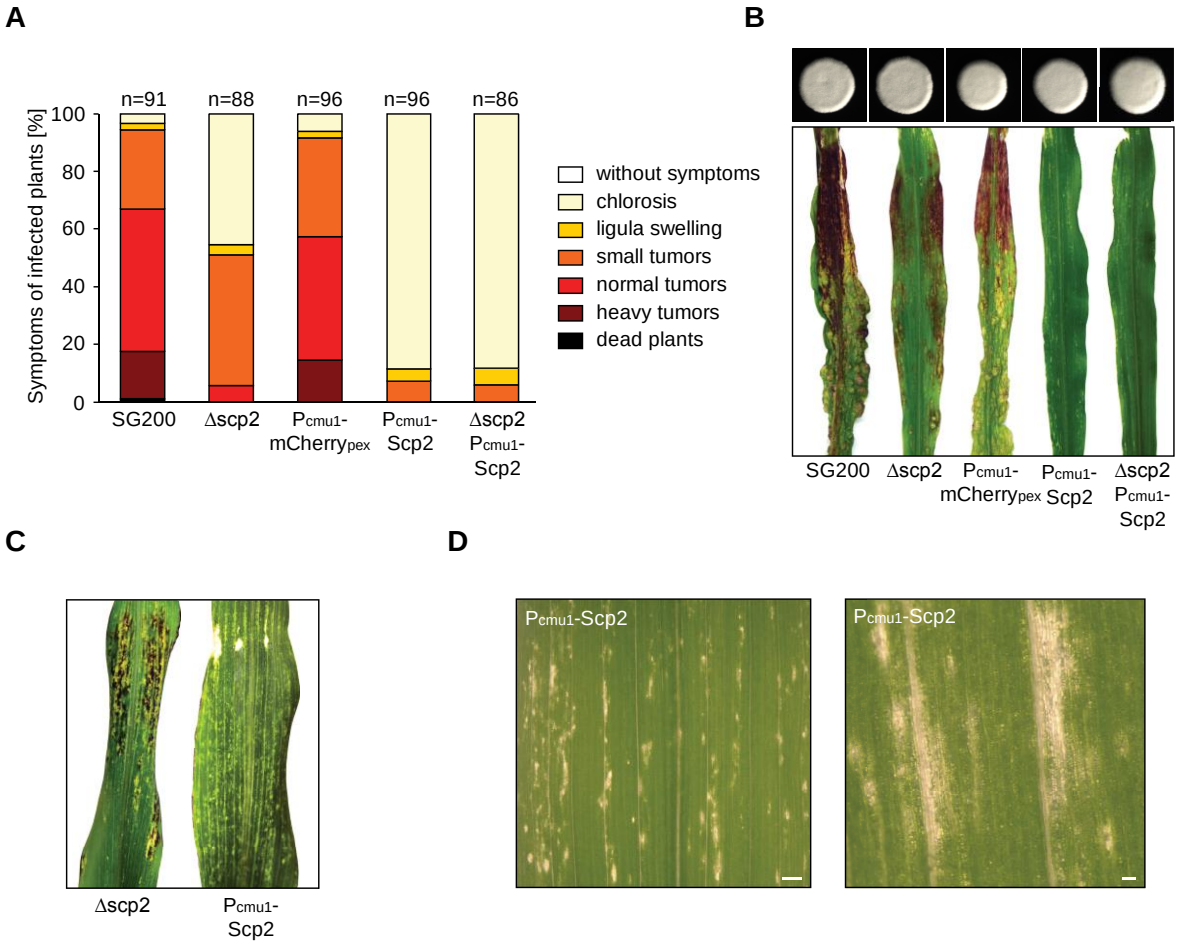

Fig. 12: Virulence of strains overexpressing *scp2* under the *cmu1* gene promoter. (A) Infection symptoms on maize seedlings infected with SG200, SG200Δscp2, SG200P_{cmu1}-mCherry$_{pex}$, SG200P_{cmu1}-Scp2 and SG200Δscp2P_{cmu1}-Scp2, respectively. Infection symptoms were evaluated twelve days post infection. The respective symptom categories are depicted on the right hand side of the diagram. For the virulence assay, average values of three independent infections were taken. The total number of plants (n) is depicted above each column. (B) Filamentous growth of the respective strains on charcoal plates (top panel). Pictures of representative leaves from plant infections (lower panel). (C) Photographs of maize leaves infected with the *scp2* deletion strain SG200Δscp2 (left) and the overexpression strain SG200P_{cmu1}-Scp2 (right). (D) Close-up pictures of maize leaves infected with the overexpression strain SG200P_{cmu1}-Scp2. The scale bars equal 1000 µm (left) and 100 µm (right).

2.4.1 Overexpression of *scp2* under the *cmu1* promoter induces plant defense reactions

To investigate reasons for the reduced virulence in *scp2* mutant strains and the strong virulence defect of SG200P$_{cmu1}$-Scp2 overexpression strains the proliferation of the respective strains was analyzed during plant colonization. To visualize fungal hyphae and plant cell walls infected leaves were stained with WGA-AF488/PI (wheat germ agglutinin / propidium iodide). WGA is a green fluorescent dye consisting of a lectin bound to Alexafluor 488. This lectin binds to chitin which is present in the fungal cell wall (Robin *et al.*, 1986). Propidium iodide is a membrane-impermeable dye that binds the plant cell wall. In dead cells the cell membrane integrity is reduced and PI is able to reach the cell interior where it binds to double-stranded DNA or RNA.

Leaves infected with SG200, SG200Δscp2 and SG200P$_{cmu1}$-Scp2, respectively, were harvested two days after infection, stained with WGA-AF488/PI and subsequently analyzed by confocal laser scanning microscopy. Scp2 mutant strains were able to colonize the plant tissue (Fig. 13). However, after two days post infection the extent of proliferation within the leaves was lower than what was observed for the SG200 progenitor strain (Fig. 13 A and B). In addition, more leaf areas displayed autofluorescence due to plant defense reactions upon infection with the *scp2* mutant strain (Fig. 13 C, D and E). SG200P$_{cmu1}$-Scp2 strains expressing *scp2* under control of the *cmu1* promoter elicited plant defense reactions more frequently than SG200 and SG200Δscp2 (Fig. 13 F and G). Successful entry of SG200P$_{cmu1}$-Scp2 fungal hyphae into the plant tissue was extremely rare (Fig. 13 H) and did not lead to a massive proliferation within the plant.

These results indicate that both the deletion as well as the overexpression of *scp2* leads to defects during the penetration step that is accompanied by plant defense responses.

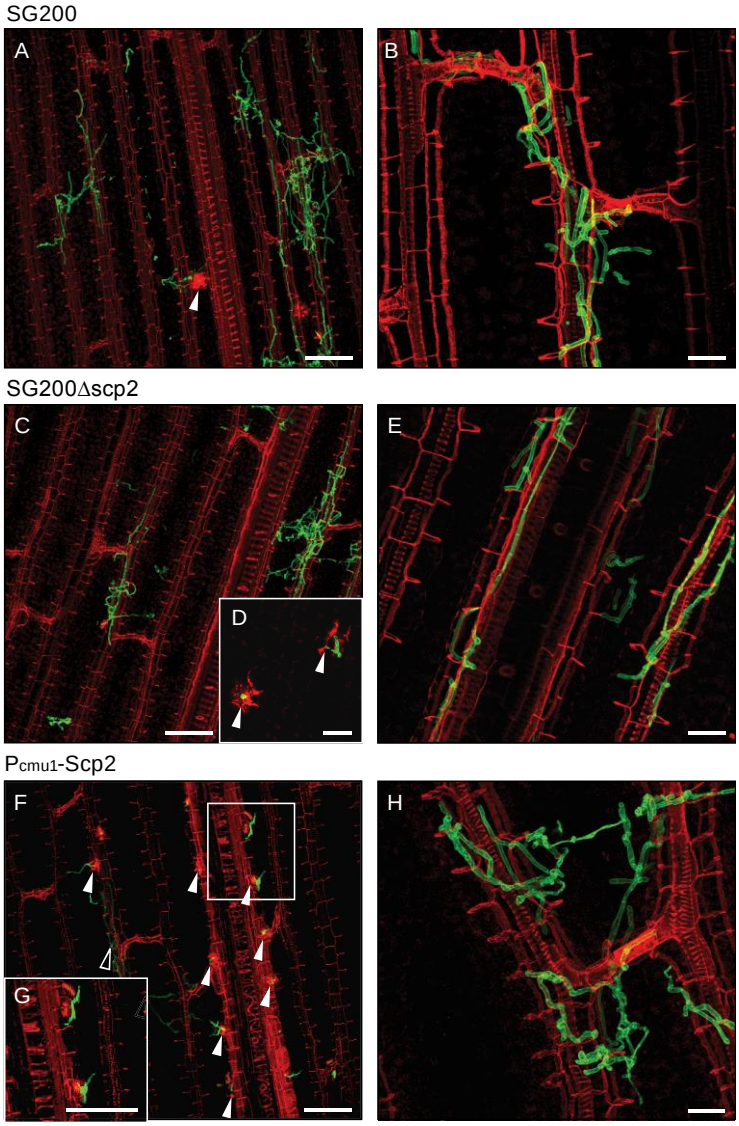

Fig. 13: WGA-AF488/PI staining of maize plants two days after infection with SG200, SG200Δscp2 and the overexpression strain SG200P$_{cmu1}$-Scp2. Fungal cells on top and within the plant tissue were stained with WGA-AF488 and are depicted in green. Plant cell walls are stained with PI and are depicted in red. (A and B) Intracellular proliferating SG200 hyphae two days after plant infection. (C and E) Intracellular proliferating SG200Δscp2 hyphae two days after plant infection. (D) SG200Δscp2 cells on the plant surface that induce plant defense. (F and G) SG200P$_{cmu1}$-Scp2 hyphae on the plant surface and hyphae within the plant tissue (empty arrowhead). (H) Intracellular proliferating SG200P$_{cmu1}$-Scp2 hyphae two days after plant infection. Scale bars for A, C, F and G equal 100 µm. Scale bars for B, D, E and H equal 25 µm. All pictures are maximum projections of confocal Z-stacks. Autofluorescence of plant defense responses with the same spectral properties as PI are marked with white arrowheads.

2.5 Scp2 is unconventionally secreted in low amounts

Previous experiments provided evidence that Scp2 is a candidate for unconventional protein secretion (see introduction). To verify unconventional secretion of Scp2, colony secretion assays (CSA) were conducted to supplement the data generated in previous studies. For CSAs cells are cultivated on a nitrocellulose membrane. Secreted proteins are captured by the membrane and Strep-HA fusion proteins can be visualized by western blot analysis. All generated constructs were integrated into the *ip* locus of the AB33 progenitor strain. AB33 is a

FB2 derivative which contains the *bE1* and *bW2* genes under the control of the nitrate inducible *nar* promoter (Brachmann *et al.*, 2001). AB33 therefore undergoes the morphological transition from saprophytic to filamentous growth in liquid medium when cells are shifted to nitrate minimal medium. All experiments included an AB33 strain that did not synthesize any Strep-HA tagged proteins to exclude unspecific background signals on the nitrocellulose membrane. This empty control strain did not give a signal in the conducted CSAs (Fig. 14 A, 1). A strain expressing a cytoplasmic *gfp-HA-strep* fusion construct under the control of the *otef* promoter (AB33GFP-HA-Strep) was included in each experiment to exclude cell lysis as a reason for detected signals (Fig. 14 A, 2). No secretion of cytoplasmic GFP could be observed. As a positive control Strep-HA-Scp2 was fused to the secretion signal of the *U. maydis* effector protein Stp1 (Schipper, 2009). A strong signal was obtained for the classically secreted SP-Strep-HA-Scp2 in all CSAs (Fig. 14 A, 5). To verify Scp2 secretion, *strep-HA-scp2* was expressed either under control of the *otef* promoter or the endogenous *scp2* promoter (Fig. 14 A, 3 and 4). CSAs could show secretion of Strep-HA-Scp2 on NM-glc as well as on CM-glc medium independently of the utilized promoter (Fig. 14 A).

To assay whether peroxisomal localization is crucial for Scp2 secretion a strain synthesizing a cytoplasmic version of the Strep-HA-Scp2 fusion protein (AB33Strep-HA-Scp2$_{cyt}$) was included in the analysis. This cytoplasmic Scp2 version carries a mutation in the peroxisomal targeting site (AKL/AAA) rendering the peroxisomal targeting signal nonfunctional. When analyzed for secretion, lower amounts of the protein were detected on the membrane suggesting a higher Scp2 secretion efficiency when the protein resides within peroxisomes (Fig. 14 A, 6). A strain producing a peroxisomal GFP fusion protein was generated (AB33Strep-HA-GFP$_{pex}$) to assay whether any protein that is localized in peroxisomes is able to reach the cell exterior (Fig. 14 A, 7). Peroxisomal localization of Strep-HA-GFP$_{pex}$ was verified by fluorescent microscopy (Fig. 14 B). Very low signals could be detected for Strep-HA-GFP$_{pex}$ in CSAs, making it unlikely that all proteins in peroxisomes can reach the extracellular space.

Cell lysates of the respective AB33 derivatives were analyzed in western blot analysis to exclude variations in CSA signal intensity due to differences in protein abundance. All analyzed Strep-HA fusion proteins, except of SP-Strep-HA-Scp2, were shown to be present in comparable amounts (Fig. 14 C). Lower protein levels of SP-Strep-HA-Scp2 in cell extracts most likely resulted from the efficient export of the protein to the cell exterior (Fig. 14 A, 5).

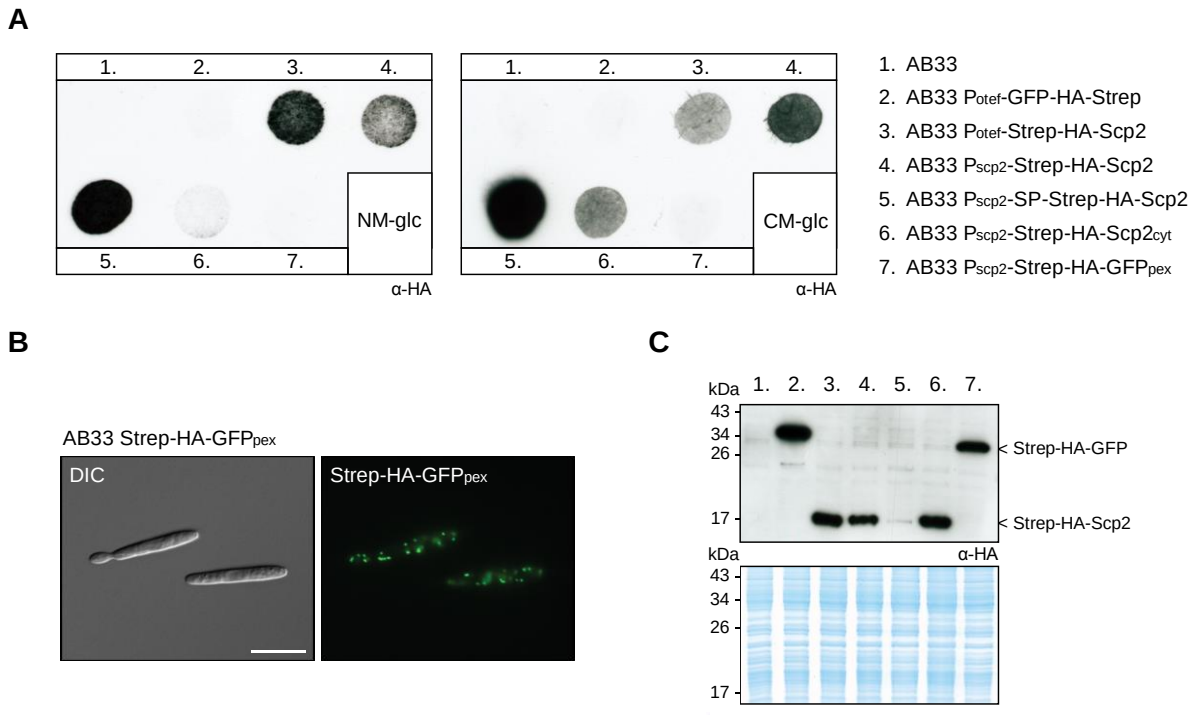

Fig. 14: Strep-HA-Scp2 is secreted in low amounts. (A) CSAs on different media. The indicated strains were grown in $YEPS_{light}$ to an OD_{600} of 0.6, washed in water and cultivated in NM-glc or Cm-glc for one hour. Subsequently, the cells were concentrated to an OD_{600} of 1.2 and 10 µl of the respective culture was spotted on nitrocellulose membranes. The plates were sealed and incubated overnight at 28 °C. In the morning, the cells were washed off the membrane and Strep-HA fusion proteins were detected by anti-HA western-blot analysis. (B) Localization of Strep-HA-GFP_{pex} in AB33 Strep-HA-GFP_{pex} grown in $YEPS_{light}$ medium. (C) Protein quantities in cells lysates of sporidia were determined for each strain by Bradford protein assays. 10 µg of total protein was separated using SDS-PAGE. Western blot analysis was used to visualize total levels for Strep-HA-fusion proteins using an anti-HA antibody (top panel). An InstantBlue stained polyacrylamide gel served as a loading control to ensure that equal protein quantities were used for the western blot analysis (lower panel).

The colony secretion analysis provides information about the secretion of a protein but does not specify the size of the secreted protein. Strep-HA-Scp2 was isolated from the CSA nitrocellulose membrane using acetone precipitation (Anderson, 1985) to prove that the Strep-HA-Scp2 fusion protein is secreted as a full length version. Full length Strep-HA-Scp2 could be isolated from nitrocellulose and was detected using anti-HA western blot analysis (Fig. 15). A cell lysate of the respective strain and the AB33 progenitor strain were used as a positive and negative control, respectively (Fig. 15). This data shows that the full length Strep-HA-Scp2 fusion protein is able to reach the cell exterior in low amounts via an unconventional secretion mechanism.

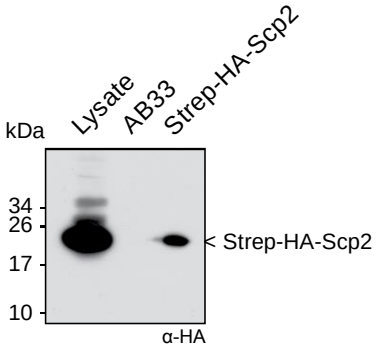

Fig. 15: Strep-HA-Scp2 is secreted as full length protein. For the isolation of secreted AB33 and AB33 Strep-HA-Scp2 proteins from nitrocellulose membranes the same set-up was used as it was described for CSAs on NM-glc and CM-glc with slight modifications (Fig. 14). To obtain higher quantities of protein, 500 µl of each culture were spotted on the nitrocellulose membrane. After washing off the cells a 1 cm^2 piece of the nitrocellulose was dissolved in acetone as described in Anderson (1985). Secreted Strep-HA tagged proteins were precipitated and detected via anti-HA western blot analysis. A cell lysate of AB33 Strep-HA-Scp2 sporidia served as a positive control. Nitrocellulose incubated with the empty progenitor strain AB33 served as a negative control. A single replicate was performed.

2.5.1 Investigation of a potential extracellular Scp2 function

After verifying that a Strep-HA-Scp2 fusion protein can be secreted, the potential role of extracellular Scp2 during pathogenic development was analyzed. Previous experiments had shown that a classically secreted SP-Strep-HA-Scp2 (AKL/AAA) fusion protein cannot complement the *scp2* deletion phenotype. This Scp2 derivative contained a mutated peroxisomal targeting sequence (AKL/AAA) to prevent dual targeting to peroxisomes and the secretory pathway (S. Krombach, unpublished). It has been hypothesized that the Scp2 C-terminus might not only contain the PTS1 targeting signal but might additionally contribute to the ligand binding activity of Scp2 (García *et al.*, 2000). To exclude that the lack of complementation observed for the SP-Strep-HA-Scp2 (AKL/AAA) fusion protein is caused by the inability of the protein to bind its ligand, a *SP-scp2-GSA* construct was generated. In this construct Scp2 was fused to the Stp1 secretion signal and expressed under transcriptional control of the endogenous *scp2* promoter. To prevent peroxisomal targeting the C-terminus was extended by adding three amino acids (GSA) (Fig. 16 A). Blocked peroxisomal targeting of SP-Scp2-GSA was verified by fluorescence microscopy of a GFP-fusion derivative of the respective construct (SP-GFP-Scp2-GSA). The plasmid carrying the sequence *SP-gfp-scp2-GSA* was integrated into the *ip* locus of the peroxisomal marker strain AB31Pex. Colocalization experiments of peroxisomes and SP-GFP-Scp2-GSA confirmed the exclusive targeting to the secretory pathway/ER (Fig. 16 B).

To test for complementation the *SP-scp2-GSA* construct was integrated into the *ip* locus of SG200Δscp2 and the resulting strain SG200Δscp2SP-Scp2-GSA was analyzed in plant infection experiments. Evaluation of plant symptom development twelve days after infection

showed no complementation of the *scp2* deletion phenotype (Fig. 16 C). As a control construct *scp2-AKL* was generated and inserted into the *ip* locus of SG200Δscp2 to exclude that the fusion of three amino acids to the Scp2 C-terminus renders the protein nonfunctional. Rather than adding three random amino acids a second three amino acid long PTS1 signal (AKL) was added to the *scp2* sequence. In plant infection experiments SG200Scp2-AKL induced virulence symptoms comparable to the SG200 progenitor strain (Fig. 16 C). Based on this, it is unlikely that the addition of amino acids at the C-terminus of Scp2 is the reason for the lack of complementation. These results show that a Scp2 protein that no longer resides in peroxisomes and that is targeted to the secretory pathway cannot complement the *scp2* deletion phenotype during pathogenic development.

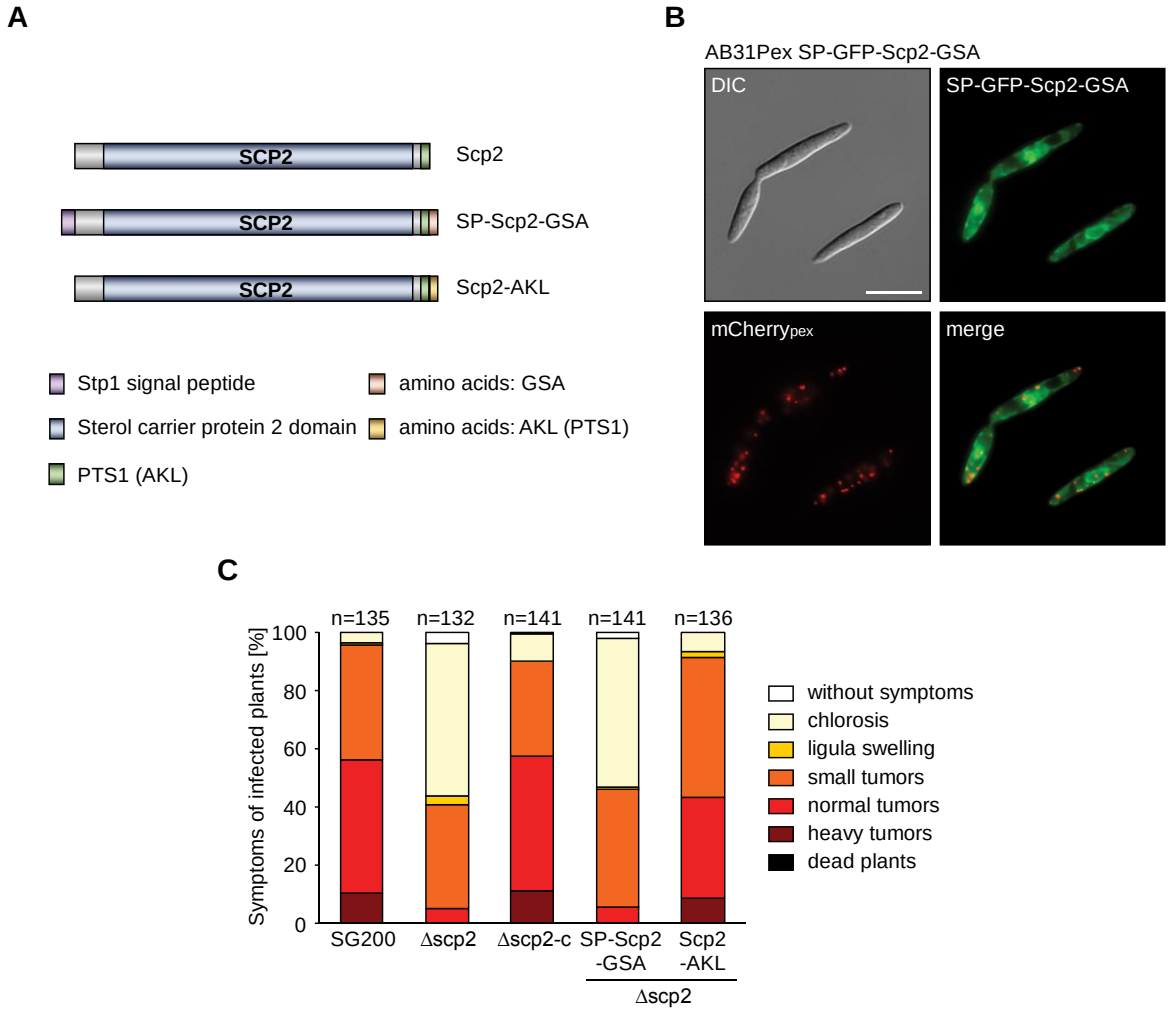

Fig. 16: Virulence of the strains SG200Δscp2SP-Scp2-GSA and SG200Δscp2Scp2-AKL. (A) Illustration of the fusion constructs used for infection assays. A legend of the respective domains is depicted underneath the scheme. (B) Fluorescent microscopy of SP-GFP-Scp2-GSA and colocalization with the peroxisomal marker protein mCherry$_{pex}$. Green fluorescence displays the SP-GFP-Scp2-GSA fusion construct localized in the secretory pathway while red fluorescence depicts the peroxisomal marker protein mCherry-SKL. The scale bar equals 10 µm. (C) Infection symptoms on maize seedlings infected with SG200, SG200Δscp2, SG200Δscp2-c, SG200Δscp2SP-Scp2-GSA and SG200Δscp2Scp2-AKL, respectively. Infection symptoms were evaluated twelve days post infection. The respective symptom categories are depicted on the right hand side of the diagram. For the virulence assay average values of four independent infections were taken. The total number of plants (n) is depicted above each column.

2.6 *Yarrowia lipolytica* and human Scp2 can partially complement the function of *U. maydis* Scp2

Sterol carrier proteins are conserved in bacteria, archaea and eukaryotes (Edqvist and Blomqvist, 2006). For the human sterol carrier protein 2 (hScp2) as well as for Scp2 from the yeast *Yarrowia lipolytica* (YLScp2) structural and experimental data is available (García *et al.*, 2000; De Berti *et al.*, 2013). Amino acid sequence alignments showed that the *U. maydis* Scp2 (UmScp2) shares a sequence identity of 38.14 % and 41.8 % with its orthologs in human and *Y. lipolytica*, respectively (t-coffee alignment) (Fig. 17 A). Furthermore, the generation of a structural model of the *U. maydis* Scp2 protein revealed a conformation comparable to the ones described for hScp2 and YLScp2 (García *et al.*, 2000; De Berti *et al.*, 2013) suggesting related functions (Fig. 17 B). *U. maydis scp2* deletion strains were complemented using *hscp2* and *YLscp2*, to demonstrate conserved functions between the three orthologs.

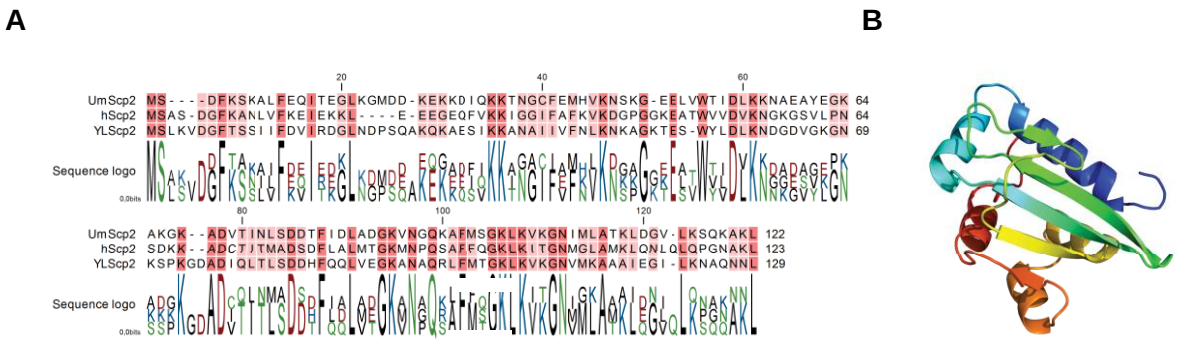

Fig. 17: Conservation between UmScp2 and its two orthologs from human (hScp2) and *Y. lipolytica* (YLScp2) and a predicted structural model of the *U. maydis* Scp2 (UmScp2). (A) Amino acid sequence alignment of UmScp2 with its two orthologs hScp2 and YLScp2. The sequence logo displaying conserved amino acids is depicted underneath the alignment. The alignment was generated using the CLC Genomics Workbench 8. (B) The structural model of UmScp2 was generated using the Phyre2 web portal for protein modeling, prediction and analysis (http://www.sbg.bio.ic.ac.uk/phyre2/html) (Kelley *et al.*, 2015). The model was generated with 100 % of the residues modelled at >90 % confidence. The 3-dimensional structure of YLScp2 was one of the four protein structure templates that were used by the database to model the structure of UmScp2.

The two genes were synthesized as codon optimized versions adapted for the expression in *U. maydis*. In mammals hScp2 is generated by posttranslational processing from a 143 amino acid precursor protein (pro-Scp2) (Stolowich *et al.*, 2002). Therefore, a start codon was added to the synthesized gene sequence of *hscp2*. Both genes were expressed under the control of the *U. maydis scp2* promoter and single copies of the respective constructs were integrated into the genome of SG200Δscp2 (SG200Δscp2-hScp2 and SG200Δscp2-YLScp2). The ability of hScp2 and YLScp2 to complement the *scp2* deletion phenotype was assayed in plant infection experiments. Single integrations of *hscp2* and *YLscp2* into SG200Δscp2 lead to a weak

complementation of the *scp2* mutant phenotype (Fig. 18 A). None of the strains showed defects in filamentation on charcoal supplemented medium (Fig. 18 B).

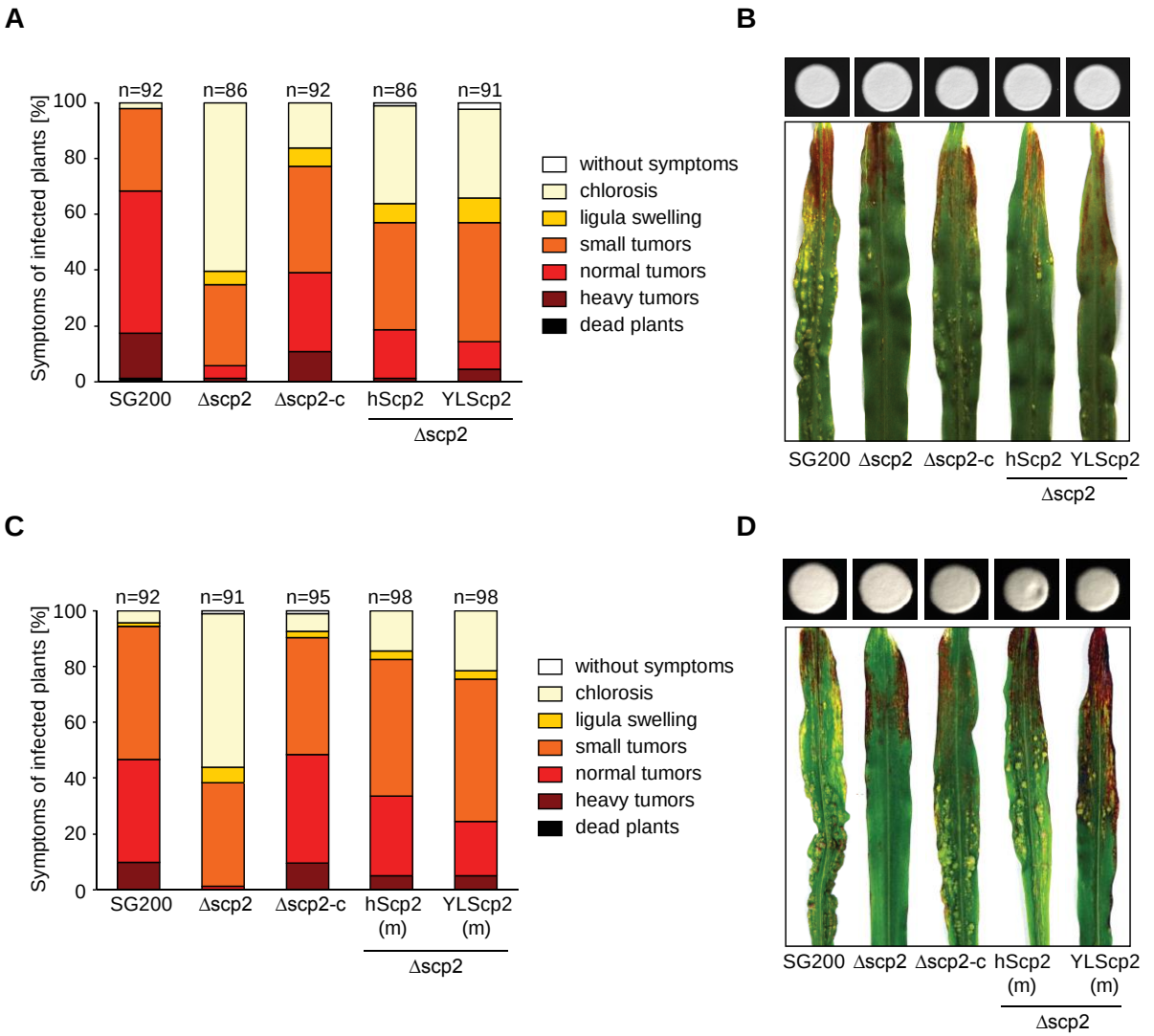

Fig. 18: Virulence of *scp2* deletion strains complemented with single and multiple integrations of *hscp2* or *YLscp2*. (A) Infection symptoms on maize seedlings infected with SG200, SG200Δscp2, SG200Δscp2-c and the complementation strains SG200Δscp2-hScp2 and SG200Δscp2-YLScp2 carrying a single copy of the *hscp2* and *YLscp2* gene. Infection symptoms were evaluated twelve days post infection. The respective symptom categories are depicted on the right hand side of the diagram. For the virulence assay average values of three independent infections were taken. The total number of plants (n) is depicted above each column. (B) Filamentous growth of the respective strains on charcoal plates (top panel). Pictures of representative leaves from plant infections (lower panel). (C) Virulence of SG200Δscp2-hScp2 and SG200Δscp2-YLScp2 complementation strains carrying multiple copies of the respective genes *hscp2* and *YLscp2*. Infections and scorings were performed as described in (A). (D) Filamentous growth of the respective strains on charcoal plates (top panel). Pictures of representative leaves from plant infections (lower panel).

As the observed level of complementation was very low, *scp2* deletion strains carrying multiple integrations of *YLscp2* or *hscp2* were analyzed in infection assays. Plant infection experiments showed that multiple integrations of *hscp2* and *YLscp2* led to a higher level of complementation (Fig. 18 C). None of the analyzed strains showed defects in filament formation on PD-charcoal

medium (Fig. 18 D). These results reinforce that Scp2 proteins from different organisms have a conserved function.

2.7 Ligand binding specificity of the *U. maydis* Scp2 protein

Sterol carrier proteins have been shown to be involved in the transport and distribution of various lipids such as fatty acids, fatty acyl-CoAs, phospholipids and sterols like cholesterol between intracellular membranes (Gallegos *et al.*, 2001). To elucidate whether the *U. maydis* Scp2 might bind cholesterol or the fungal counterpart ergosterol SG200 and SG200Δscp2 were treated with the naturally fluorescent stain filipin. Filipin is an antifungal polyene antibiotic which forms complexes with sterols in the fungal membrane (Alvarez *et al.*, 2007).

In *U. maydis* SG200 sporidia filipin localized predominantly at the emerging bud, the bud tip and was further found in a dotted pattern along the membrane. These observations were in line with the findings of previous work which described that filipin accumulates at the sites of active growth and in ergosterol sterol-rich membrane domains, termed lipid rafts (Cánovas and Pérez-Martín, 2009). The analysis of saprophytically growing cells revealed no significant differences between *scp2* deletion strains and SG200 (Fig. 19 A).

Since *scp2* has been shown to be upregulated in early stages of plant infection, the sterol distribution in filamentous growing cells and in *in vitro* induced appressoria was analyzed. *U. maydis* filamentation and appressorium formation can be initiated by spraying cells on a hydrophobic surface like parafilm. Enhanced appressorium formation can be induced by the addition of hydroxy fatty acids (HFA) (16-hydroxyhexadecanoic acid) (Mendoza-Mendoza *et al.*, 2009). Approximately sixteen hours after induction, the formed appressoria and filaments can be visualized by microscopy. In SG200 filaments filipin accumulated in a dotted pattern along the membrane and further localized to the tip of appressorium. The evaluation of the sterol distribution in SG200 and SG200Δscp2 filaments did not show a significant difference of staining patterns after filipin treatment (Fig. 19 B).

Interestingly, in the course of analyzing the distribution of membrane sterols it was found that the majority of SG200Δscp2 filaments were unable to form appressoria on the hydrophobic surface (not shown). Accordingly, SG200Δscp2 appressorium formation was analyzed in more detail in chapter 2.8.

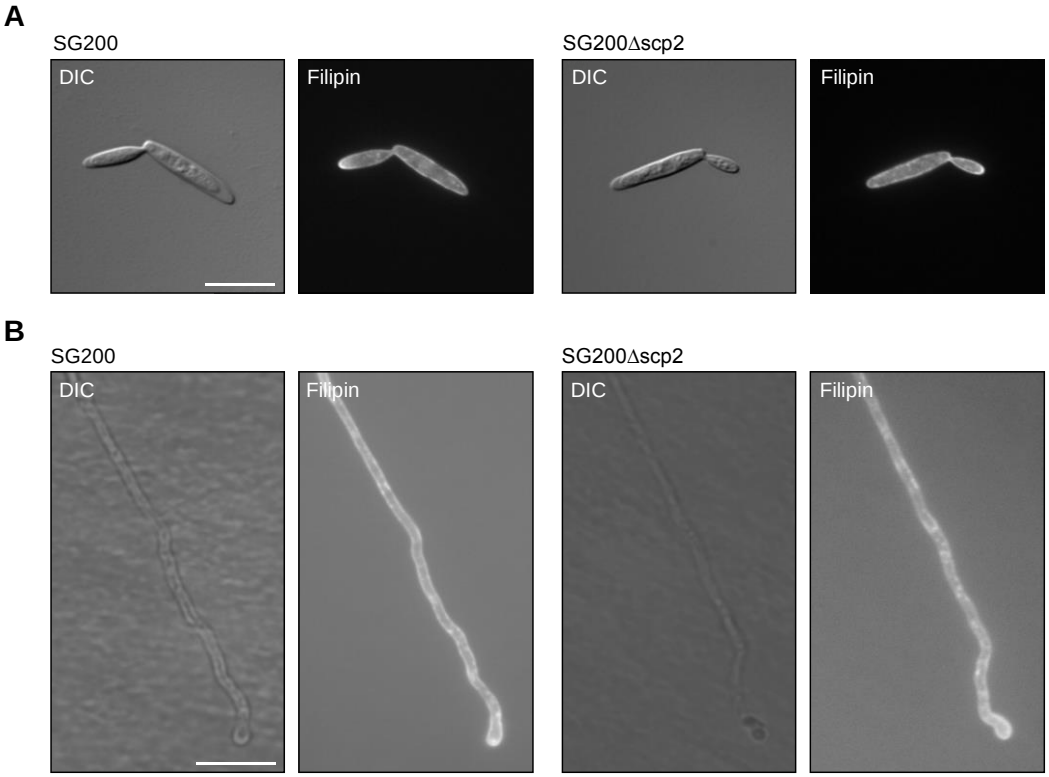

Fig. 19: Filipin staining of SG200 and SG200Δscp2. (A) SG200 and SG200Δscp2 were grown in $YEPS_{light}$ to an OD_{600} of 0.6 and stained with 5 µM filipin in PBS for 5 min. Sterol distribution was visualized using fluorescence microscopy (DAPI channel) immediately after staining. (B) Filament and appressorium formation was induced by treating cells with 100 µM HFA and subsequently spraying the cells on parafilm. Sixteen hours after induction of filaments, the distribution of sterols was visualized using filipin staining as described above. Scale bars equal 10 µm.

Differences in plasma membrane sterol content can change the resistance to polyene antibiotics like the described filipin or the related antibiotic nystatin (Berger *et al.*, 2005). Like filipin the antifungal drug nystatin binds to ergosterols and causes permeabilization of the plasma membrane by the formation of ion channels.

A nystatin growth assay was conducted to examine whether fungal membrane integrity might differ between SG200 and the *scp2* mutant. In comparison to the SG200 progenitor strain no difference in resistance to nystatin was observed for *scp2* mutant strains when treated with 2.5 µg/ml or 5.0 µg/ml nystatin demonstrating that membrane integrity of *scp2* deletion strains is intact (Fig. 20). It is therefore unlikely that Scp2 alters the sterol distribution or composition in the fungal plasma membrane.

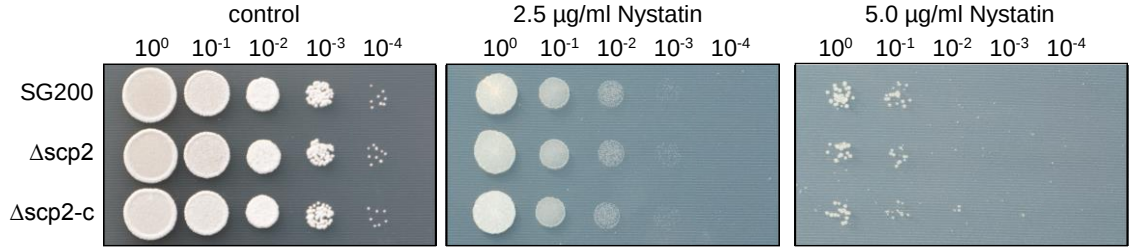

Fig. 20: Sensitivity of *scp2* deletion strains to nystatin. The respective strains were grown in $YEPS_{light}$ to an OD_{600} of 0.8. Serial dilutions were spotted on CM-glc (control) as well as CM-glc supplemented with either 2.5 µg/ml or 5.0 µg/ml nystatin. The plates were incubated at room temperature for two days (CM-glc), four days (2.5 µg/ml) and six days (5.0 µg/ml), respectively.

2.7.1 Scp2 shows binding affinity to phosphatidylinositol 4-phosphate and cardiolipin

To determine whether the binding specificity of the *U. maydis* Scp2 is similar to the ligand specificity of its two orthologs hScp2 and YLscp2 a Strep-Scp2 fusion protein was heterologously expressed in *E. coli* and analyzed in a protein-lipid overlay assay. In protein-lipid overlay assays a hydrophobic membrane is spotted with biologically relevant membrane lipids and then incubated with purified protein to determine the spectrum of potential lipid ligands. For the synthesis in *E. coli* the *scp2* gene was amplified from *U. maydis* cDNA and fused N-terminally to a Strep affinity tag. The respective fusion construct *strep-scp2* was inserted into a pET21a(+) expression vector resulting in the plasmid pSR226 which was transformed into the *E. coli* derivative Rosetta (DE3)pLysS. As a control for unspecific binding, the *U. maydis* effector Tin2 (TwinStrep-Tin2) (Tanaka *et al.*, 2014) encoded in the plasmid pPR-IBA102-Tin2dSP was purified in parallel and included in the analysis. Protein synthesis of transformed *E. coli* cells grown in dYT complete medium was induced by treatment with 1 mM IPTG for 4 hours at 37 °C. Both proteins were found to be soluble and synthesized in sufficient amounts. Successfully produced Strep-Scp2 and Twin-Strep-Tin2 were purified via Strep-affinity purification and subsequent gel-filtration chromatography (Fig. 21 A). The purified proteins were used for the protein-lipid overlay assay. Bound protein was detected by western blot analysis using an anti-Strep-HRP coupled antibody. A lipid strip membrane developed without the addition of any recombinant protein was used to exclude unspecific binding of the anti-Strep-HRP antibody (Fig. 21 B). The control protein TwinStrep-Tin2 did not display strong affinities for any of the provided lipids in the assay (Fig. 21 B). The Strep-Scp2 protein, however, showed a specific interaction with cardiolipin as well as phosphatidylinositol 4-phosphate (PI4P) (Fig. 21 B). These results indicate that the *U. maydis* Scp2 protein binds the mitochondrial lipid cardiolipin and PI4P rather than cholesterol.

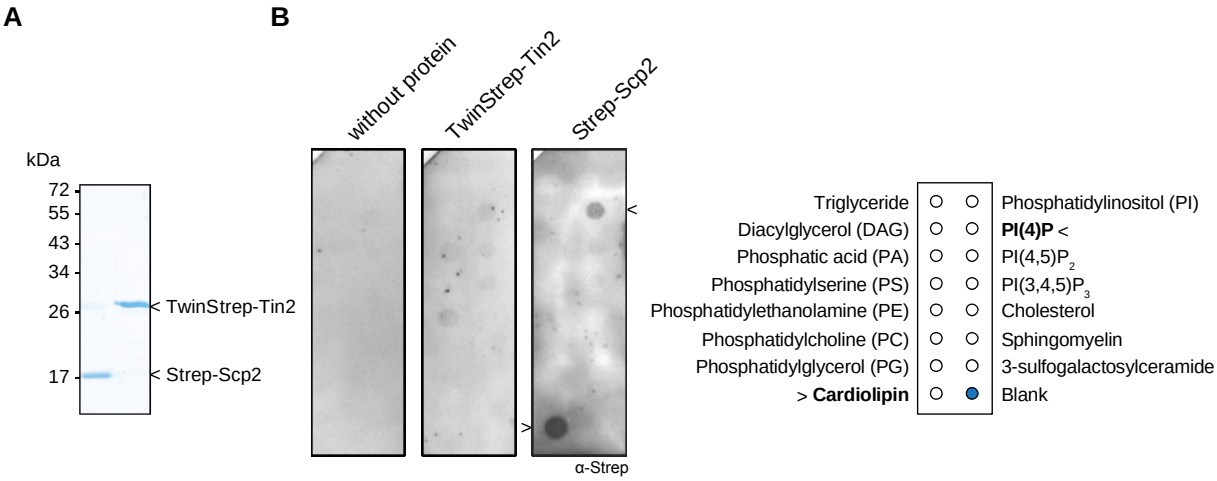

Fig. 21: Scp2 lipid binding properties. (A) Purified Strep-Scp2 and TwinStrep-Tin2 were separated by SDS-PAGE and visualized using InstantBlue protein stain. Heterologously expressed recombinant Strep-Scp2 and TwinStrep-Tin2 were purified from *E. coli* Rosetta(DE3)pLysS transformed with the plasmids pSR226 and pPR-IBA102-Tin2dSP, respectively. Protein synthesis was induced by treatment with 1 mM IPTG for 4 hours at 37 °C. Expressed proteins were purified using Strep-affinity purification and gel-filtration chromatography. Both proteins run slightly higher as expected in the performed SDS-PAGE (Strep-Scp2: 14.7 kDa and TwinStrep-Tin2: 24.0 kDa) (B) Echelon membrane lipid strip assays for Strep-Scp2 and the control protein TwinStrep-Scp2. Left: The membrane was incubated without addition of any recombinant protein to exclude unspecific binding of the anti-Strep-HRP coupled antibody to the membrane. Middle: The membrane was incubated with 0.5 µg/ml TwinStrep-Tin2 to detect unspecific binding of a control protein subjected to the same practical scheme. Right: The membrane was incubated with 0.5 µg/ml Strep-Scp2 to determine the lipid binding specificity of the *U. maydis* Scp2 protein. For western blot analysis an anti-Strep-HRP-coupled antibody was used. Arrowheads indicate specific binding of Scp2 to cardiolipin and PI4P.

2.8 Deletion of *scp2* causes a defect in appressoria formation on artificial surfaces but not on planta

During the analysis of membrane sterols in filaments of the *scp2* deletion strain on parafilm a potential appressorium formation defect was noted (chapter 2.7). To examine *scp2* mutant strain appressoria in more detail multiple copies of the *appressorial marker 1* (AM1) were integrated into SG200Δscp2 (SG200Δscp2AM1). The marker construct *am1* consists of a *triple-gfp* fusion which is expressed under the control of the appressorium-specific promoter P_{01779}. The AM1-marker therefore allows detection and quantification of filaments that induce the genetic program for appressorium formation by fluorescence microscopy (Mendoza-Mendoza *et al.*, 2009). *U. maydis* appressoria are characterized by a crook that precedes the development of the slightly swollen appressorium (Snetselaar, 1993). Appressorium and filament formation of SG200AM1 and SG200Δscp2AM1 on parafilm was induced as described in chapter 2.7.

In an initial experiment it was assayed whether SG200AM1 and SG200Δscp2AM1 show a similar amount of filaments expressing the AM1 marker (AM-positive). Thereby, the morphology of the filaments was disregarded. Analysis of the AM1-marker expression on parafilm showed that the ratio between filaments expressing *am1* and filaments not expressing the appressorial marker (AM1-negative) was comparable in SG200AM1 and SG200Δscp2AM1

(Fig. 22 A). In a second experiment the AM1-marker expressing filaments of SG200AM1 and SG200AM1Δscp2 were compared with respect to the formation of appressoria sixteen hours after spraying on parafilm. The quantification of appressoria in SG200AM1 and SG200Δscp2AM1 revealed that only around 10 % of the AM1-positive *scp2* deletion strain filaments were able to form appressoria. In contrast to that, around 80 % of the SG200AM1 filaments that expressed *am1* formed appressoria (Fig. 22 B).

To investigate whether the formation of appressoria in the *scp2* deletion strains is reduced or only delayed appressoria development on parafilm was also analyzed 24 hours after spraying. While 87 % of SG200AM1 filaments formed an appressorium after 24 hours, only 5 % of SG200Δscp2AM1 had generated appressoria (Fig. 22 C). This experiment confirmed that the ability of *scp2* deletion strains to form appressoria on a hydrophobic surface is significantly reduced in comparison to SG200AM1. Interestingly, the appressorium formation defect of SG200Δscp2AM1 on parafilm was not observed for filaments on the leaf surface (not shown). This indicates that additional plant derived signals are involved in the initiation of appressorium formation on the plant.

U. maydis hyphae grow by extension of the cell apex and by the periodic insertion of septa at the posterior pole. The cytoplasm migrates towards the growing tip leaving empty sections in the hindmost part of the filament (Steinberg *et al.*, 1998). The cytoplasm filled tip compartment of SG200Δscp2AM1 filaments which did not form an appressorium appeared thinner and longer in comparison to SG200AM1 (Fig. 22 D). The average length of the tip compartments in SG200AM1 and SG200Δscp2AM1 AM1-marker expressing filaments was determined starting at the hyphal tip until the first integrated septum. This quantification verified that the cytoplasm filled tip compartment of SG200Δscp2AM1 filaments was with an average length of 89.6 µm (± 8.0) significantly longer than in SG200AM1 filaments that only reached an average length of 54.0 µm (± 9.6) (n=15).

These experiments show that although *scp2* deletion strains do express the AM1-marker SG200Δscp2AM1 shows a significantly lower frequency of appressorium formation on parafilm than SG200AM1. Instead *scp2* deletion strain filaments show extended growth of the cytoplasm filled tip compartment.

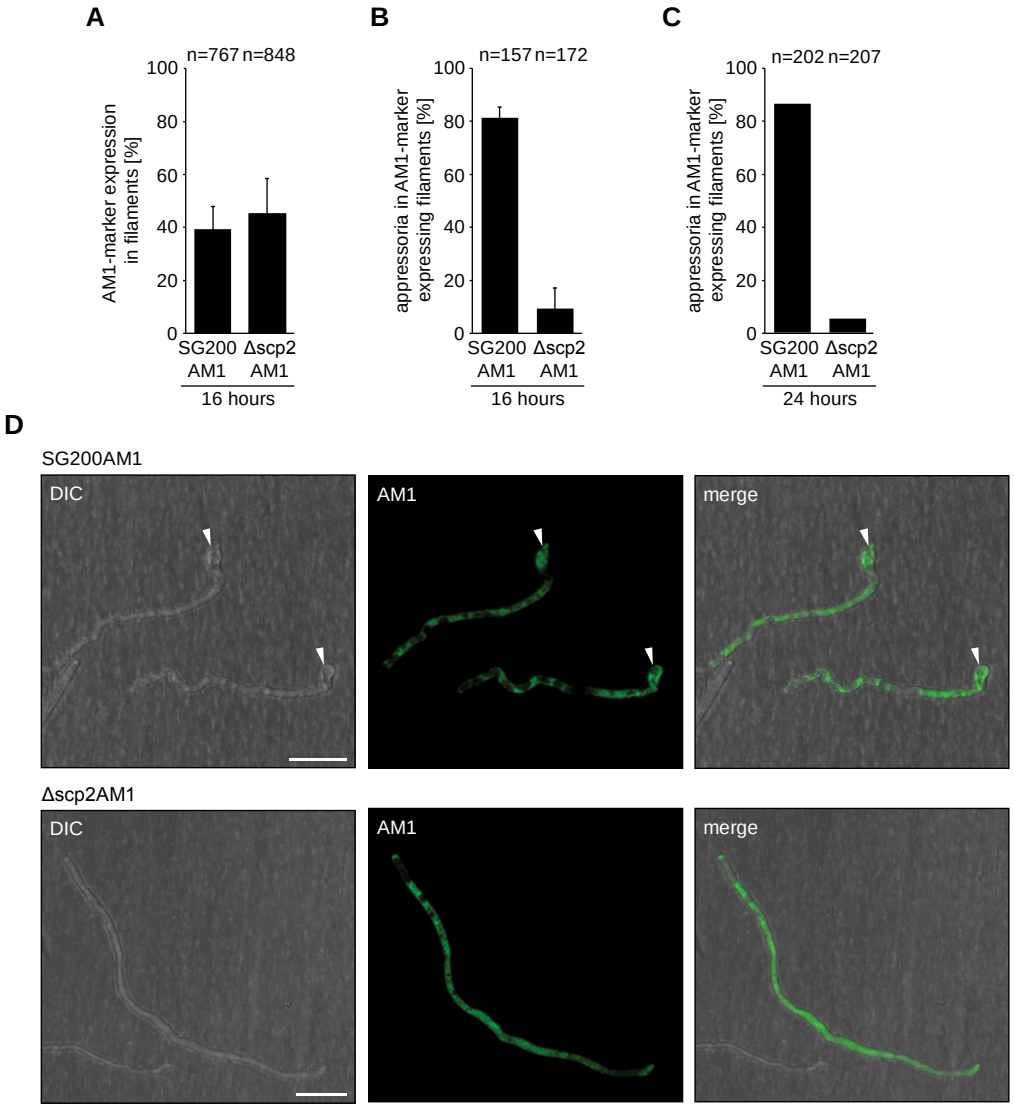

Fig. 22: Appressorium formation of *scp2* deletion strains on parafilm. (A) Quantification of filaments expressing the AM1-marker on parafilm sixteen hours after spraying. Average values of three independent replicates are depicted in the graph. The error bars indicate the ± standard deviation. (B) Quantification of AM1-marker expressing filaments that form appressoria on parafilm sixteen hours after spraying. Average values of four independent replicates are depicted in the graph. The error bars indicate the ± standard deviation. The majority of AM1-marker expressing SG200AM1 filaments formed appressoria while the frequency of appressoria formation in SG200Δscp2AM1 was significantly reduced. (C) Quantification of AM1-positive filaments that formed appressoria on parafilm 24 hours after spraying. A single replicate is depicted in the graph. The total number of evaluated cells (n) is depicted above each column. (D) Fluorescence microscopy of SG200AM1 and SG200Δscp2AM1 filaments on parafilm sixteen hours after induction. Filaments and appressoria were induced as described in chapter 2.7. Cytoplasmic GFP indicates the expression of the AM1-marker. White arrowheads indicate appressoria. Scale bars equal 10 µm.

2.8.1 Mutants of s*cp2* display a higher mortality after growth on parafilm

The elongation of the tip compartment might reduce the viability of the SG200Δscp2AM1 hyphae. A viability assay was conducted to quantify the numer of living and dead cells for SG200 as well as for the *scp2* mutant strain after induction of filament formation on parafilm. Filament and appressorium formation of SG200, SG200Δscp2 and the complementation strain SG200Δscp2-c were induced as described in chapter 2.7. After sixteen hours of incubation the parafilm slides were treated with a double fluorescent stain containing propidium iodide (PI)

and fluorescein diacetate (FDA). Propidium iodide only penetrates into dead cells while FDA is passively taken up by all cells and is subsequently converted to fluorescein. Non-viable cells are not able to hydrolyze FDA and therefore show no green fluorescence (Kwolek-Mirek and Zadrag-Tecza, 2014). The quantification of viable cells on parafilm showed that in comparison to SG200 and the complementation strain SG200Δscp2-c, SG200Δscp2 filaments displayed an approximately two-times higher mortality (15% versus 31% versus 12%) (Fig. 23).

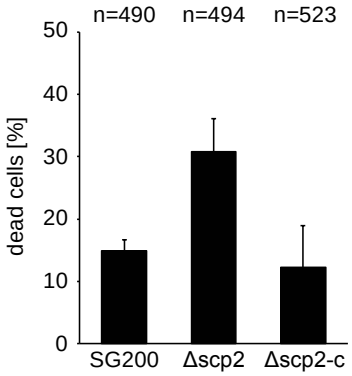

Fig. 23: Quantification of dead SG200, SG200Δscp2 and SG200Δscp2-c filaments on parafilm. Filament and appressorium formation was induced as described in chapter 2.7. Living and dead cells were visualized by a FDA/PI double stain. Dead filaments were stained in red (PI) and viable cells were stained in green (FDA). Average values of dead cells from two replicates are depicted in the graph. The total number of counted cells (n) is indicated above each column. Error bars indicate the ± standard deviation.

2.9 Cuticle penetration and plant colonization is reduced in *scp2* mutants

Even though the appressorium formation defect of *scp2* deletion strains on parafilm was not observed for filaments on the plant surface appressorial function might be compromised during plant cuticle penetration. A new penetration marker was established to monitor successful breaching of the plant cuticle and to determine whether appressorium mediated penetration is less efficient in *scp2* mutants.

2.9.1 Establishment of a marker for successful cuticle penetration

The penetration marker construct was composed of two elements. First, it contained the already established AM1-marker (Mendoza-Mendoza *et al.*, 2009) that indicates appressorium formation. Second, it comprised a *mCherry-HA* fusion under the control of the *rsp3* promoter (Fig. 24 A) which had been shown to be expressed during penetration (L. Ma, unpublished). To study the generated penetration marker construct (AM1PM) the respective plasmid pSR422 was integrated in single or multiple copies in the *ip* locus of the SG200 and the SG200Δscp2 (SG200AM1PM and SG200Δscp2AM1PM). Maize plants were infected with SG200AM1PM carrying a single integration of the penetration marker to verify functionality of the construct.

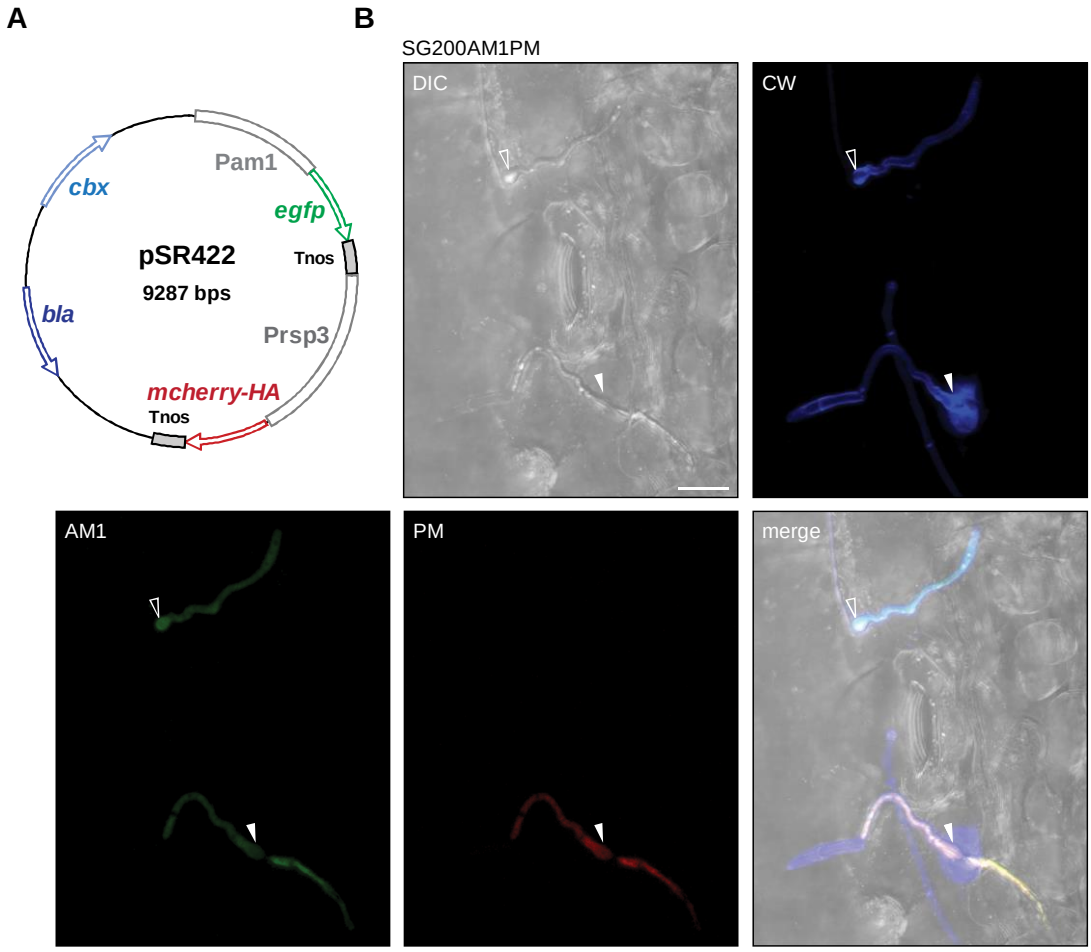

Fig. 24: Vector map of the penetration marker construct pSR422 and microscopic analysis of SG200AM1PM on the plant surface. (A) Schematic drawing of pSR422 expressing both the AM1-marker and the penetration marker (PM). *Egfp* expression is controlled by the appressorium specific *am1* promoter (P_{am1}) and indicates appressorium formation. Expression of cytoplasmic *mcherry-HA* under the control of the *rsp3* promoter (P_{rsp3}) serves as a marker for penetration (B) Confocal laser scanning microscopy of SG200AM1PM on the leaf surface sixteen hours after infection. Filaments on the leaf surface were stained with calcofluor white (CW). Expression of the appressorial marker construct (P_{am1}-*egfp)* is displayed in the green channel (AM1). Expression of the penetration marker construct (P_{rsp3}-*mcherry-HA*) is depicted in the red channel (PM). Cells that do not penetrate glow in green due to appressorium formation but do not show red fluorescence that indicates successful penetration. An overlay of all channels is shown in the merge image. White arrowheads mark penetrating appressoria. Hollow arrowheads mark non-penetrating appressoria. The scale bar equals 10 µm.

Confocal laser scanning microscopy of the plant surface sixteen hours post infection verified AM1-marker expression upon appressorium formation. In contrast to that, fluorescence of the penetration marker (PM) was only observed when appressoria successfully breached the plant cuticle (Fig. 24 B). To exclude unspecific expression of the penetration marker SG200AM1PM and SG200Δscp2AM1PM were sprayed on parafilm and expression of the two markers was analyzed sixteen hours after spraying. The hydrophobic composition of parafilm promotes *U. maydis* appressorium formation but does not allow penetration of the rigid parafilm surface. Due to this, e*gfp* expression should be visible in filaments that initiate the genetic program for appressorium formation but no cytoplasmic mCherry-HA fluorescence should be detectable. Quantification of fluorescence signals in a single replicate experiment verified that only one

out of 141 (0.71%) AM1-positive SG200AM1PM filaments and one out of 153 (0.65%) AM1-marker expressing SG200Δscp2AM1PM filaments showed a slight red fluorescence. These results confirm that the PM marker is specifically induced upon penetration of the plant epidermis.

In infection assays virulence of strains carrying single and multiple copies of the construct were analyzed to exclude an impact of the penetration marker on biotrophic growth. While single integrations of the penetration marker construct did not influence virulence of SG200AM1PM and SG200Δscp2AM1PM, multiple integrations of the construct caused a slight reduction of disease severity in both strains (Fig. 25). No effect on filament formation was observed for any of the analyzed strains (Fig. 25). Based on these findings, only single integrations of the penetration marker construct were used for the evaluation of penetration efficiency of SG200AM1PM and SG200Δscp2AM1PM.

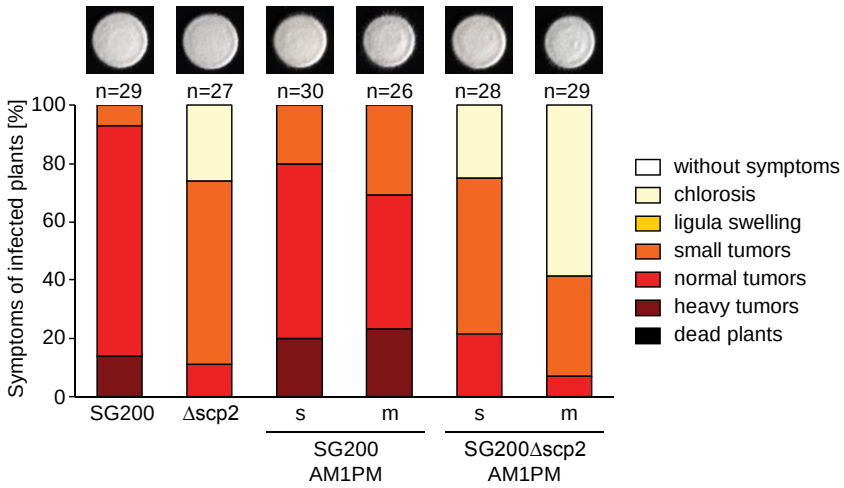

Fig. 25: Virulence of the penetration marker strains SG200AM1PM and SG200Δscp2AM1PM. Infection symptoms on maize seedlings infected with SG200, SG200Δscp2 as well as SG200AM1PM and SG200Δscp2AM1PM carrying single (s) and multiple (m) integrations of the penetration marker construct pSR422. Infection symptoms were evaluated twelve days post infection. The respective symptom categories are depicted on the right hand side of the diagram. For the virulence assay a single round of infections was conducted. The total number of infected plants (n) is indicated above each column. Filamentous growth of the respective strains on PD charcoal plates is depicted above each column.

2.9.2 Penetration efficiency of *scp2* deletion strains is reduced

After establishment of a functional penetration marker, the penetration efficiency of SG200AM1PM versus SG200Δscp2AM1PM was assayed on the plant surface. For this, maize seedlings were infected with SG200AM1PM and SG200Δscp2AM1PM, respectively, and the penetration efficiency of each strain was evaluated sixteen hours after infection by fluorescence microscopy. Quantification of AM1-marker expressing cells that successfully penetrated the plant surface revealed a penetration frequency of about 70 % for SG200AM1PM. In contrast, only around 35 % of the SG200Δscp2AM1PM appressoria were able to successfully breach the

plant cuticle (Fig. 26). These results support the previous hypothesis that appressoria formation and function might be influenced by the absence of Scp2.

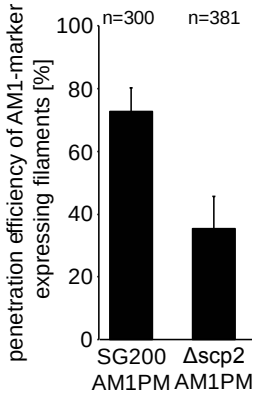

Fig. 26: Penetration efficiency of *scp2* deletion strains on maize leaves. Seven day old maize seedling were infected with SG200AM1PM and SG200Δscp2AM1PM, respectively. Successful penetration events were quantified sixteen hours after plant infection by fluorescence microscopy using the PM-marker (red fluorescence). The graph shows successful penetration events in ratio to all quantified AM1-marker expressing filaments (green fluorescence). Average values of three independent experiments are shown with error bars indicating the ± standard deviation. The total number of evaluated AM1-marker expressing filaments (n) is given above each column.

2.9.3 Plant tissue colonization is reduced in *scp2* deletion strains

To analyze whether the reduced penetration efficiency of *scp2* deletion mutants causes a decrease of plant tissue colonization, the relative fungal biomass was quantified in SG200 and SG200Δscp2 infected maize plants. For this, seven day old maize seedling were infected with SG200 and SG200Δscp2 and leaf samples were harvested 20 hours, 2 days and 4 days after infection. All leaf samples, except of the 20 hour time point samples, were washed with 0.1 % Tween 20 and subsequently in H_2O to remove sporidia that remained on the leaf surface. Plant and fungal gDNA was extracted from the leaves and a quantitative real-time PCR (qPCR) approach was used to amplify the fungal gene *ppi* and the plant derived *gapdh* for determining the ratio between fungal and maize plant biomass.

Two days after infection the biomass assays showed that in comparison to SG200 the colonization of the maize plant tissue by *scp2* deletion strains was reduced by factor 4.4. At four days post infection the relative biomass of SG200Δscp2 was reduced by factor 1.9 compared to SG200 (Fig. 27). These experiments support the observation that *scp2* deletion mutants penetrate the plant surface with a lower efficiency than the SG200 progenitor strain which in turn causes a reduction of overall plant tissue colonization at later stages of the infection.

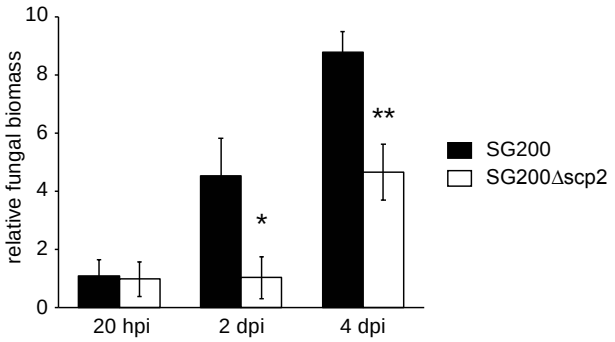

Fig. 27: Colonization of the plant tissue by *scp2* deletion mutants. Relative fungal biomass was determined by qPCR. For this, gDNA was prepared from infected maize leaves 20 hpi, 2 dpi and 4 dpi. The fungal gene *ppi* and the plant gene *gapdh* were used for the estimation of relative fungal biomass. SG200 biomass at 20 hpi was used as the reference and was set to 1. The average value of three biological replicates is depicted in the graph. Error bars indicate the ± standard deviation. Significance of differences between SG200 and SG200Δscp2 was calculated using the student's t-test: (*) P = 0.015, (**) P = 0.004.

2.10 Deletion of isocitrate lyases attenuates growth and virulence

A possible reason underlying the reduction of fungal penetration frequency is an alteration in energy metabolism pathways like the glyoxylate cycle (Dunn *et al.*, 2009). It has been shown for *M. oryzae* and *Colletotrichum lagenarium* that deleting key enzymes of the glyoxylate cycle can affect virulence and reduce appressorium mediated plant cuticle penetration (Wang *et al.*, 2003; Asakura *et al.*, 2012). By using acetyl-CoA produced during fatty acid β-oxidation the glyoxylate cycle allows to retrieve 4-carbon units like succinate for energy production and biosynthesis (Voet and Voet, 2004). A key enzyme of the glyoxylate cycle is the enzyme isocytrate lyase (ICL) which catalyzes the cleavage of isocitrate to succinate and glyoxylate. To mimic a defect in energy metabolism the peroxisomal isocytrate lyase gene *UMAG_04285* (*um04285*) was deleted in the *U. maydis* strain SG200 (SG200Δ04285). Virulence of SG200Δ04285 in comparison to the SG200 progenitor strain and the *scp2* deletion strain was analyzed in maize seedling infections (one mutant only).

Deletion of the peroxisomal ICL Um04285 caused a weak reduction of normal and heavy tumor development. The observed phenotype did, however, not mimic the phenotype observed for the *scp2* deletion strain (Fig. 28). The weak virulence defect of SG200Δ04285 could be complemented by integration of a *gfp-um04285* fusion gene into the *ip* locus of the deletion strain (SG200Δ04285-c) (Fig. 28).

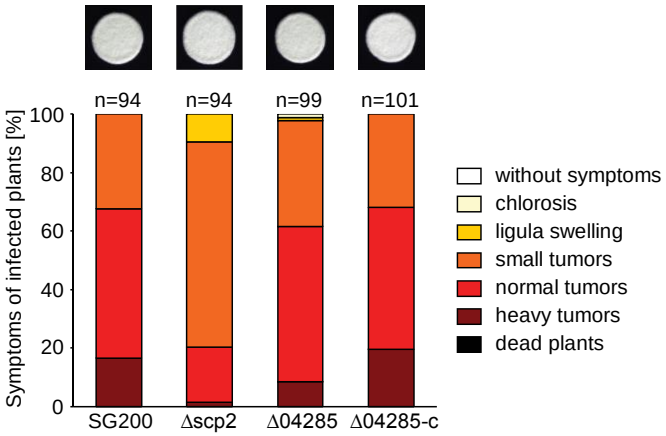

Fig. 28: Virulence of the peroxisomal ICL knock-out mutant SG200Δ04285. (A) Infection symptoms on maize seedlings infected with SG200, SG200Δscp2, the *icl* deletion strain SG200Δ04285 and the respective complementation strain SG200Δ04285-c. Infection symptoms were evaluated twelve days post infection. The respective symptom categories are depicted on the right hand side of the diagram. For the virulence assay average values of three independent infections were taken. The total number of plants (n) is indicated above each column. Filamentous growth of the respective strains on PD charcoal plates is depicted above each column.

Since the peroxisomal isocitrate lyase had only a minor effect on virulence, a double deletion mutant lacking the peroxisomal ICL Um04285 as well as the mitochondrial ICL *UMAG*_01892 (Um01892) was generated (SG200ICLΔΔ). Unfortunately, growth rates of two independent double deletion strains in liquid culture were strongly reduced. To verify the growth phenotype serial dilutions of the two mutants SG200ICLΔΔ #10 and #15 were spotted on CM-glc solid medium. Both strains displayed a strong reduction of colony size indicating a reduction of the overall growth rate (Fig. 29). On the basis of these findings, the *icl* double deletion strains were not analyzed in more detail. Since the phenotype of *icl* single and double deletions did not resemble the *scp2* deletion phenotype it seems unlikely that the penetration defect observed in the absence of Scp2 is caused by a disturbed fatty acid driven energy metabolism.

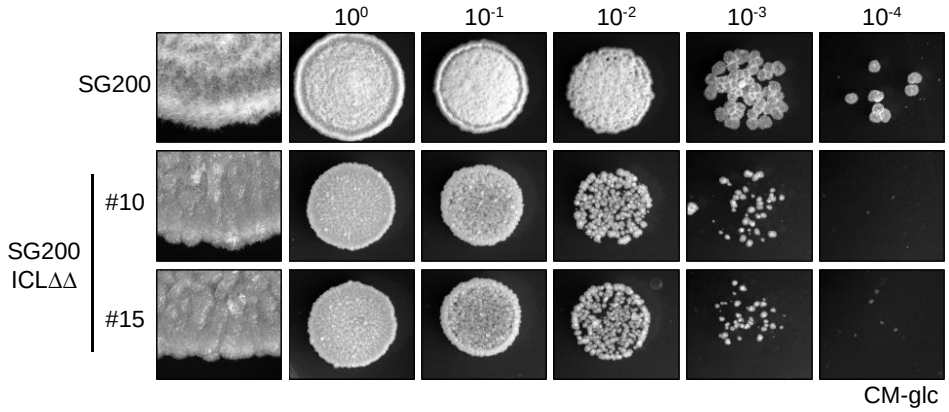

Fig. 29: **Growth phenotype of ICL double deletion strains on CM-glc plates.** Serial dilutions of SG200 and the two *icl* double deletion strains SG200ICLΔΔ #10 and #15 were spotted on CM-glc medium and incubated for 48 hours at 28 °C. A close-up picture of the10^0 dilution colony was added for the respective strains on the left hand side of the figure to show colony morphology in more detail. A dark background was used for imaging the colonies.

2.11 Peroxisome distribution is altered in filaments of *scp2* deletion strains

Colocalization studies of a GFP-Scp2 fusion protein showed that the majority of Scp2 is targeted to peroxisomes (S. Krombach, unpublished). Furthermore, qPCR data revealed an upregulation of *scp2* expression twenty hours after infection. This time point correlates with the initiation of appressorium formation and penetration on the plant surface. Based on these findings, peroxisome distribution and morphology during appressorium formation was analyzed in *scp2* deletion strains.

2.11.1 Peroxisome distribution is altered in *scp2* deletion strains when filamentation is induced on parafilm or on the leaf surface

Strains were generated expressing the peroxisomal marker protein GFP-PTS1 in addition to the appressorial AM1-marker to visualize peroxisome distribution. In contrast to the AM1-marker used previously, the appressorial marker used for this experiment consisted of a mCherry under transcriptional control of an appressorium specific promoter (Mendoza-Mendoza *et al.*, 2009). The respective construct was integrated into the *mig2* locus of SG200Pex and SG200Δscp2Pex already carrying a multiple integration of the peroxisomal maker construct *gfp-PTS1* in their *ip* locus. The resulting strains SG200AM1Pex and SG200Δscp2AM1Pex allowed the examination of peroxisomes in filaments that activated the genetic program for appressorium formation. To exclude an impact of the integrated constructs on the pathogenicity of *U. maydis* the respective strains were tested in a single round of plant infection experiments. For both strains a slight reduction of normal tumor rate was observed (Fig. 30 A). Peroxisome distribution in SG200AM1Pex and SG200Δscp2AM1Pex was first analyzed in budding cells grown in $YEPS_{light}$. Confocal laser scanning microscopy revealed no significant differences in morphology or distribution of peroxisomes between SG200AM1Pex and SG200Δscp2AM1Pex (Fig. 30 B).

SG200AM1Pex and SG200Δscp2AM1Pex were sprayed on parafilm to induce filament and appressorium formation as described in chapter 2.7. AM1-postive filaments were examined sixteen hours after spraying with respect to their peroxisome distribution using confocal microscopy. While SG200AM1Pex showed an even distribution of peroxisomes SG200Δscp2AM1Pex showed an accumulation of peroxisomes in the posterior part of the hyphal cytoplasm as well as in the hyphal tip (Fig. 31 A). In successive experiments, the percentage of filaments showing this altered distribution of peroxisomes was quantified for SG200AM1Pex and SG200Δscp2AM1Pex. Sixteen hours after induction approximately 60 % of the *scp2* mutant filaments expressing the AM1-marker displayed a misdistribution of

peroxisomes (Fig. 31 B). In contrast, only 2 % of filaments with an altered distribution of peroxisomes were detected for SG200AM1Pex (Fig. 31 B).

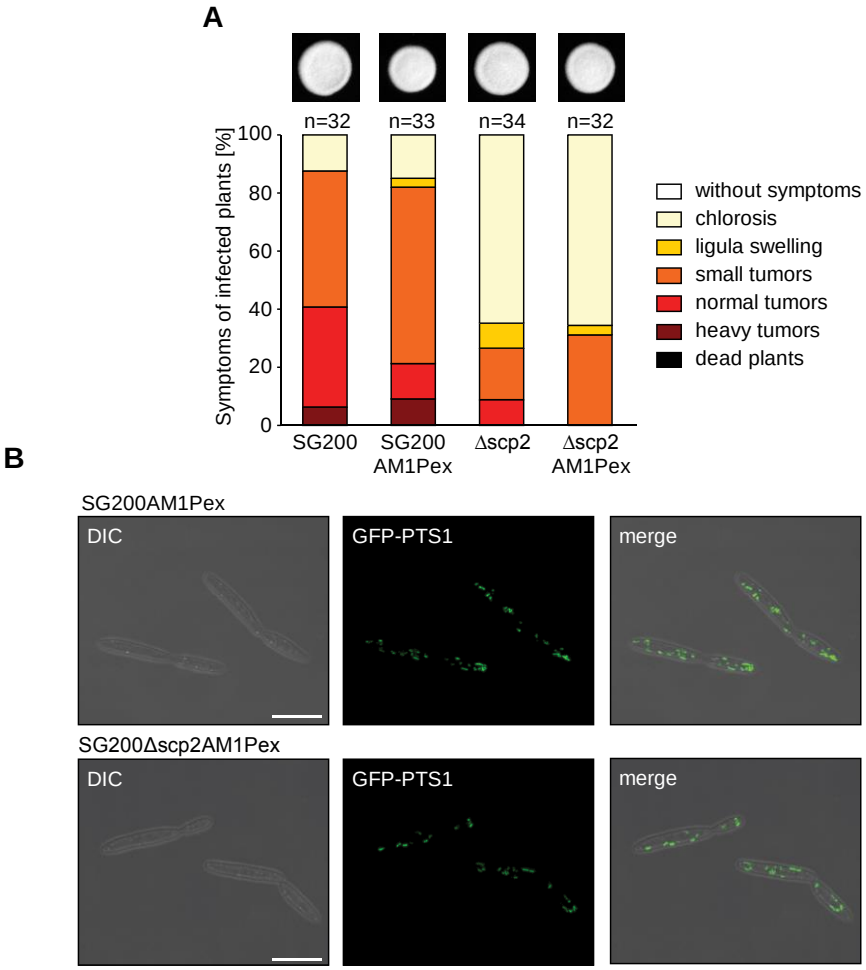

Fig. 30: Virulence of the peroxisomal marker strains SG200AM1Pex and SG200Δscp2AM1Pex. (A) Infection symptoms on maize seedlings infected with SG200, SG200AM1Pex, SG200Δscp2 and SG200Δscp2AM1Pex, respectively. Infection symptoms were evaluated twelve days post infection. The respective symptom categories are depicted on the right hand side of the diagram. For the virulence assay a single round of infections was conducted. The total number of infected plants (n) is indicated above each column. Filamentous growth of the respective strains on PD charcoal plates is depicted above each column. (B) Peroxisome distribution in saprophytically growing SG200AM1Pex and SG200Δscp2AM1Pex in liquid culture. Green fluorescence indicates localization of the peroxisomal marker protein GFP-PTS1. The scale bar equals 10 µm.

A complementation strain was generated by integrating *scp2*, fused to a nourseothricin resistance cassette, into the *ip* locus of SG200Δscp2AM1Pex (SG200Δscp2AM1Pex-c) to verify that the observed defect is caused by the *scp2* gene deletion. Since the *ip* locus of the respective strain was already occupied by the peroxisomal marker construct the integration was verified using a PCR based method targeting the open reading frame of *scp2*. Reintegration of *scp2* into SG200Δscp2AM1Pex fully complemented the aberrant peroxisomal distribution (Fig. 31 B). To determine whether the altered distribution is restricted to filaments expressing the AM1-marker the analysis was repeated in AM1-negative cells. For this, SG200AM1Pex, SG200Δscp2AM1Pex and SG200Δscp2AM1Pex-c were sprayed on parafilm without prior

HFA-treatment. On a hydrophobic surface without HFA-treatment filament formation can be observed but appressorium formation efficiency is significantly reduced (Mendoza-Mendoza *et al.*, 2009). The quantification revealed that 76 % of AM1-negative filaments displayed the altered distribution of peroxisomes in *scp2* mutants in comparison to 13 % and 11 % for SG200AM1Pex and SG200Δscp2AM1Pex-c, respectively (Fig. 31 C). These results indicate, that the altered peroxisomal distribution does not coincide with induction of the AM1-marker.

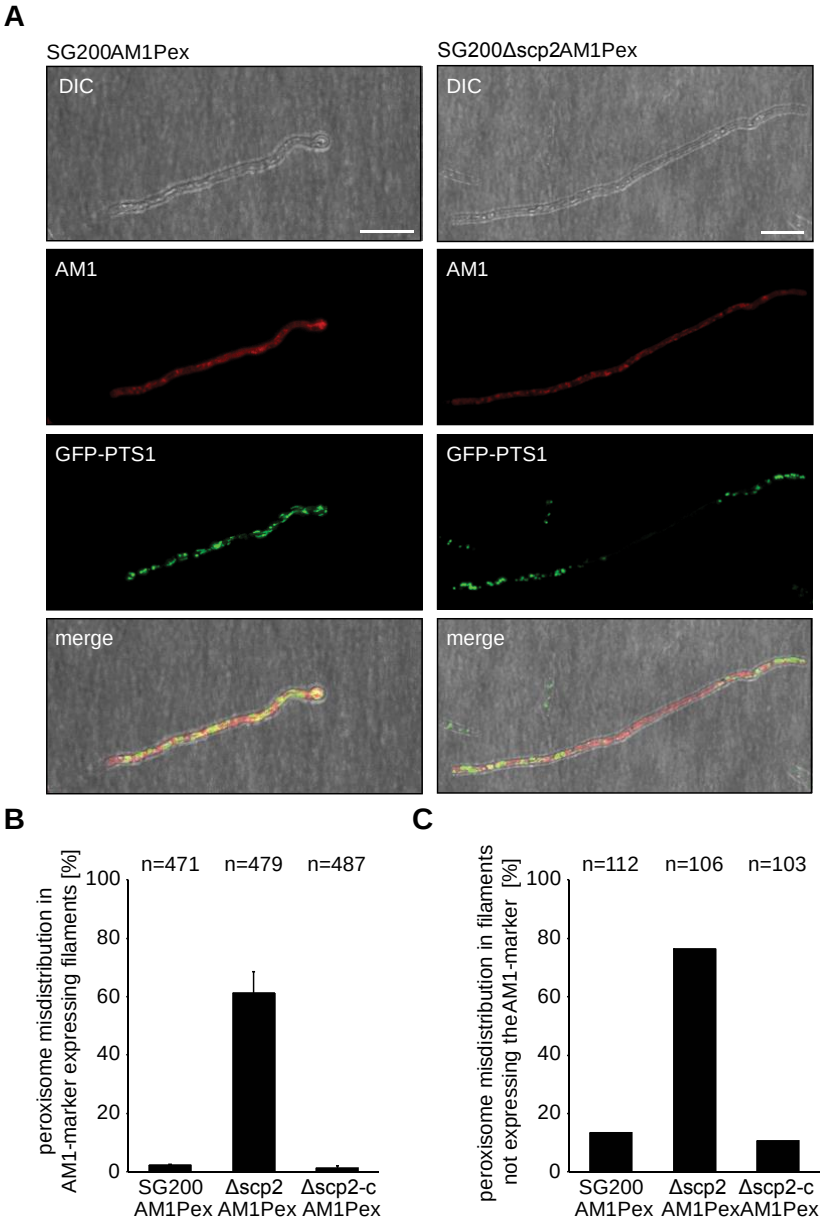

Fig. 31: Distribution of peroxisomes in SG200AM1Pex and SG200Δscp2AM1Pex growing on parafilm. (A) Confocal microscopy of the peroxisomal distribution in SG200AM1Pex and SG200Δscp2AM1Pex on parafilm sixteen hours after spraying. Filament and appressorium formation was induced as described in chapter 2.7. Red fluorescence shows expression of the appressorial AM1-marker. Green fluorescence shows localization of the peroxisomal marker protein GFP-PTS1. All pictures are maximum projections generated from confocal Z-stacks. Scale bars equal 10 µm. (B) Distribution of peroxisomes in filaments expressing the AM1-marker. The percentage of all AM1-positive filaments with a misdistribution of peroxisomes was determined. Average values of three independent replicates are shown. Error bars indicate the ± standard deviation. (C) Quantification of peroxisomal misdistribution in filaments, which are not expressing the AM1-marker on parafilm. Only one replicate was performed. The total number (n) of analyzed filaments is indicated above each column.

To quantify the altered distribution of peroxisomes in SG200AM1Pex and SG200Δscp2AM1Pex filaments on parafilm fluorescence intensity plots of 15 AM1-positive filaments were generated by measuring the fluorescence intensity of the peroxisomal marker protein GFP-PTS1 over the entire length of the tip compartment. Fig. 32 shows the results in a bar diagram, whereby the fluorescence intensity of peroxisomes and the filament length have been normalized to allow direct comparison between tip compartments of variable length.

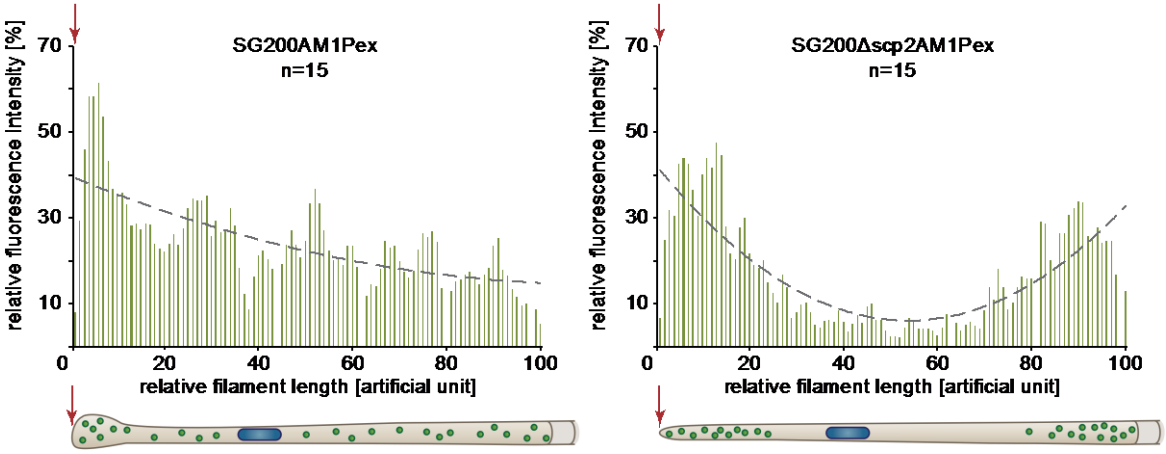

Fig. 32: Visualization of peroxisome distribution in SG200AM1Pex and SG200Δscp2AM1Pex filaments using signal intensity plots. Filament and appressorium formation was induced as described in chapter 2.7. Sixteen hours after induction Z-stacks imaging the GFP-PTS1 fluorescence were taken in AM1-marker expressing filaments and transformed into maximum projections (Leica software). ImageJ was used to plot intensity values along a line that was drawn from the last septum to the tip of the cytoplasm filled tip compartment. The fluorescence intensity measured for GFP-PTS1 in each filament was normalized to values ranging from 0 -100 %. The length of all filaments was normalized to values ranging from 1 to 100 (artificial units). For each of the 100 sections along the length of the filament the average fluorescence intensity was plotted. Bar graphs were generated using average values of 15 filaments per strain. Polynomial trend lines were added to illustrate the tendency of peroxisomal distribution throughout the filament. The total number of analyzed filaments (n) is depicted above each graph. A schematic distribution of peroxisomes within the hyphae is illustrated below each graph. Red arrows indicate the hyphal tip.

These diagrams emphasize the low number of peroxisomes in the middle part of SG200Δscp2AM1Pex filaments and the accumulation at the tip and in proximity to the septum of the hyphal tip compartment. In SG200AM1Pex, a rather even distribution of peroxisomes was observed with an increase of intensity at the hyphal tip.

Peroxisomal distribution in SG200AM1Pex and SG200Δscp2AM1Pex was further analyzed in filaments on the maize leaf surface to exclude that the peroxisomal misdistribution is an *in vitro* artefact. For this, maize seedlings were infected with the respective strains and peroxisome distribution was analyzed sixteen hours after infection using confocal microscopy. While peroxisomes in SG200AM1Pex filaments were mostly scattered throughout the cell, a high frequency of SG200Δscp2AM1Pex filaments displayed the unusual distribution of peroxisomes that was already observed on parafilm (Fig. 33). These experiments confirmed that the

peroxisomal distribution defect does not only occur on parafilm and thus might play a crucial role during plant infection.

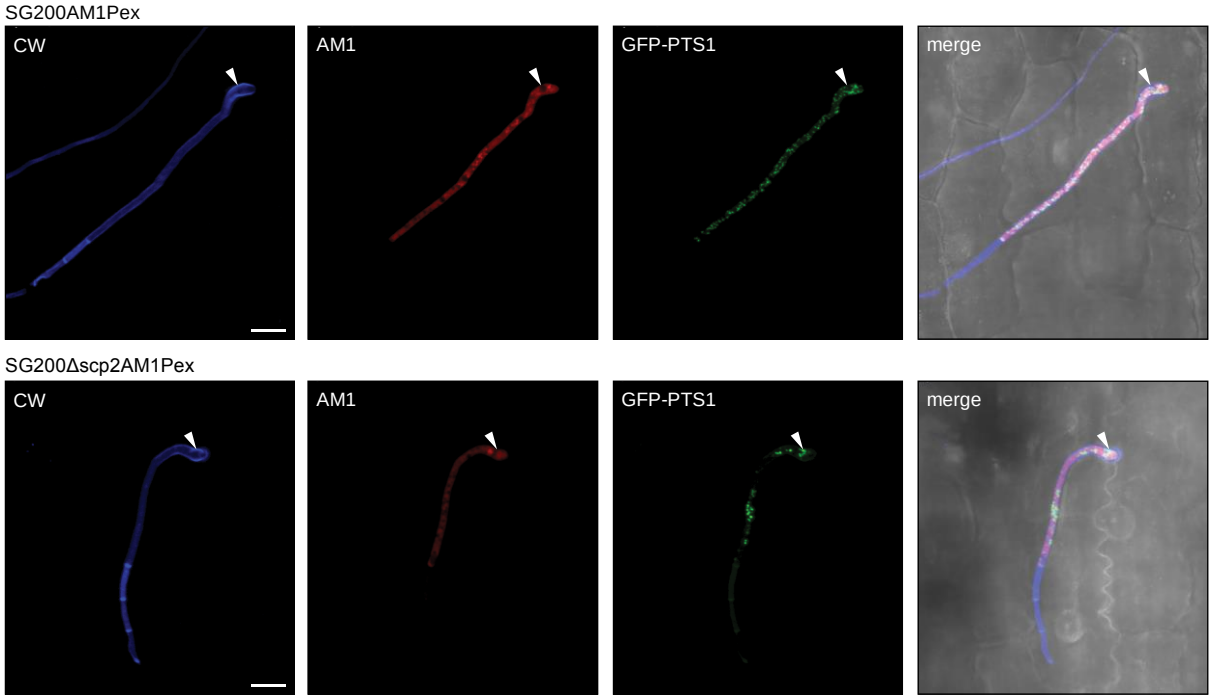

Fig. 33: Visualization of the peroxisomal misdistribution in SG200AM1Pex and SG200Δscp2AM1Pex on the plant surface. (A) Confocal microscopy of peroxisome distribution in SG200AM1Pex and SG200Δscp2AM1Pex filaments on the leaf surface. Seven day old maize seedlings were infected with the indicated strains. Sixteen hours after infection leaves were stained with calcofluor white (CW) to visualize cells on the leaf surface. Red fluorescence indicates expression of the appressorial marker (AM1) while green fluorescence indicates the localization of the peroxisomal marker protein GFP-PTS1. Appressoria are marked with white arrowheads. Scale bars equal 10 µm.

2.11.2 The peroxisomal misdistribution is not visible in *b* induced filaments

To elucidate whether the induction of filamentation or the contact to HFAs causes the altered peroxisome distribution, peroxisomes were analyzed in *b*-filaments of SG200AM1Pex and SG200Δscp2AM1Pex in liquid culture. Filament formation can be induced by incubation of exponentially growing cells in 2 % $YEPS_{light}$ supplemented with 500 µM HFAs for at least six hours. Confocal microscopy of SG200AM1Pex and SG200Δscp2AM1Pex revealed that shifting the strains to filaments by using HFAs did not induce the misdistribution of peroxisomes that was observed on parafilm or on the plant surface (Fig. 34).

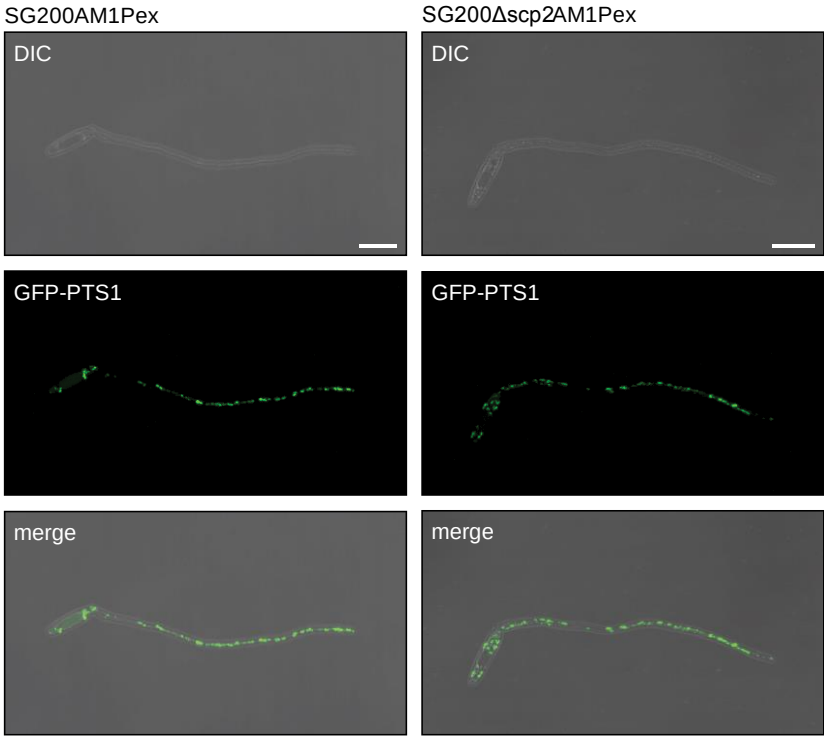

Fig. 34: Peroxisome distribution in SG200AM1Pex and SG200Δscp2AM1Pex filaments induced by HFA treatment. Filament formation was induced by shifting exponentially growing sporidia from complete medium to 2% $YEPS_{light}$ supplemented with 500 µM HFAs. Peroxisome distribution in filaments was analyzed after overnight incubation at 28 °C using confocal microscopy. Confocal Z-stacks were taken for each filament and illustrated as maximum projections. Scale bars equal 10 µm.

Peroxisome distribution was also analyzed in *b*-filaments of the *U. maydis* strain AB33. In this strain *b*-filament formation can be induced by shifting saprophytically growing cells from ammonium-containing medium to nitrate minimal medium. The *bE1* and *bW2* genes of AB33 are controlled by the nitrate inducible *nar* promoter allowing the transition from saprophytic to filamentous growth in liquid culture (Brachmann *et al.*, 2001). For the microscopic analysis of peroxisomes the peroxisomal marker construct *gfp-PTS1* was integrated into the *ip* locus of AB33 and AB33Δscp2 (AB33Pex and AB33Δscp2Pex). Analysis of saprophytically growing AB33Pex and AB33Δscp2Pex strains in $YEPS_{light}$ medium revealed no differences in peroxisome distribution between the two strains (Fig. 35 A). To evaluate the distribution of peroxisomes in AB33 hyphae, *b*-filament formation was induced by transferring exponentially growing cell cultures to nitrate-minimal medium for six hours. A microscopic analysis revealed that the induction of *b*-dependent filaments did not induce a misdistribution of peroxisomes in the analyzed strains (Fig. 35 B).

Taken together, these experiments confirm that the altered distribution of peroxisomes is not triggered by treatment with HFA or by activation of the *b*-cascade.

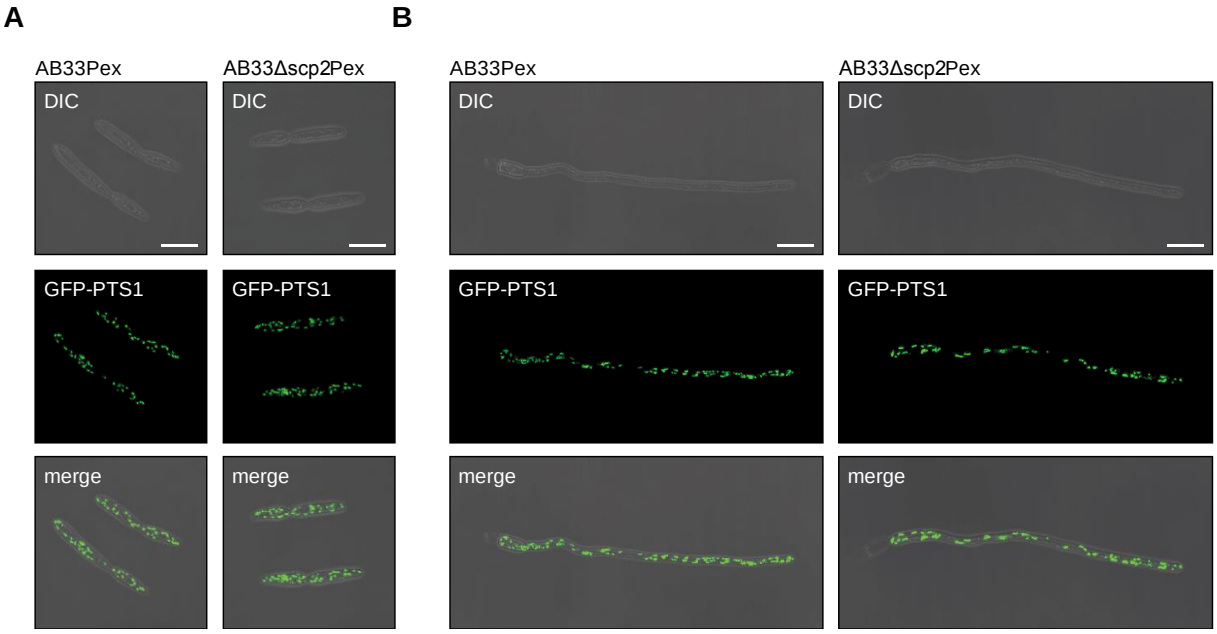

Fig. 35: Peroxisome distribution in AB33Pex and AB33Δscp2Pex sporidia and filaments in liquid culture. Peroxisome distribution of exponentially growing sporidia and *b*-induced filaments was analyzed using confocal microscopy. Z-stacks were taken for each cell and depicted as maximum projections. (A) Peroxisome distribution in exponentially growing sporidia. (B) Peroxisome distribution in AB33Pex and AB33Δscp2Pex filaments. Filament formation was induced by shifting exponentially growing sporidia from ammonium-containing medium to nitrogen-minimal medium. Forming filaments were analyzed after 6 hours of incubation at 28 °C. Scale bars equal 10 µm.

2.12 Lipid droplet distribution is altered in *scp2* deletion strains

Apart from their impact on peroxisomes it is known that sterol carrier 2 proteins also modulate the protein and lipid composition of lipid droplets (Atshaves *et al.*, 2001). Lipid droplets are dynamic organelles which are not exclusively involved in free fatty acid storage but have been shown to provide substrates for energy metabolism, membrane synthesis and for the production of several lipid-derived signaling molecules (Pol *et al.*, 2014). More importantly, in different pathogenic fungi like *M. oryzae* and *C. orbiculare* lipid droplets have been shown to be essential for appressorium formation and appressorium mediated cuticle penetration (Wang *et al.*, 2003; Asakura *et al.*, 2012). Based on this, lipid droplet distribution and morphology was analyzed in SG200AM1 and SG200Δscp2AM1 filaments on parafilm. SG200AM1 and SG200Δscp2AM1 filaments were induced as described in chapter 2.7 and intracellular lipid droplets were stained using the lipophilic dye nile red. Nile red is a benzophenoxazine dye which is almost non-fluorescent in water but is strongly fluorescent in the presence of a hydrophobic environment (Greenspan *et al.*, 1985). Confocal microscopy of SG200AM1 revealed a strong accumulation of lipid droplets in the posterior part of the filament cytoplasm. While the central part of the hyphae showed only few lipid droplets, several intermediate sized lipid droplets accumulated in the forming appressorium (Fig. 36). In SG200Δscp2AM1 the lipid depot in the posterior part

of the filament was comparable to the one observed in SG200AM1. In contrast to that, abundance of lipid droplets in SG200Δscp2AM1 decreased towards the tip of the filament and lipid droplets of a considerable size only rarely migrated into the hyphal tip (Fig. 36).

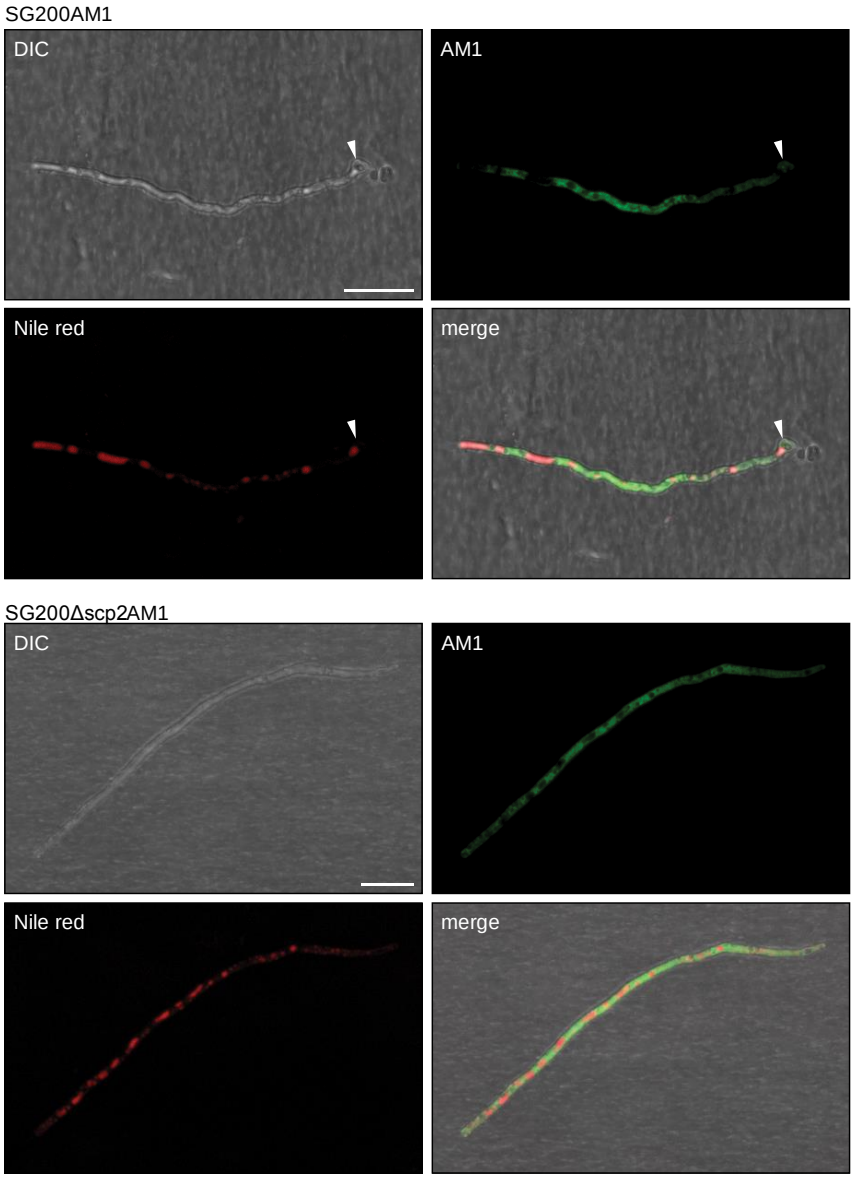

Fig. 36: Visualization of lipid droplet distribution in SG200AM1 and SG200Δscp2AM1 filaments growing on parafilm. Filament and appressorium formation was induced as described in chapter 2.7. Lipid droplets were visualized with nile red. Confocal microscopy of the lipid droplet distribution in SG200AM1 and SG200Δscp2AM1 filaments growing on parafilm was performed sixteen hours after spraying. Green fluorescence shows expression of the AM1-marker. Red fluorescence shows localization of nile red stained lipid droplets. All pictures are maximum projections generated from confocal Z-stacks. Scale bars equal 10 µm.

To quantify the altered distribution of lipid droplets in SG200AM1 and SG200Δscp2AM1 filaments growing on parafilm, fluorescence intensity plots of 15 AM1-positive filaments were generated by measuring the fluorescence intensity of the lipid droplet stain nile red over the entire length of the tip compartment. Fig. 37 shows the results in a bar diagram whereby the fluorescence intensity and the filament length have been normalized to allow direct comparison

of different filaments of variable length. The graph emphasized the accumulation of lipid droplets in the most posterior and anterior parts of the SG200AM1 filaments. In contrast, lipid droplet intensity plots of SG200Δscp2AM1 illustrate the decreasing amount of lipid droplets towards the tip of the filaments (Fig. 37).

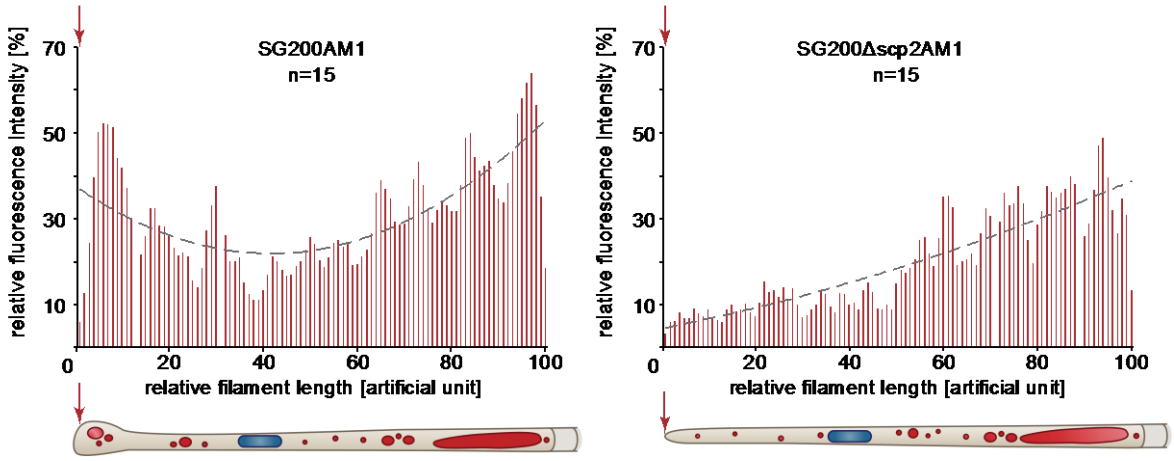

Fig. 37: Visualization of lipid droplet distribution in SG200AM1 and SG200Δscp2AM1 filaments using signal intensity plots. Filament and appressorium formation was induced as described in chapter 2.7. Sixteen hours after induction, Z-stacks of nile red fluorescence were taken in AM1-marker expressing filaments and transformed into maximum projections (Leica software). ImageJ was used to plot intensity values along a line that was drawn from the septum to the tip of the cytoplasm filled tip compartment. The fluorescence intensity measured for nile red in each filament was normalized to values ranging from 0 -100 %. The length of all filaments was normalized to values ranging from 1 to 100 (artificial units). For each of the 100 sections along the length of the filament the average fluorescence intensity was plotted. Bar graphs were generated using average values of 15 filaments per strain. Polynomial trend lines were added to illustrate the tendency of lipid droplet distribution throughout the filament. The total number of analyzed filaments (n) is depicted above each graph. A schematic distribution of peroxisomes within hyphae is illustrated below each graph. Red arrows indicate the hyphal tip.

2.13 Distribution of early endosomes in *scp2* deletion strains is not altered

Peroxisomes and lipid droplets are known to transiently bind to early endosomes and thus to "hitchhike" along the cytoskeleton of the cell (Guimaraes *et al.*, 2015). Defects in early endosome movement can cause the accumulation of these organelles at the hyphal tip (Salogiannis *et al.*, 2016). To exclude that the altered distribution of peroxisomes and lipid droplets observed in *scp2* deletion strains is caused by an alteration of early endosome movement, early endosome motility was analyzed in *scp2* deletion strains. Strains were generated that simultaneously expressed the peroxisomal marker GFP-PTS1 and the early endosome marker mCherry-Rab5a (EE), to visualize peroxisomes and early endosomes (SG200PexEE and SG200Δscp2PexEE). Rab5a is small endosomal GTPase which has been shown to localize to early endosomes in *U. maydis* (Schuster *et al.*, 2011). As expected, no difference of early endosome distribution or movement was observed in exponentially growing SG200PexEE or SG200Δscp2PexEE sporidia (Fig. 38 A). Filament and appressorium formation of SG200PexEE and SG200Δscp2PexEE on parafilm was induced as described in

chapter 2.7. Fluorescence microscopy of SG200PexEE peroxisomes and the highly motile early endosomes showed that both organelles were distributed evenly throughout the hyphae (Fig. 38 B). Likewise, analysis of SG200Δscp2PexEE filaments that displayed an altered distribution of peroxisomes did not reveal any differences in early endosome localization or movement when compared to SG200PexEE (Fig. 38 B). These results suggest that the altered distribution of peroxisomes and lipid droplets is not caused by a defect of early endosome motility or distribution.

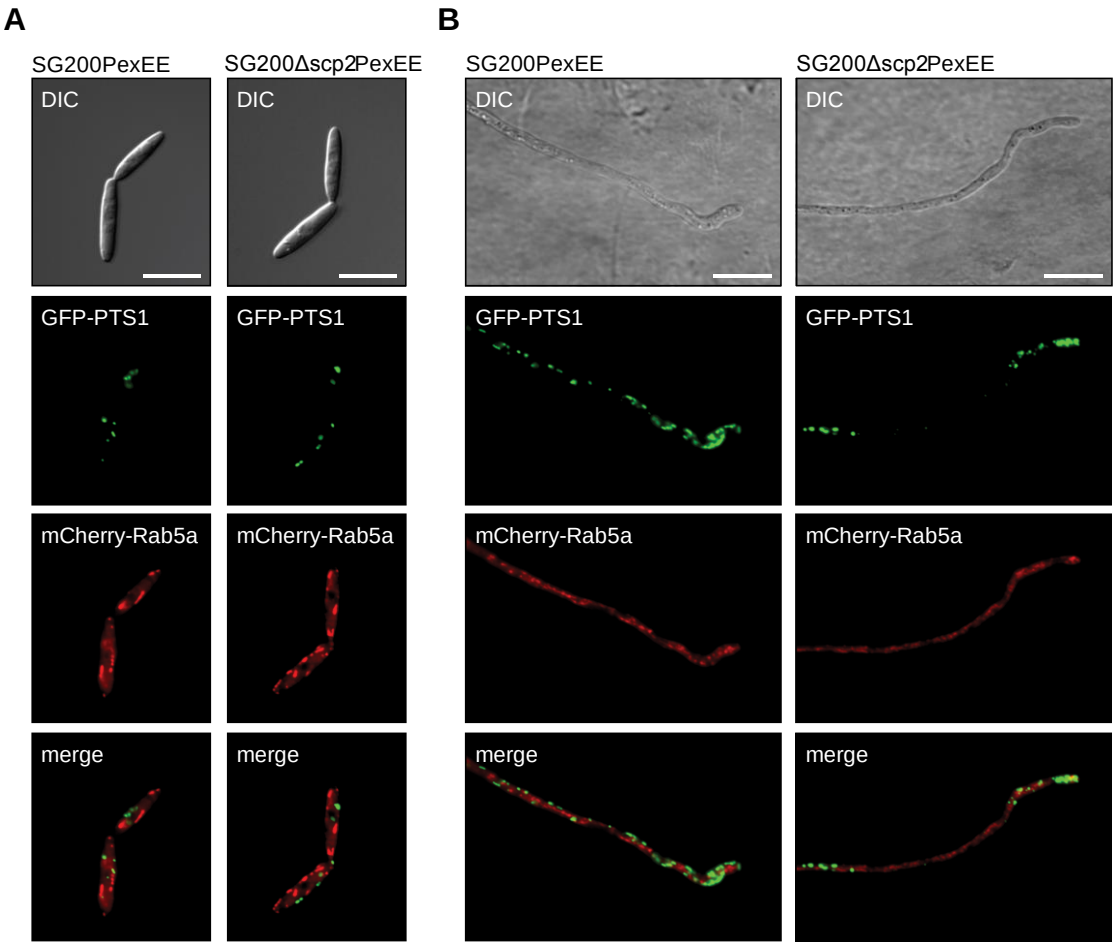

Fig. 38: Peroxisome and early endosome distribution in SG200PexEE and SG200Δscp2PexEE. (A) Distribution of peroxisomes and early endosomes in saprophytically growing sporidia. Exponentially growing cell cultures of the respective strains were analyzed using fluorescence microscopy. Green fluorescence displays the localization of the peroxisomal marker protein GFP-PTS1. Red fluorescence displays the localization of the early endosome marker protein mCherry-Rab5a. The merge channel shows colocalization of peroxisomes and early endosomes. (B) Distribution of peroxisomes and early endosomes in filaments growing on parafilm. Filament and appressorium formation was induced as described in chapter 2.7. Scale bars equal 10 µm.

3. Discussion

Sterol carrier proteins are highly conserved throughout all domains of life. Their major task seems to be the intracellular binding and distribution of different lipid species between membranes and organelles. Dependent on the individual organism the functions of sterol carrier proteins can vary to meet the requirements of the distinct life styles. In the present work the peroxisomal *U. maydis* protein Scp2 was characterized and determined to be a pathogenicity factor with an important role during host plant infection. While saprophytically growing sporidia were found to be independent of Scp2 function, the protein seemed to be important upon appressorium formation and host plant penetration. Low amounts of a Strep-HA-Scp2 fusion protein were found to reach the cell exterior by an unconventional secretion mechanism but no biological relevant function could be attributed to extracellular Scp2. Further experiments link Scp2 with the distribution of peroxisomes in *U. maydis* filaments during pathogenic development. In the following chapters the phenotypes of *U. maydis scp2* deletion strains will be discussed with respect to the potential biological function of Scp2.

3.1 Low amounts of Scp2 are secreted via an unconventional mechanism

Unconventional secretion of proteins has been observed in various organisms and was established as an important eukaryotic secretion mechanism besides the classical secretory pathway. A multitude of unconventionally secreted proteins has been described in the past years (Rabouille *et al.*, 2012). In the ascomycete fungus *Magnaporthe oryzae* it has been shown that effector proteins that target the plant cytoplasm undergo SP-mediated translocation into the ER but subsequently circumvent the Golgi-apparatus following a nonconventional secretion pathway. These unconventionally secreted effectors accumulate in the plant-derived biotrophic interfacial complex (BIC) before entering the plant host cell (Giraldo *et al.*, 2013). *Neurospora crassa* chitin synthases (CHS) have been shown to be exported independently of the ER-Golgi system by microvesicles that are insensitive to the treatment with BFA, a drug that inhibits the classical secretory pathway. Unconventional secretion of the *U. maydis* endochitinase Cts1 has been shown to depend on the endosome-mediated transport of its mRNA along microtubules (Stock *et al.*, 2012). Subsequent secretion of Cts1 was suggested to be mediated by multivesicular bodies that fuse with the plasma membrane and release the enclosed intracellular vesicles into the extracellular space (Shoji *et al.*, 2014). Furthermore, the two isochorismatases PsIsc1 and VdIsc1 from *P. sojae* and *V. dahlia*, which seem to target the host plant cytoplasm

and are required for full virulence, are exported via an undefined unconventional secretion mechanism (Liu *et al.*, 2014).

These examples emphasize that a significant proportion of yet uncharacterized fungal effectors might be secreted by non-classical secretion mechanisms.

Consistent with earlier studies (S. Krombach, unpublished) CSAs showed that a Strep-HA-Scp2 fusion protein can be unconventionally secreted in low amounts by *U. maydis* filaments. Beyond that, the present study addressed new aspects of Strep-HA-Scp2 secretion. An important observation in the performed CSAs was that the cytoplasmic version of Scp2 (Strep-HA-Scp2$_{cyt}$) is not as efficiently exported as the peroxisomal Scp2 (Strep-HA-Scp2). Moreover, previous experiments showed that cytoplasmic Strep-HA-Scp2$_{cyt}$ cannot complement the virulence phenotype of *scp2* deletion mutants (S. Krombach, unpublished). Therefore, peroxisomal targeting seems to be required for the unconventional secretion of Scp2. The reason why more peroxisomal Strep-HA-Scp2 is secreted remains unclear, but the binding to a peroxisome derived ligand could mediate changes in conformation, charge or hydrophobicity that allows the protein to traverse the fungal plasma membrane with a higher efficiency. This potential ligand might not or only rarely be present in the cytosol which in turn could lead to a less efficient secretion of Scp2 when it is forced to remain in the cytosolic compartment. Taken together, peroxisomal targeting seems to be important for efficient Scp2 secretion and Scp2 function is disturbed when peroxisomal localization is hindered.

Importantly, no secretion of peroxisomal localized GFP (Strep-HA-GFP$_{pex}$) could be observed in CSAs, suggesting that unique Scp2 characteristics like ligand binding properties or its conformation allow the protein to be externalized. These experiments prove that peroxisomal localization *per se* is not sufficient for unconventional protein secretion.

Externalization of Scp2 could be demonstrated but the mode of secretion remains unclear. Proteomic data from *U. maydis* exosomes suggests that Scp2 might reach the cell exterior via extracellular vesicles (EVs) which are released from *U. maydis* filaments (S. Uszkoreit and L. Lo Presti, personal communication). EVs represent an important mechanisms of intercellular communication by transporting proteins, lipids and RNA (Raposo and Stoorvogel, 2013). Furthermore, EVs have been shown to mediate the delivery of virulence factors to host cells in filamentous fungi (Silva *et al.*, 2014). Interestingly, the Scp2 peptide detected in exosome fractions vanished when the vesicles were pre-treated with trypsin indicating that Scp2 adheres to the outside of exosomes (S. Uszkoreit and L. Lo Presti, personal communication). An exosome-based secretion mechanism has been shown for the unconventional secreted tissue transglutaminase (tTG). The mammalian cytoplasmic tTG is recruited to perinuclear recycling

endosomes by binding to phosphoinositide and is subsequently internalized and transported to the plasma membrane (Zemskov *et al.*, 2011).

The remaining question is whether Scp2 is actively secreted by *U. maydis* filaments because of an extracellular function, whether secretion occurs passively due to its lipid binding or biochemical properties or whether the unconventional secretion of Scp2 is part of a default turnover mechanism for cellular components.

3.2 Is there a biologically relevant function of the extracellular form of Scp2?

In previous experiments it was shown that an Scp2 protein which lacks the peroxisomal targeting sequence and is externalized via the conventional secretory pathway by fusing it to the signal peptide of the secreted effector Stp1 (Schipper, 2009) did not complement the *scp2* deletion phenotype in plant infection experiments (S. Krombach, unpublished). Since it was hypothesized that the C-terminus of Scp2 might contribute to lipid binding and function of Scp2 (García *et al.*, 2000), the original construct was modified in a way that the peroxisomal targeting sequence of Scp2 was kept intact but was concealed by the addition of three amino acid residues. The expression of this conventionally secreted form of Scp2 (SP-Scp2-GSA), however, did also not rescue the *scp2* deletion phenotype during plant infections. In conclusion, two independent attempts to secrete Scp2 via the conventional secretory pathway failed to yield strains in which the virulence phenotype of the *scp2* deletion mutant was at least partially complemented.

This leaves several interpretations: First, Scp2 may have no biological function in the extracellular space and secretion might be an effect of passive diffusion due to the biochemical and physiological properties of Scp2 rather than to active secretion. Further, the transition through the ER-Golgi system might render Scp2 fusion proteins nonfunctional. For the unconventionally secreted fibroblast growth factor FGF2 was shown that its secretion through the ER-Golgi network was successful but the externalization via this pathway led to an artificial O-glycosylation resulting in a non-functional protein (Wegehingel *et al.*, 2008). These observations led Wegehingel *et al*. (2008) to propose that unconventional secretion might be an ancient mechanism that allows secretion of proteins for which the secretion via the classical secretory pathway is fatal for protein function.

Moreover, as mentioned in chapter 3.1 it might be crucial for cytoplasmically produced Scp2 to bind a certain pathogenicity related ligand within or in close proximity to the peroxisome which is subsequently externalized by Scp2. Therefore, the inability of SP-Scp2-GSA to

complement the *scp2* deletion phenotype could be attributed to a missing Scp2-bound ligand rather than to posttranslational modifications within the secretory pathway.

Another aspect of SP-mediated secretion is that the targeting to the secretory pathway causes secretion of the respective proteins once the mRNA is made. Unconventional secretion systems, by contrast, are often tightly regulated and many unconventional secretion pathways are only activated upon certain triggers as it has been shown for the *Pichia pastoris* Acb1 and the mammalian GAPDH (Manjithaya *et al.*, 2010; Takenouchi *et al.*, 2015). Furthermore, SP-mediated secretion of Scp2 led to large amounts of extracellular protein whereas protein levels of unconventionally secreted Scp2 were comparatively low. Both scenarios might interfere with the potential function of Scp2 in the extracellular space.

Another reason for the lack of complementation could be that Scp2 belongs to the group of moonlighting proteins that do not only exhibit an extracellular function but which are also crucial for processes within the cell as it was shown for the unconventional secreted protein enolase (Karkowska-Kuleta and Kozik, 2014). Several moonlighting proteins are housekeeping enzymes that do not contain a classical secretion signal. Nonetheless, in several pathogens, including fungi, these proteins are able to reach the extracellular space via unconventional secretion mechanisms where they have been shown to fulfill critical roles in the interaction with the extracellular matrix or in the evasion of the host immune system (Karkowska-Kuleta and Kozik, 2014).

Taken together, the combined results from the present and previous studies (S. Krombach, unpublished) indicate that the conventional secretion of Scp2 renders the protein non-functional and that the protein must access peroxisomes to fulfill its virulence related function.

3.3 Deletion of *scp2* causes an appressorium defect

U. maydis forms non-melanized appressoria on the leaf surface that mediate the entry into the plant tissue. In contrast to *Magnaporthe oryzae* and *Colletotrichum* spp. that invade the host plant through melanized appressoria and mechanical force, appressoria of *U. maydis* seem to penetrate the plant cuticle by locally secreting plant cell wall degrading enzymes (Tucker and Talbot, 2001; Schirawski *et al.*, 2005). Several steps are important for successful appressoria formation and penetration. First, the pathogen needs to locate and perceive the host surface by detecting extracellular signals. These signals are transmitted to intracellular signaling cascades which initialize the reorganization of the fungal cytoskeleton thus allowing the formation of appressoria and the redirection of growth towards the plant surface prior to penetration (Tucker and Talbot, 2001; Patkar *et al.*, 2010). During this process the fungal appressorium has to

adhere tightly to the host surface to allow appressorium mediated entry into the host plant tissue (Tucker and Talbot, 2001). In *U. maydis*, appressorium formation can be induced *in vitro* by providing hydroxy-fatty acids and a hydrophobic surface as stimulus (Mendoza-Mendoza *et al.*, 2009).

A qPCR approach revealed an upregulation of *scp2* during appressorium formation and penetration at around 20 hours after maize seedling infection. Microscopic analysis showed that filaments of *scp2* deletion strains express the appressorial marker *am1* on parafilm and on the leaf surface suggesting that the genetic program for appressorium formation has been initiated. However, *scp2* deletion strains showed a significantly lower amount of appressoria on parafilm when compared to the respective progenitor strain sixteen hours after appressorium induction. This defect could not be attributed to a delayed appressorium initiation since 24 hours after induction no enhanced appressorium formation frequency was observed in the mutant. An impaired sensing of external fatty acid stimuli was excluded by demonstrating the induction of filament formation in liquid culture using HFA. Interestingly, the appressorial defect observed on parafilm was not apparent on the plant surface where appressoria could be frequently detected for *scp2* deletion strains.

The appressorium formation defect of *scp2* mutants on parafilm coincided with an extension of the cytoplasm-filled part of the filaments. Compared to wild type hyphae in which the cytoplasm filled tip compartment had an average length of 54.0 µm (± 9.6) the tip compartments of *scp2* mutants had an average length of 89.6 µm (± 8.0). This extension occurred without the additional integration of septa causing the formation of elongated hyphae and coincided with a higher mortality rate of filaments on parafilm when compared to the progenitor strain.

During the elongation process several filaments appeared to attempt the formation of appressoria by forming a crook-like structure but failed to form an appressorium and continued hyphal growth. In *M. oryzae*, the loss of the polarized growth regulator Tea4 has been shown to cause a zigzag morphology in aerial hyphae and defects in appressoria formation on inductive surfaces while vegetative growth was mostly unaffected (Patkar *et al.*, 2010). In contrast to the phenotype observed for the polarized growth mutants in *M. oryzae*, however, *U. maydis scp2* deletion strains are able to form appressoria on the maize leaf surface and to penetrate the host plant cuticle to a certain extent. Considering this, it seems unlikely that the observed *scp2* appressorium formation phenotype is caused by a defect in polarized growth of forming filaments.

This might indicate that *scp2* deletion strains are not impaired in polarized growth of filaments and are capable to initiate appressoria but that these appressoria are not firmly attached to the

hydrophobic parafilm. Such an effect could be caused by a reduction of filament hydrophobicity. A general reduction of hydrophobicity in *scp2* deletion mutant filaments, however, seems unlikely. First, the parafilm slides used for the analysis of appressoria were washed in water prior to microscopic examination. In case of a less effective overall attachment washing would have caused a significant loss of filaments. Further, the hydrophobicity of *scp2* deletion strain filaments was not significantly reduced. This was demonstrated by a water soaking assay (Müller *et al.*, 2008). For this, water drops were spotted on filamentous growing SG200 and *scp2* deletion strains on PD-charcoal solid medium and the time until the water drop was fully absorbed by the colony was measured as an indication for the surface hydrophobicity of the respective strains. No difference of hydrophobicity was observed for SG200 and SG200Δscp2 (not shown).

Furthermore, the secretion of glycolipids such as mannosylerythritol lipids (MELs) leads to a reduced surface tension of *U. maydis* culture medium (Hewald, 2005). The biosynthesis of MELs takes partially place in peroxisomes and is coupled to peroxisomal fatty acid degradation (Freitag *et al.*, 2014). The surface tension of liquid medium incubated with the *U. maydis* strains MB215 and MB215Δscp2, however, showed that both strains are able to reduce the surface tension of the medium to a comparable extent (not shown) indicating that Scp2 is not involved in MEL production.

Adhesion of lily pollen tubes has been shown to depend on a lipid transfer-like protein (nsLTP), a class of extracellular cystein-rich proteins with a broad affinity for various lipids (Park *et al.*, 2000). In this system the secreted nsLTP either mediate adhesion of the pollen tube directly or act indirectly as a transporter of lipophilic compounds involved in signaling (Park *et al.*, 2000). Even though sterol carrier proteins like Scp2 do not share specific motifs of lipid transfer proteins both protein classes contain a hydrophobic cavity that allows the unspecific transport of different lipid species (De Berti *et al.*, 2013; Liu *et al.*, 2015). Interestingly, several fungal species produce an extracellular matrix (ECM) presumably consisting of glycoproteins, polysaccharides and lipids which promote appressorial adhesion (Tucker and Talbot, 2001; Ahn *et al.*, 2004). This might indicate that components of the fungal ECM depend on nsLTP or sterol carrier protein mediated transport. With respect to this, the *U. maydis* Scp2 protein could be involved in the generation, transport or secretion of compounds that help the forming appressorium to effectively attach to the parafilm surface. On the maize leaf surface, however, additional factors like topography and structure or the presence of plant derived cuticle waxes and fatty acids could help to overcome the appressorium formation defect.

3.3.1 Scp2 is required for efficient penetration of the host plant surface

A question arising from the observed appressorium formation defect on parafilm was whether the presence of appressoria on planta necessarily correlates with appressorium functionality. This question was addressed by the quantification of penetration efficiency which showed that appressoria of *scp2* deletion strains are less efficient in successful invasion of the epidermal layer of the leaf than wild type appressoria. The penetration defect indicates that although appressoria formation is restored on the plant surface *scp2* deletion strain appressoria are less efficient in breaching the plant cuticle. This data was supported by the quantification of fungal biomass which revealed that *scp2* deletion strains accumulate significantly less biomass within the maize plant when compared to the SG200 progenitor strain.

A phenotype similar to that of *scp2* deletion strains was observed for mutants of the plasma membrane spanning protein Sho1 and the transmembrane mucin Msb2. Both proteins are involved in the perception of surface signals and the induction of the MAP-kinase cascade that induces pathogenic development in *U. maydis* (Lanver *et al.*, 2010). Single gene deletions of *sho1* and *msb2* caused a strong reduction of appressorium formation on parafilm. Interestingly, this defect was partially compensated on the plant surface. In contrast to *scp2* deletion strains, however, *sho1* and *msb2* did not express the appressorial marker on parafilm indicating that Scp2 either functions downstream of the signaling cascade which triggers appressorium induction or is involved in a separate pathway.

3.4 *Scp2* deletion strains show a misdistribution of peroxisomes and lipid droplets

Peroxisomes and lipid droplets are independent organelles but seem to be functionally and physically associated (Shai *et al.*, 2016). In yeast it has been demonstrated that peroxisomes can stably adhere to lipid droplets. The two organelles can undergo hemifusion by so-called pexopodia which bring lipids and fatty acids in contact with the peroxisomal fatty acid oxidation machinery (Binns *et al.*, 2006). *In vitro* induced filaments of *scp2* deletion strains displayed an unusual distribution of peroxisomes and lipid droplets. In around 60 % of the hyphae growing on parafilm, peroxisomes accumulated in the posterior and anterior parts of the filaments. In contrast, lipid droplets mostly accumulated in the posterior part of the filament without migrating to the hyphal tip.

The melanized appressoria of *M. oryzae* and *Colletotrichum orbiculare* penetrate the plant surface by mechanical force. The required turgor pressure is generated by the production of the osmolyte glycerol which is obtained through rapid lipolysis of lipid droplets (Thines *et al.*, 2000; Asakura *et al.*, 2012). Lipolysis is the lipase-mediated mobilization and break-down of

lipid droplet-derived triglycerides which allows cells to regain fatty acids for energy production, membrane synthesis and signaling functions (Zechner and Madeo, 2009). The process of lipolysis appears closely associated with the fatty-acid β-oxidation in peroxisomes (Shai *et al.*, 2016). The appressorium mediated penetration in *U. maydis* presumably depends on the localized secretion of cell wall-degrading enzymes rather than on turgor pressor and mechanic force. Therefore, it is unlikely that *U. maydis* depends on the generation of osmolytes from lipid droplets. Nevertheless, while lipid droplets accumulate in appressoria of SG200AM1 growing on parafilm only very few lipid droplets were detected in the tip of AM1-marker expressing filaments of the *scp2* deletion strain suggesting that there might be a correlation of lipid droplet distribution and appressorium formation. In future experiments, it would be interesting to investigate the lipid droplet distribution in the 10 % of *scp2* deletion strain filaments that did form appressoria on parafilm.

Interestingly, the misdistribution of peroxisomes was not only visible in hyphae on parafilm but also in hyphae on the plant surface indicating that these defects might contribute to the decreased pathogenicity of *scp2* deletion mutants. Further experiments, however, are required to determine whether the altered distribution of peroxisomes and lipid droplets is causing the inability of filaments to penetrate the epidermal layer of the host plant.

In *U. maydis*, peroxisomes and lipid droplets have been shown to be distributed by hitchhiking on early endosomes. Defects in early endosome movement can cause a clustering of peroxisomes in the hyphal tip (Guimaraes *et al.*, 2015). Colocalization experiments of peroxisomes and early endosomes in *scp2* deletion mutants, however, demonstrated that in filaments which showed an altered peroxisomal distribution early endosome localization and motility was not affected.

On a glass surface *U. maydis* is not able to form appressoria but filament formation can be induced by treatment with HFA. In the course of this work *scp2* deletion strains were treated with HFA and applied to a glass slide to determine whether the presence of a solid surface induces the misdistribution of peroxisomes and lipid droplets. These experiments showed that the contact to a solid surface is not sufficient to induce the misdistribution (not shown).

In contrast to that, filaments induced by HFA treatment on paraffin wax slides showed a similar misdistribution of peroxisomes as it was observed for *scp2* deletion filaments on parafilm (not shown). These results suggest that either the strong hydrophobicity or distinct components of the wax and parafilm slides are the reason for the peroxisomal misdistribution. Both parafilm and the wax slides are composed of paraffin, a mixture of saturated hydrocarbons with a hydrocarbon chain length ranging from 20 to 30 carbon atoms (Mortimer and Müller, 2003).

Interestingly, waxes consisting of very long-chain fatty acids (VLCFAs) with carbon chains ranging from 20 to 40 carbon atoms have been shown to be a major component of the plant cuticle (Reina-Pinto and Yephremov, 2009). Further experiments like the treatment of *scp2* deletion strain filaments with VLCFAs like erucic acid (C22) or lignoceric acid (C24) could clarify whether the contact to these compounds induces the altered distribution of peroxisomes and/or lipid droplets. Although it was shown that the misdistribution does not necessarily correlate with the expression of the AM1-marker it has to be considered that the misdistribution could be initialized by intracellular changes prior to appressorium formation such as differences in gene expression or rearrangements of the fungal cytoskeleton.

The altered accumulation of lipid droplets and peroxisomes in filaments of the *scp2* deletion strain could also be caused by changes in the overall membrane phospholipid content of the two organelles. Peroxisomes and lipid droplets are not able to synthesize their own membrane lipids. Therefore, they depend on the provision of structural phospholipids such as phosphatidylcholine (PC) by extraperoxisomal pathways like the Kennedy pathway (Flis *et al.*, 2015). In yeast, defects in PC biosynthesis resulted in alterations of peroxisomal membrane properties and stability (Flis *et al.*, 2015). Moreover, PC has been shown to act as a surfactant in the phospholipid monolayers that surrounds lipid droplets. The presence of PC prevents the coalescence of lipid droplets that would otherwise result in the formation of large, lipolysis-resistant lipid droplet aggregates (Krahmer *et al.*, 2011). Overexpression of murine Scp2 in mouse cells is suspected to influence key enzymes of the Kennedy pathway, thereby altering the synthesis of phospholipids like PC (Murphy *et al.*, 2000). The absence of Scp2 could therefore alter the composition of peroxisomal and lipid droplet membranes. These alterations could either interfere with binding of peroxisomes and lipid droplets to the early endosome transport machinery or it could cause an accumulation of these organelles thereby preventing the efficient transport throughout the cell. Contradicting the above interpretation, Murphy and coworkers (Murphy *et al.*, 2000) suspected that the overrepresentation of Scp2 causes a downregulation of PC. Therefore it has to be established how the deletion of *scp2* influences the overall phospholipid composition in *U. maydis*.

The assumption that the observed misdistribution of peroxisomes and lipid droplets might causes the virulence phenotype in *scp2* deletion strains raised the question why the equal distribution of organelles is of such an importance during this specific stage of the fungal lifecycle. Considering the most prominent function of peroxisomes, their equal distribution might be important for the protection of *U. maydis* filaments from oxidative stress (Rodriguez-Serrano *et al.*, 2009). The accumulation of peroxisomes in certain areas of the hyphae would

therefore leave the midsection of the filament unprotected and vulnerable to plant derived defense reactions. But even though peroxisomes are usually regarded as hydrogen peroxide (H_2O_2) detoxifying organelles peroxisomes have also been shown to be important producers of potent signaling molecules like H_2O_2 and nitric oxide (·NO) in plants and in fungi (Corpas *et al.*, 2001; Del Río, 2011; Wei *et al.*, 2013). The aggregation of peroxisomes in a very restricted area of the filament might therefore cause the accumulation of toxic compound like H_2O_2 which might damage the cell from within during the sensitive state of host plant infection. Further, the equal distribution of organelles could support the distribution and exchange of lipid substrates between peroxisomes and lipid droplets (Gao and Goodman, 2015). Taken together, the even distribution of peroxisomes and lipid droplets might ensure a comprehensive protection of filaments from external factors like plant defense responses and allow the distribution of metabolic substrates within the cell. Preliminary experiments using DAB-stain suggested that *scp2* deletion strains might elicit increased hypersensitive responses upon infection of maize leaves when compared to SG200 (not shown). Future experiments have to address whether the altered distribution of peroxisomes and lipid droplets is responsible for the presumably enhanced defense reaction. Expression analysis of maize genes involved in defense responses against pathogens like pr1, pr3 and pr5 (Heimel *et al.*, 2013) or maize marker genes for enhanced ROS production (Campbell *et al.*, 2015) could help to describe the defense reaction observed in *scp2* deletion strains in a quantitative manner.

3.5 Precise regulation of *scp2* gene expression might be crucial for Scp2 function

While the overexpression of *scp2* under the native promoter did not influence *U. maydis* virulence, expression of *scp2* under the control of the *cmu1* promoter caused a severe virulence defect during plant infection. The defect was observed after single copy integration of the construct P_{cmu1}-*scp2* into the SG200 as well as into the SG200Δscp2 genome, indicating that the overexpression of *scp2* under the *cmu1* promoter causes a dominant negative effect on virulence. This defect was characterized by the absence of anthocyanin and tumors and the presence of chlorotic lesions that were distributed throughout the entire leaf. Furthermore, WGA/PI stains of the respective leaves indicated that the overexpression strains elicit strong plant defense reactions in early stages of infection. An overloading of peroxisomes by the overexpressed Scp2 protein is considered unlikely because overexpression of a peroxisomal $mCherry_{pex}$ using the *cmu1* promoter did not result in a comparable effect on SG200 virulence. In addition, several other fluorescent proteins as well as effector proteins were expressed in *U. maydis* using the *cmu1* promoter without encountering a virulence phenotype comparable to

the phenotype observed for Scp2 overexpression strains (Tanaka *et al.*, 2014; Lo Presti *et al.*, 2016). RNAseq and qPCR data shows that *scp2* is naturally downregulated two days after infection and expression increases again 4 dpi. Expression under control of the *cmu1* promoter would not follow this pattern but would lead to a constitutive overexpression of *scp2* in the plant. This could indicate that it is important to rapidly suppress *scp2* expression during plant colonization, since excess of Scp2 at two days after infection elicits strong plant defense reactions. This is in line with the observation that *scp2* deletion strains show a milder phenotype than the overexpression strain since here the presumably dangerous presence of Scp2 at later stages of plant infection is not given. Interestingly, besides Scp2, several other peroxisomal *U. maydis* proteins involved in metabolic processes like peroxisomal β-oxidation (Mfe2 and Scpx), the degradation of hydrogen peroxide (catalase) and the synthesis of glycolipids (Mac1 and Mac2) show a significant drop of expression two days after infection (D. Lanver, personal communication). This might indicate that the tight transcriptional regulation of peroxisomal proteins during pathogenic development is crucial for the establishment of the biotrophic interaction between plant and fungus. Analyzing the phenotype of genes like *mfe2* and *scpx* under control of the *cmu1* promotor could clarify whether the phenotype observed for SG200P_{cmu1}-Scp2 and SG200Δscp2P_{cmu1}-Scp2 is Scp2-specific or whether peroxisomal protein expression under the *cmu1* promoter in general elicits a hypersensitive response in the host plant.

3.6 Binding properties of Scp2

Most of the known sterol carrier proteins in other organisms exhibit a high affinity for cholesterol. In contrast, no binding to cholesterol was observed for the *U. maydis* Scp2 protein in protein-lipid overlay assays. The fungal cholesterol counterpart ergosterol has a similar but not identical structure and further experiments have to be performed to elucidate whether ergosterol can be bound by the *U. maydis* Scp2. However, Scp2 showed a significant affinity for cardiolipin and the phospholipid PI4P. Cardiolipin is a non-bilayer phospholipid considered to be a signature lipid of mitochondrial membranes (Tatsuta and Langer, 2016). Cardiolipin initially seemed an unlikely candidate for interacting with Scp2 since it has been shown to mainly localize at the inner mitochondrial membrane *in vivo*. However, in the yeasts *Pichia pastoris* and *S. cerevisiae* cardiolipin was found to be present in peroxisomal membrane fractions (Zinser *et al.*, 1991; Wriessnegger *et al.*, 2007). Interestingly, *Y. lipolytica* Scp2 was shown to transfer fatty acids by a collision-mediated mechanism and the transfer frequency of lipids to a certain target membrane could be significantly enhanced by enrichment of the

membranes with cardiolipin (Falomir Lockhart *et al.*, 2009). This suggests that the fatty acid composition may dictate the binding of Scp2 proteins to their target membranes (Falomir Lockhart *et al.*, 2009). The analysis of cardiolipin contents in *U. maydis* peroxisomes could help to determine the relevance of the cardiolipin-binding properties for the Scp2 function.

PI4P has been localized to Golgi membranes but has also been associated with the plasma membrane as well as late endosomes and/or lysosomes and is thought to assist protein targeting to specific organelle membranes (Hammond *et al.*, 2014). PI4P does not reside in peroxisomes which raises the question whether a small proportion of Scp2 functions as a lipid transfer protein in the cytoplasm. This assumption is supported by previous studies that could show that SCP-2 of fibroblasts is not only localized in peroxisomes but that it is also present in the ER (Starodub *et al.*, 2000). Immunogold labeling coupled with electron microscopy analysis could help to identify small amounts of Scp2 outside of peroxisomes and to evaluate the possibility that Scp2 binds to extraperoxisomal lipids in *U. maydis*.

Several sterol carrier proteins have been shown to influence plasma membrane composition and robustness by binding and distributing sterols between membranes (Berger *et al.*, 2005; Zhao *et al.*, 2014). However, filipin stains of sterols in the *U. maydis* membrane as well as nystatin sensitivity assays gave no clear cut indication that Scp2 is involved in the maintenance of fungal membrane integrity. Nevertheless, minor differences of overall sterol content in the fungal plasma membranes could be quantified using a lipidomic approach. Furthermore, previously performed stress assays which did not show differences in stress sensitivity (F. Bochen, personal communication) should be repeated by using filamentous growing cells since all defects of *scp2* deletion strains were exclusively observed in filamentous hyphae.

An interesting question concerning the binding specificity of Scp2 is why the two Scp2 homologs hScp2 and YLScp2 are able to partially complement the *U. maydis scp2* deletion phenotype even though the observed lipid binding capacity of the three proteins does not seem to coincide. A potential reason could be that Scp2 ligand binding is relatively unspecific. Rather than a lock-and-key mechanism sterol carrier proteins harbor their respective ligands loosely in a hydrophobic cavity that is formed by a conserved conformation of β-sheets and α-helices (De Berti *et al.*, 2013). This fold has been shown to be conserved in sterol carrier proteins from various species including bacteria and mammals (De Berti *et al.*, 2013). Due to this lack of specificity sterol carrier proteins were also termed nonspecific lipid transfer proteins. The mammalian Scp2 protein, for instance, has been shown to not only transfer cholesterol but to bind poly- and monounsaturated fatty acids, branched-chain isoprenoids and branched-chain phytol-derived fatty acids (Frolov *et al.*, 1997). YLScp2 and hScp2 might thus be able to

transfer similar lipid ligands as the *U. maydis* Scp2 and are therefore able to partially complement the *scp2* deletion phenotype. In contrast, the two Scp2 paralogs Um01850 and Um11277 do not seem to be able to exhibit a Scp2-like function. In case of a related function, the two paralogs should partially substitute for the Scp2 function and therefore the pathogenicity defect observed for the triple deletion strain SG200Δ*um01850*Δ*um11277*Δ*scp2* should have been stronger than the one observed for *scp2* deletion strains. The documented lack of complementation, however, could also be attributed to the different expression levels of the three genes. In axenic culture, expression levels of *scp2* are approximately 5.0 times higher than *um11277* and approximately 20 times higher than *um01850*. Twelve hours after infection the expression levels of *scp2* are approximately 5.7 times higher than *um11277* and approximately 8.0 times higher than *um01850* (D. Lanver, personal communication). Therefore, to substantiate the absence of complementation a *scp2* deletion strain should be complemented with constructs that contain *um01850* and *um11277* under the control of the *scp2* promoter.

Furthermore it should be considered that the virulence related function of Scp2 is lipid binding-independent. By using the structural information of hScp2 and YLScp2, essential amino acids in the *U. maydis* Scp2 hydrophobic cavity could be mutated to abolish lipid binding and to analyze whether the ligand binding characteristics are essential for Scp2 function.

3.7 A potential model for the function of Scp2 during *U. maydis* infection

In the following chapter a hypothetical model of the Scp2 function in *U. maydis* and potential ways to prove this model will be discussed.

U. maydis Scp2 may function as an intracellular lipid carrier and pool former which binds and transfers a yet undetermined lipidic ligand. This transfer might not only occur within peroxisomes but could also include intracellular membranes like the fungal plasma membrane, the ER or the Golgi apparatus. The presence of Scp2 at the cytosolic phase of exosomal membranes could support the hypothesis that Scp2 is present in the cytoplasm of *U. maydis* filaments. Correct extraperoxisomal targeting of Scp2 could be supported by the presence of marker lipids like cardiolipin or PI4P in the destination organelles. As a lipid carrier Scp2 could help to maintain the equilibrium of structural phospholipid components in peroxisomes and lipid droplet membranes. Loss of Scp2 might therefore cause alterations of peroxisomal and lipid droplet membrane content which in turn could promote the coalescence of lipid droplets and an inefficient attachment of peroxisomes to the early endosome transport machinery (Fig. 39). As a consequence, the access to certain metabolic products of peroxisomes and lipid droplets at the site of appressorium formation might be decreased and the attachment of

appressoria to surfaces weakened. This product could be a precursor lipid or glycolipid that serves as a glue for the appressorium and mediates its strong attachment to the respective surface (Fig. 40). Alternatively, the appressorium formation and adhesion defects might result from a lack of locally produced energy caused by the lipid droplet and peroxisome misdistribution. This defect would have to occur in early steps of lipolysis since defects in later stages of energy metabolism like defects in peroxisomal β-oxidation or the glyoxylate cycle did not resemble the *scp2* deletion phenotype. The impaired appressorium function could manifest itself on the plant surface as a penetration defect resulting in reduced plant colonization and a reduction of overall symptom development. Appressoria that manage to gain access into the leaf tissue, however, proliferate effectively and are able to complete the entire biotrophic *U. maydis* life cycle, reinforcing a specific defect prior or during penetration.

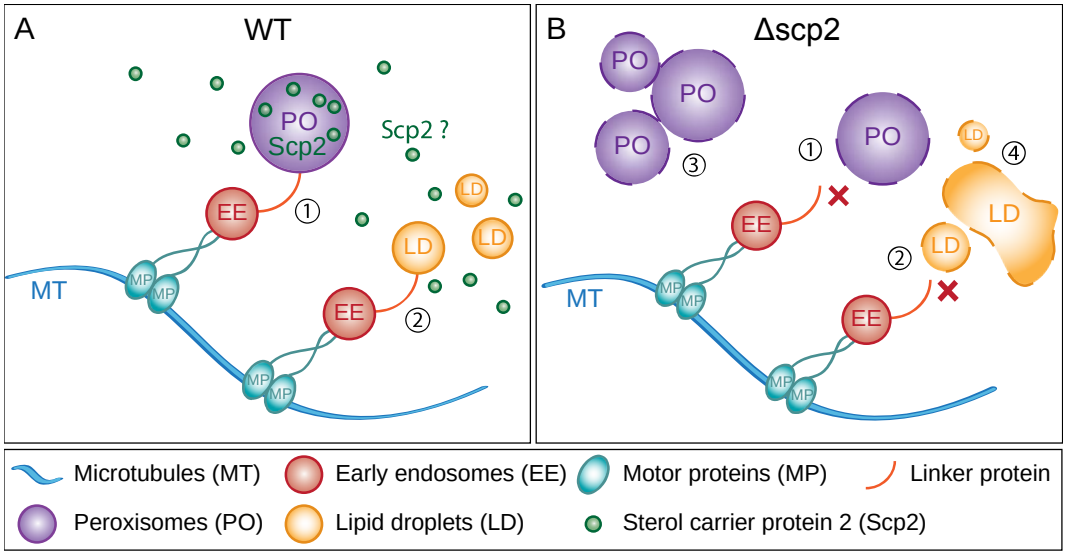

Fig. 39: Hypothetical model for the Scp2 function within *U. maydis* cells. (A) Scp2 could function as a pool former and lipid carrier that stabilizes the equilibrium of lipids within organelle membranes. Thereby Scp2 might function exclusively within peroxisomes or might be distributed throughout the cell. Peroxisomes [1] and lipid droplets [2] are transported through the cell by hitchhiking on early endosomes that travel via a motor protein/microtubule depended mechanism. (B) In the absence of Scp2 the membrane composition of peroxisomes and lipid droplets may be altered. The changes in lipid components might prohibit the binding of peroxisomes [1] and lipid droplets [2] to the early endosome transport machinery resulting in an accumulation of the organelles at the cell poles. Alternatively peroxisomes [3] and lipid droplets [4] might form aggregates as a result of changes in membrane lipid components, thereby prohibiting their effective transportation and distribution within the cell.

Several experiments have to be performed to verify the proposed model. Peroxisomes and lipid droplets from SG200 and SG200Δscp2 filaments on parafilm have to be isolated and analyzed in terms of lipid composition. Differences between the two strains could indicate the involvement of Scp2 in the regulation of biosynthesis or the distribution of lipid compounds between intracellular membranes and organelles. Further, SG200 and SG200Δscp2 appressoria on parafilm have to be examined with respect to the extracellular matrix that potentially mediates appressorium adhesion. The extracellular matrix could be analyzed by

immunohistochemical examination and electron microscopy (Zelinger *et al.*, 2006; Inoue *et al.*, 2008). The adhesion strength of filaments and appressoria to surfaces could be assessed by using single-cell force spectroscopy (SCFS) (Alsteens *et al.*, 2013).

The misdistribution of peroxisomes and lipid droplets on the plant surface has to be quantified to compare the frequency of misdistribution events between the *in vitro* and the *in vivo* system. In order to validate that an even organelle distribution is a prerequisite for effective cuticle penetration it should further be analyzed whether the misdistribution of peroxisomes and lipid droplets in filaments on the plant surface correlates with an unsuccessful penetration attempt. Besides the investigation of SG200 and SG200Δscp2 the inclusion of the overexpression strain SG200P_{cmu1}-Scp2 might give valuable clues on the function of Scp2 in the course of *U. maydis* infection.

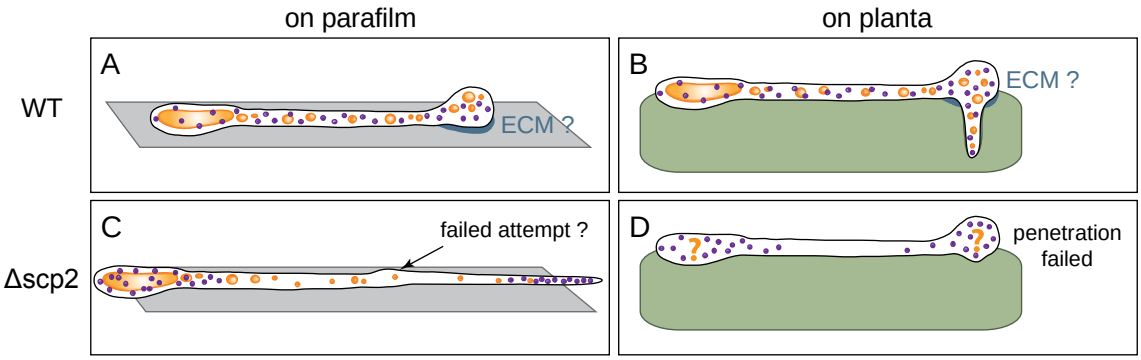

Fig. 40: Hypothetical model for the Scp2 function during *U. maydis* pathogenic development. The model summarizes the observed phenotypes of *scp2* deletion strains on parafilm and on the plant surface in comparison to the respective progenitor strains, here termed wild type strains (WT). Lipid droplets are colored in yellow while peroxisomes are colored in purple. (A) Appressorium formation of wild type strains on parafilm. A large lipid droplet depot is localized in the posterior part of the filament and lipid droplets of intermediate size are evenly distributed throughout the cytoplasm. Peroxisomes are distributed evenly within the filament. The presence of an extracellular matrix (ECM) might mediate stable attachment of the appressorium to the parafilm surface. (B) Appressorium formation and penetration of WT filaments on the plant surface. Lipid droplet and peroxisome distribution correlates with the distribution on parafilm. The ECM might grant attachment to the plant cuticle allowing efficient appressorium-mediated penetration of the plant cuticle. (C) Appressorium formation defect of *scp2* deletion strains on parafilm. A large lipid droplet depot is localized in the posterior part of the filament whereas lipid droplets only rarely migrate to the tip of the filament. Peroxisomes accumulate in the posterior and anterior parts of the hyphae. Some filaments seem to attempt appessorium formation but do not succeed and continue filamentous growth. This appressorium formation defect might be caused by the absence of an ECM that mediates the adhesion of the appressorium to the parafilm surface. (D) Appressorium formation and attempted penetration of *scp2* deletion strains on the plant surface. The appressorium formation defect observed on parafilm does not manifest on the plant, probably due to physical or chemical leaf surface cues. The formed appressoria, however, display a reduction in penetration frequency that may result from the inability of appressoria to adhere tightly enough to the leaf cuticle. Peroxisomes seem to display a similar misdistribution as it was observed for *scp2* deletion strains filaments on parafilm. The distribution of lipid droplets on the plant surface still has to be examined (yellow quotation mark).

4. Materials and Methods

4.1 Materials and source of supplies

4.1.1 Chemicals

All chemicals used in this study were obtained from Becton Dickinson (BD) (Heidelberg, Germany), Merck (Darmstadt, Germany), Roth (Karlsruhe, Germany), Sigma-Aldrich (Munich, Germany), GE Healthcare (Freiburg, Germany), Roche Diagnostics (Mannheim, Germany) and Invitrogen (Karlsruhe, Germany).

4.1.2 Solutions and buffers

All standard solutions and buffers used in this study were prepared as described in Ausubel *et al*. (1987) and Sambrook *et al*. (1989). All additional solutions and buffers are listed in the corresponding method sections. All media, solutions and buffers were autoclaved for 5 min at 121 °C. Heat-sensitive solutions were filter sterilized (pore size 0.2 µm; Merck, Darmstadt, Germany).

4.1.3 Enzymes and antibodies

All restriction enzymes, T4 DNA ligase, Polynucleotide kinase and Antarctic Phosphatase were obtained from New England Biolabs (NEB) (Frankfurt am Main, Germany). Phusion DNA Polymerase was obtained from Thermo Scientific (Darmstadt, Germany). KOD Extreme Polymerase was obtained from Merck (Darmstadt, Germany). Enzymatic digestion of RNA was accomplished using RNase A from Roth (Karlsruhe, Germany). Enzymatic digestion of cell walls was accomplished by using Novozym 234 (Interspex Products, Foster City, CA, USA). Antibodies were obtained from Sigma-Aldrich (Munich, Germany), Cell Signaling Technology (Leiden, Netherlands), Eurogentec (Seraing, Belgium) and IBA GmbH (Goettingen, Germany). A detailed table of all antibodies can be found in chapter 4.6.7 (Antibodies).

4.1.4 Utilized kits

The following kits were used in this study according to the manufacturers' specifications: Wizard® SV Gel and PCR Clean-Up System (Promega, Mannheim, Germany) was used to purify PCR products and DNA fragments from agarose gels. QIAprep® Spin MiniPrep Kit (Qiagen, Hilden, Germany) was used to isolate and purify plasmid DNA before sequencing. The TOPO® TA Cloning® Kit (Invitrogen, Karlsruhe, Germany) was used for the cloning of PCR products. More specific kits are listed under the respective method descriptions.

4.2 Cell cultivation and media

4.2.1 *E. coli*

For the cultivation of *E. coli*, dYT liquid medium and YT solid medium were used (Ausubel *et al.*, 1987; Sambrook *et al.*, 1989). Ampicillin (Amp) was added to a final concentration of 100 µg/ml. Liquid cultures were incubated at 37 °C and 200 rpm. Solid media were incubated under aerobic condition at 37 °C. For preparing frozen stocks exponentially growing cultures containing the appropriate antibiotic were mixed with dYT-glycerol at a 1:1 ratio and stored at -80 °C.

dYT liquid medium
1.6 % (w/v) Tryptone (Bacto)
1.0 % (w/v) Yeast-Extract (Bacto)
0.5 % (w/v) NaCl (Roth)
Dissolve in H_2O_{bid} and autoclave.

YT solid medium
0.8 % (w/v) Tryptone (Bacto)
0.5 % (w/v) Yeast-Extract (Bacto)
0.5 % (w/v) NaCl (Roth)
1.3 % (w/v) Agar (Bacto)
Dissolve in H_2O_{bid} and autoclave.

dYT glycerol medium
1.6 % (w/v) Tryptone (Bacto)
1.0 % (w/v) Yeast-Extract (Bacto)
0.5 % (w/v) NaCl (Roth)
80.0 % (v/v) 87 % Glycerin (f. c. 69.6 %)
Dissolve in H_2O_{bid} and autoclave.

4.2.2 *U. maydis*

U. maydis strains were grown on PD or CM-glc solid medium or cultivated in $YEPS_{light}$ or CM-glc liquid media. To select transformants hygromycin B (HY) (Duchefa, Haarlem, Netherlands), geneticin (NE) (Sigma G-8168), nourseothricin (trade name: clonNAT) (NA) (WERNER BioAgents GmbH, Jena, Germany) and carboxin (CB) (Sigma-Aldrich; Munich, Germany) were added to a final concentration of 200 µg/ml (HY), 400 µg/ml (NE), 75 µg/ml (NA) and 2 µg/ml (CB), respectively. To prepare frozen stocks exponentially growing cultures were mixed with NSY-glycerol at a 1:1 ratio and stored at -80 °C.

$YEPS_{light}$ liquid medium
1.0 % (w/v) Yeast-Extract (Bacto)
0.4 % (w/v) Peptone (Bacto)
0.4 % (w/v) Sucrose (Roth)
Dissolve in H_2O_{bid} and autoclave.

CM liquid medium (CM-glc)
0.25 % (w/v) Casaminoacids (Difco)
0.1 % (w/v) Yeast-Extract (Bacto)
1.0 % (v/v) Vitamin solution (Holliday, 1974)

6.25 % (v/v) Salt solution (Holliday, 1974)
0.05 % (w/v) DNA from herring sperm degr. (Sigma, D-3159)
0.15 % (w/v) NH_4NO_3 (Roth)
1.0 % (v/v) 1 M Tris/HCl pH 8.0 (f. c.10 mM)
Dissolve in H_2O_{bid} adjust pH to 7.0 with 5 M NaOH and autoclave. After autoclaving add 4.0 % (v/v) 50 % glucose solution (f. c. 2 %).

double CM solid medium

0.4 % (w/v) Casaminoacids (Difco)
0.2 % (w/v) Yeast-Extract (Bacto)
2.0 % (v/v) Vitamin solution (Holliday, 1974)
25.0 % (v/v) Salt solution (Holliday, 1974)
0.1 % (w/v) DNA from herring sperm degr. (Sigma, D-3159)
0.6 % (w/v) NH_4NO_3 (Roth)
1.0 % (v/v) 1 M Tris/HCl pH 8.0 (f. c.10 mM)
2.0 % (w/v) Agar (Bacto)
Dissolve in H_2O_{bid} adjust pH to 7.0 with 5 M NaOH and autoclave. After autoclaving add 4.0 % (v/v) 50 % glucose solution (f. c. 2 %).

Vitamin solution (Holliday, 1974)

0.1 ‰ (w/v) Thiamine hydrochloride (Sigma T-4625)
0.05 ‰ (w/v) Riboflavin (Sigma R-4500)
0.05 ‰ (w/v) Pyridoxine hydrochloride (Sigma P-9755)
0.2 ‰ (w/v) D-Pantothenic acid hemicalcium salt (Sigma P-2250)
0.05 ‰ (w/v) 4-Aminobenzoic acid (Sigma A-9878)
0.2 ‰ (w/v) Nicotinic acid (Sigma N-4126)
0.2 ‰ (w/v) Choline chloride (Sigma C-1879)
1.0 ‰ (w/v) myo-Inositol (Sigma I-5125)
Dissolve in H_2O_{bid} prepare 40 ml aliquots in 50 ml tubes and freeze at -20 °C.

Salt solution (Holliday, 1974)

16.0 ‰ (w/v) KH_2PO_4
4.0 ‰ (w/v) Na_2SO_4
8.0 ‰ (w/v) KCl
2.0 ‰ (w/v) $MgSO_4 * 7H_2O$
1.32 ‰ (w/v) $CaCl_2 * 2H_2O$
8.0 ‰ (v/v) Trace elements
Dissolve in H_2O_{bid} and sterile filtrate.

Trace elements (Holliday, 1974)

0.06 ‰ (w/v) H_3BO_3
0.14 ‰ (w/v) $MnCl * 4H_2O$
0.4 ‰ (w/v) $ZnCl_2$
0.4 ‰ (w/v) $Na_2MoO_4 * 2H_2O$
0.1 ‰ (w/v) $FeCl_3 * 6H_2O$

	0.03 ‰ (w/v) $CuSO_4$ Dissolve in H_2O_{bid}.
50 % glucose solution	55.0 % (w/v) Glucose * H_2O (Roth) Dissolve in H_2O_{bid} and sterile filtrate.
PD solid medium	2.4 % (w/v) Potato Dextrose Broth (Difco) 2.0 % (w/v) Agar (Bacto) Dissolve in H_2O_{bid} and autoclave.
PD charcoal solid medium	2.4 % (w/v) Potato Dextrose Broth (Difco) 1.0 % (w/v) Charcoal (Sigma C-9157) 2.0 % (w/v) Agar (Bacto) Dissolve in H_2O_{bid} and autoclave.
NSY glycerol medium	0.8 % (w/v) Nutrient broth (Difco) 0.1 % (w/v) Yeast-Extract (Bacto) 0.5 % (w/v) Sucrose (Roth) 80.0 % (v/v) 87 % Glycerin (f. c. 69.6 %) Dissolve in H_2O_{bid} and autoclave.
NM liquid medium	0.3 % (w/v) KNO_3 6.25 % (v/v) Salt solution (Holliday ‘74) 1.0 % (v/v) 1 M Tris/HCl pH 8.0 Dissolve in H_2O_{bid} adjust pH to 7.0 with 5 M NaOH and autoclave. After autoclaving add 4.0 % (v/v) 50 % glucose solution (f. c. 2 %).
NM solid medium	0.3 % (w/v) KNO_3 6.25 % (v/v) Salt solution (Holliday, 1974) 2.0 % (w/v) Agar (Bacto) 1.0 % (v/v) 1 M Tris/HCl pH 8.0 Dissolve in H_2O_{bid} adjust pH to 7.0 with 5 M NaOH and autoclave. After autoclaving add 4.0 % (v/v) 50 % glucose solution (f. c. 2 %).

4.2.2.1 Fatty acid growth assay

The respective strains were grown to an OD_{600} of 0.8 in $YEPS_{light}$. Subsequently, the cells were washed twice in H_2O_{bid} (3,500 rpm, 5 min, RT) and adjusted to an OD_{600} of 1.0. Serial dilutions ranging from 10^0 to 10^{-4} were generated in H_2O_{bid} and 7 µl of each dilution were spotted on YNB-plates (w/o amino acids) supplemented with the respective fatty acid. The plates were incubated at 28 °C for 3-5 days. Fatty acids were purchased from Sigma-Aldrich (Munich, Germany). Following concentrations were used for the preparation of YNB fatty acid supplemented plates: 1.2 % stearic acid stock solution, 0.3 % palmitic acid stock solution, 0.3 % oleic acid solution (Sigma O1008), 0.03 % linoleic acid solution (Sigma L1376).

Stearic acid stock solution	79.1 mM Stearic acid (Sigma S-4751) Dissolved in 100 % EtOH.
Palmitic acid stock solution	281.2 mM Palmitic acid (Sigma P0500) Dissolved in 100 % EtOH.
YNB w/o amino acids solid medium	0.67 % (w/v) yeast nitrogen base without amino acids (Difco) 2.0 % (w/v) Agarose (Roth) Dissolve in H_2O_{bid} and autoclave.

4.2.2.2 Nystatin growth assay

For nystatin growth assays serial dilutions of the respective strains were prepared as described in chapter 4.2.2.1 (Fatty acid growth assay). 7 µl of each dilution were spotted on CM-glc plates containing either only DMSO (as control) or 2.5 µg or 5.0 µg nystatin.

Nystatin stock solution	5 mg/ml Nystatin (Sigma N3503) Dissolve in 100 % DMSO.

4.2.3 Determination of cell density

The cell density of liquid cultures was determined photometrically using an Ultrospec 3000 pro UV/Visible Spectrophotometer (Biochrom, Cambridge) at 600 nm (OD_{600}). To determine the optical density cell cultures were diluted 1:10 in the respective medium. As a reference value the OD_{600} of sterile medium was used. For *U. maydis* cell cultures an OD_{600} of 1.0 equals approximately 1-5 x 10^7 cells.

4.3 Strains, oligonucleotides and plasmids

4.3.1 *E. coli* strains

The *E. coli* strains DH5α and TOP10 were used for the cloning and amplification of plasmids while the *E. coli* strain Rosetta(DE3)pLysS was used for the IPTG-induced gene expression needed for the purification of *U. maydis* proteins from *E. coli*.

DH5α (Thermo Scientific, Darmstadt, Germany): (*F– endA1 glnV44 thi-1 recA1 relA1 gyrA96 deoR nupG purB20 φ80dlacZΔM15 Δ(lacZYA-argF)U169, hsdR17(rK–mK+), λ–*)

TOP10 (Invitrogen, Karlsruhe, Germany): (*F– mcrA Δ(mrr-hsdRMS-mcrBC) Φ80lacZΔM15 ΔlacX74 recA1 araD139 Δ(ara leu) 7697 galU galK rpsL (StrR) endA1 nupG*)

Rosetta(DE3)pLysS (Novagen/Merck, Darmstadt, Germany): *F- ompT hsdSB(RB- mB-) gal dcm λ(DE3 [lacI lacUV5-T7 gene 1 ind1 sam7 nin5]) pLysSRARE (CamR)*

4.3.2 *U. maydis* strains

In the following chapter pre-existing *U. maydis* progenitor strains (Tab. 1), progenitor strains that were generated during this thesis (Tab. 2) and the strains utilized for this work (Tab. 3) are

listed. For the generation of deletion mutants, the respective gene was replaced by a resistance cassette as described in Kämper (2004) and in Brachmann *et al*. (2004). Plasmids containing a carboxin resistant *ip*-allele (ip^R) (Broomfield and Hargreaves, 1992) were used for the integration of genes into the *ip* locus. These plasmids were integrated into the carboxin-sensitive *ip*-allele (ip^S) of the *U. maydis* genome via homologous recombination. If not indicated otherwise all generated strains were verified via southern blot analysis and carry a single copy insertion of the respective plasmid in the *ip* locus. The plasmids that were used for the generation of the listed strains are described in chapter 4.3.4.

Table 1. *U. maydis* progenitor strains.

Serial number	Name	Genotype	Resistance[2]	Reference
SR18	SG200	*a1: mfa2 bW2 bE1*	PH	Kämper *et al*., 2006
SR142	SG200AM1	*a1: mfa2 bW2 bE1 $ip^R[P_{um01779}$:egfp$]ip^S$*	PH, CB	Mendoza-Mendoza *et al.*, 2009
SR146	AB33	*a2: P_{nar}: bW2 bE1*	PH	Brachmann *et al.*, 2001
SR256[1]	AB33 P_{otef}-GFP-HA-Strep	*a2: P_{nar}: bW2 bE1 $ip^R[P_{otef}$-gfp-HA-Strep$]ip^S$*	PH, CB	S. Krombach, unpublished
SR306[1]	AB33 P_{otef}-Strep-HA-Scp2	*a2: P_{nar}: bW2 bE1 $ip^R[P_{otef}$- gfp -myc-Strep-P_{otef}-Strep-HA-um11938$]ip^S$*	PH, CB	S. Krombach, unpublished
SR336	SG200Δscp2	*a1: mfa2 bW2 bE1 Δum11938*	HY, PH	S. Kreibich, unpublished
SR388[1]	SG200Δscp2-c #10 (m)	*a1: mfa2 bW2 bE1 Δum11938 $ip^R[P_{um11938}$-um11938$]ip^S$*	HY, CB	F. Ahrens, unpublished
SR389	SG200Δscp2-c	*a1: mfa2 bW2 bE1 Δum11938 $ip^R[P_{um11938}$-um11938$]ip^S$*	HY, CB, PH	F. Ahrens, unpublished
SR390[1]	SG200Δscp2-c #13 (m)	*a1: mfa2 bW2 bE1 Δum11938 $ip^R[P_{um11938}$-um11938$]ip^S$*	HY, CB	F. Ahrens, unpublished
SR405[1]	SG200AM1Δscp2	*a1: mfa2 bW2 bE1 Δum11938 $ip^R[P_{um01779}$-gfp$]ip^S$*	PH, HY, CB	S. Winterberg, unpublished
SR460	AB31Pex	*a2: P_{crg}: bW2 bE1 ect[P_{otef}-mcherry-SKL]*	PH, HY	J. Freitag, unpublished
SR500[1]	AB33 P_{scp2}-Strep-HA-Scp2	*a2: P_{nar}: bW2 bE1 $ip^R[P_{um11938}$-Strep-HA-um11938$]ip^S$*	PH, CB	S. Krombach, unpublished
SR523	FB1	*a1 b1*	-	Banuett and Herskowitz, 1989
SR524	FB2	*a2 b2*	-	Banuett and Herskowitz, 1989
SR704	SG200Δpex6	*a1: mfa2 bW2 bE1 Δpex6 ect[P_{otef} : mcherry-SKL]*	HY, PH, NA	Freitag *et al*., 2012
SR1057	SG200Δ04285	*a1: mfa2 bW2 bE1 Δum04285*	PH, HY	L. Bender, unpublished
SR1207	SG200Δ04285-c	*a1: mfa2 bW2 bE1 Δum04285 $ip^R[P_{um04285}$-gfp-um04285$]ip^S$*	PH, HY, CB	L. Bender, unpublished

[1] strains contain multiple integrations of the respective plasmid

[2] phleomycin (PH), hygromycin (HY), carboxin (CB), neomycin (NE), nourseothricin (NA).

Table 2. *U. maydis* progenitor strains generated in this study

Serial number	Name	Genotype	Resistance[2]	Progenitor strain	Plasmid
SR727	AB33Δscp2	*a2: P_{nar}: bW2 bE1 Δum11938*	HY	AB33	pSR209
SR809	SG200Δscp2Δ11277	*a1: mfa2 bW2 bE1 Δum11938 Δum11277*	PH, HY, NE	SR336	pSR239
SR1334[1]	SG200Δscp2Pex	*a1: mfa2 bW2 bE1 Δum11938 $ip^R[P_{etef}$-gfp-PTS1]ip^S*	PH, CB, HY	SR336	JF1742
SR1340[1]	SG200Pex	*a1: mfa2 bW2 bE1 $ip^R[P_{etef}$-gfp-PTS1]ip^S*	PH, CB	SG200	JF1742

[1] strains contain multiple integrations of the respective plasmid
[2] phleomycin (PH), hygromycin (HY), carboxin (CB), neomycin (NE), nourseothricin (NA).

Table 3. *U. maydis* strains used in this study.

Serial number	Name	Genotype	Resistance[2]	Progenitor strain	Plasmid
SR540[1]	AB33 P_{scp2}-SP-Strep-HA-Scp2	*a2: P_{nar}: bW2 bE1 $ip^R[P_{um11938}$-SP-Strep-HA-um11938]ip^S*	PH, CB	SR146	pSR140
SR558[1]	AB33 P_{scp2}-Strep-HA-$Scp2_{cyt}$	*a2: P_{nar}: bW2 bE1 $ip^R[P_{um11938}$-Strep-HA-um11938(AKL/AAA)]ip^S*	PH, CB	SR146	pSR162
SR728	FB2Δscp2	*a2 b2 Δum11938*	HY	SR524	pSR209
SR748	FB1Δscp2	*a1 b1 Δum11938*	HY	SR523	pSR209
SR812	SG200Δ11277	*a1: mfa2 bW2 bE1 Δum11277*	PH, NE	SR18	pSR239
SR822	SG200Δ01850	*a1: mfa2 bW2 bE1 Δum01850*	PH, NA	SR18	pSR241
SR872[3]	AB33Pex	*a2: P_{nar}: bW2 bE1 $ip^R[P_{etef}$-gfp-PTS1]ip^S*	PH, CB	SR146	JF1742
SR875[3]	AB33Δscp2Pex	*a2: P_{nar}: bW2 bE1 Δum11938 $ip^R[P_{etef}$-gfp-PTS1]ip^S*	PH, CB, HY	SR727	JF1742
SR930	SG200Δscp2 Scp2-AKL	*a1: mfa2 bW2 bE1 Δum11938 $ip^R[P_{um11938}$-um11938-AKL]ip^S*	CB, HY	SR336	pSR263
SR953	SG200Δscp2 SP-Scp2-GSA	*a1: mfa2 bW2 bE1 Δum11938 $ip^R[P_{um11938}$-SP-um11938-GSA]ip^S*	CB, HY	SR336	pSR261
SR959[1]	AB31Pex SP-GFP-Scp2-GSA	*a2: P_{crg}: bW2 bE1 ect[P_{otef}-mcherry-SKL] $ip^R[P_{um11938}$-SP-gfp-um11938-GSA]ip^S*	CB, HY, PH	SR460	pSR319
SR1213	SG200ΔΔΔ	*a1: mfa2 bW2 bE1 Δum11938 Δum01850 Δum11277*	PH, HY, NA, NE	SR809	pSR241
SR1246	SG200ΔΔΔ-c	*a1: mfa2 bW2 bE1 Δum11938 Δum01850 Δum11277 ip^R [$P_{um11938}$-um11938]ip^S*	PH, HY, NA, NE, CB	SR1213	pSR110

SR1251	SG200ICLΔΔ #10	*a1: mfa2 bW2 bE1 Δum04285 Δum01892*	PH, HY, NE	SR1057	pSR324
SR1252[1]	AB31Pex GFP-11277	*a2: P_{crg}: bW2 bE1 ect[P_{otef}-mcherry-SKL] ip^R[$P_{um11938}$-gfp-um11277]ip^S*	HY, PH, CB	SR460	pSR398
SR1256[1]	AB31Pex GFP-01850	*a2: P_{crg}: bW2 bE1 ect[P_{otef}-mcherry-SKL] ip^R[$P_{um11938}$-gfp-um01850]ip^S*	HY, PH, CB	SR460	pSR399
SR1258[1]	AB33 P_{scp2}-Strep-HA-GFP_{pex}	*a2: P_{nar}: bW2 bE1 ip^R[$P_{um11938}$-Strep-HA-gfp-AKL]ip^S*	PH, CB	SR146	pSR397
SR1261	SG200ICLΔΔ #15	*a1: mfa2 bW2 bE1 Δum04285 Δum01892*	PH, HY, NE	SR1057	pSR324
SR1266[1]	SG200Δscp2-hScp2 (m)	*a1: mfa2 bW2 bE1 Δum11938 ip^R[$P_{um11938}$-hScp2]ip^S*	PH, HY, CB	SR336	pSR395
SR1267	SG200Δscp2-hScp2	*a1: mfa2 bW2 bE1 Δum11938 ip^R[$P_{um11938}$-hScp2]ip^S*	PH, HY, CB	SR336	pSR395
SR1270	SG200Δscp2-YLScp2	*a1: mfa2 bW2 bE1 Δum11938 ip^R[$P_{um11938}$-YLScp2]ip^S*	PH, HY, CB	SR336	pSR396
SR1271[1]	SG200Δscp2-YLScp2 (m)	*a1: mfa2 bW2 bE1 Δum11938 ip^R[$P_{um11938}$-YLScp2]ip^S*	PH, HY, CB	SR336	pSR396
SR1277[1]	SG200 P_{cmu1}-$mCherry_{pex}$	*a1: mfa2 bW2 bE1 ip^R[P_{cmu1}-mcherry-AKL]ip^S*	PH, CB	SR18	pSR405
SR1283	SG200 P_{cmu1}-Scp2	*a1: mfa2 bW2 bE1 ip^R[P_{cmu1}-Scp2]ip^S*	PH, CB	SR18	pSR404
SR1287	SG200Δscp2 P_{cmu1}-Scp2	*a1: mfa2 bW2 bE1 Δum11938 ip^R[P_{cmu1}-Scp2]ip^S*	PH, HY, CB	SR336	pSR404
SR1326	SG200AM1PM	*a1: mfa2 bW2 bE1 ip^R[$P_{um01779}$-gfp_$P_{um03274}$-mcherry]ip^S*	PH, CB	SR18	pSR422
SR1328[1]	SG200AM1PM (m)	*a1: mfa2 bW2 bE1 ip^R[$P_{um01779}$-gfp_$P_{um03274}$-mcherry]ip^S*	PH, CB	SR18	pSR422
SR1331	SG200Δscp2 AM1PM	*a1: mfa2 bW2 bE1 Δum11938 ip^R[$P_{um01779}$-gfp_$P_{um03274}$-mcherry]ip^S*	PH, CB, HY	SR336	pSR422
SR1332[1]	SG200Δscp2 AM1PM (m)	*a1: mfa2 bW2 bE1 Δum11938 ip^R[$P_{um01779}$-gfp_$P_{um03274}$-mcherry]ip^S*	PH, CB, HY	SR336	pSR422
SR1360[1]	SG200Δscp2 AM1Pex	*a1: mfa2 bW2 bE1 Δum11938 ip^R[P_{etef}-gfp-PTS1]ip^S mig2-6[$P_{um01779}$-mcherry]*	PH, NE, CB, HY	SR1334	pMM69
SR1361[1]	SG200AM1Pex	*a1: mfa2 bW2 bE1 ip^R[P_{etef}-gfp-PTS1] ip^S mig2-6[$P_{um01779}$-mcherry]*	PH, NE, CB,	SR1340	pMM69
SR1370	SG200PexEE	*a1: mfa2 bW2 bE1 ip^R[P_{etef}-gfp-PTS1]ip^S ect[P_{otef}-mcherry-rab5-1]*	PH, CB, NA	SR1340	pomChrab5a
SR1371	SG200Δscp2 PexEE	*a1: mfa2 bW2 bE1 Δum11938 ip^R[P_{etef}-gfp-PTS1]ip^S ect[P_{otef}-mcherry-rab5-1]*	PH, CB, HY, NA	SR1334	pomChrab5a
SR1382[4]	SG200Δscp2 AM1Pex-c	*a1: mfa2 bW2 bE1 Δum11938 ip^R[P_{etef}-gfp-PTS1; $P_{um11938}$-um11938]ip^S mig2-6[$P_{um01779}$-mcherry]*	PH, NE, CB, HY, NA	SR1360	pSR429

[1] strains contain multiple integrations of the respective plasmid
[2] phleomycin (PH), hygromycin (HY), carboxin (CB), neomycin (NE), nourseothricin (NA).

[3] integration of the respective plasmids was verified by microscopy
[4] integration of the respective plasmids was verified by PCR

4.3.3 Oligonucleotides

All oligonucleotides in this study were purchased from Eurofins Genomics (Ebersberg/Munich, Germany). The name, the nucleotide sequences, potential restriction sites integrated by the oligonucleotide and the respective applications are listed in Table 4. The primers were utilized for cloning of plasmids as well as for Quantitative Real-Time PCR.

Table 4: Oligonucleotides used in this study

Name	Sequence[1]	Restriction site	Application[2]
OLL248	TTTTGGTACCTGCGGCGTGGGGAAAACC	*kpnI*	Amplification of the *cmu1* (*um05731)* promoter sequence (f) (L. Lo Presti)
OLL294	TTTTGGATCCCGTAACCTAGAGCTCTTGC	*bamhI*	Amplification of the *cmu1* (*um05731)* promoter sequence (r) (L. Lo Presti)
SI34	GTCGTCCTGGGCCTGAGTGGCCATGGTGAGCAAGGGCG	*sfiI*	Amplification of *gfp* (f)
SI35	AACGACGACGGCCGCGTTGGCCCTTGTACAGCTCGTCCATGC	*sfiI*	Amplification of *gfp* (r)
SK109	TTCGGCCATCTAGGCCTGTGGATATGAGTGGTAGGTTGG	*sfiI*	Amplification of the *scp2* left border (r) (S. Kreibich)
SK110	CGCTCAAACGCAGTGGGTGGAAG	/	Amplification of the *scp2* left border (f) (S. Kreibich)
SR91	CATGGCGTGGTCGCACCCGCAGTTCGAGAAGGCCTCGCCCTACCCCTA	/	Oligo assembly: *ncoI-Strep-HA-sfiI-sfiI-notI* (f)
SR92	CGACGTGCCCGACTACGCCGGCCTGAGTGGCCACTGTACGAGGCCAACGCGGCCCCTAAGC	/	Oligo assembly: *ncoI-Strep-HA-sfiI-sfiI-notI* (f)
SR93	TAGTCGGGCACGTCGTAGGGGTAGGGCGAGGCCTTCTCGAACTGCGGGTGCGACCACGC	/	Oligo assembly: *ncoI-Strep-HA-sfiI-sfiI-notI* (r)
SR94	GGCCGCTTAGGGGCCGCGTTGGCCTCGTACAGTGGCCACTCAGGCCGGCG	/	Oligo assembly: *ncoI-Strep-HA-sfiI-sfiI-notI* (r)
SR95	GATCCGGCCTGAGTGGCCACTGTACGAGGCCAACGCGGCCCGGCGTCGT	/	Oligo assembly: *ncoI-sfiI-sfiI-HA-Strep-notI* (f)
SR96	ACCCCTACGACGTGCCCGACTACGCCGCCTCGCCCTGGTCGCACCCGCAGTTCGAGAAGTAAGC	/	Oligo assembly: *ncoI-sfiI-sfiI-HA-Strep-notI* (f)
SR97	CACGTCGTAGGGGTACGACGCCGGGCCGCGTTGGCCTCGTACAGTGGCCACTCAGGCCCC	/	Oligo assembly: *ncoI-sfiI-sfiI-HA-Strep-notI* (r)
SR98	GGCCGCTTACTTCTCGAACTGCGGGTGCGACCAGGGCGAGGCGGCGTAGTCGGG	/	Oligo assembly: *ncoI-sfiI-sfiI-HA-Strep-notI* (r)
SR116	TAGATGTCGGGCCTGAGTGGCCCAATGTCTGACTTCAAGTCCAAGG	*sfiI*	Amplification of *scp2* (f)
SR117	CTACGATCAGGCCGCGTTGGCCTTAGAGCTTGGCCTTCTGG	*sfiI*	Amplification of *scp2* (r)

SR135	AAAGAACACCGGACTTGG	/	qPCR primer, amplifies *ppi* (r)
SR136	ACATCGTCAAGGCTATCG	/	qPCR primer, amplifies *ppi* (f)
SR137	CTTCGGCATTGTTGAGGGTTTG	/	qPCR primer, amplifies *gapdh* (f)
SR138	TCCTTGGCTGAGGGTCCGCT	/	qPCR primer, amplifies *gapdh* (r)
SR168	CCATCAACCTCTCCGATGAC	/	qPCR primer, amplifies *scp2* (f)
SR169	GCATGATGTTGCCCTTGAC	/	qPCR primer, amplifies *scp2* (r)
SR281	ATCGTCGGTGGTACCGTGCTCGCTCATTGATGTTC	*acc65I*	Amplification of the *scp2* promoter (f)
SR282	AAGCATGACGCGGCCGCTTAGAGCTTGGCCTTCTGG	*notI*	Amplification of the *scp2* gene and promoter sequence (f)
SR300	ACCCAGTCACCATGGTGTGGATATGAGTGGTAGG	*ncoI*	Amplification of the *scp2* promoter (r)
SR322	GGTCTAGGCCTGAGTGGCCATGCATTCGCTGTAATG	*sfiI*	Amplification of the *scp2* right border (f)
SR323	ATCGGCTCTACTTGCTCTAC	/	Amplification of the *scp2* right border (r)
SR334	CCAACCTACCACTCGGATCCAAATCTAGAACAATGTCTGAC	*bamhI, xbaI*	Mutagenic primer that inserts restriction sites into the *scp2* promoter sequence (f)
SR335	GACTGGATCCATGGTGAGCAAGGGCGAGG	*bamhI*	Amplification of *gfp* (f)
SR336	AGTCTCTAGAGGTGGCGATCGAGCGCTTGTACAGCTCGTCC	*xbaI*	Amplification of *gfp* (r)
SR338	CTCAAGTCCCAGAAGGCCGCGGCCTAAGCGGCCGCCCGGCTGCAG	/	Mutagenic primer that changes the *scp2* PTS1 from AKL to AAA (f)
SR341	GATCCATGAGAGCCGTGCTCTCGCTCAACA	/	Oligo assembly: *bamhI-SP-HA-Strep-xbaI* (f)
SR342	TGACCAAGCTGCTCGCCTTGTTGCTGGTCATCCTGCCGAT	/	Oligo assembly: *bamhI-SP-HA-Strep-xbaI* (f)
SR343	ACTTGTCGCCGTTCAGGCCTGGTCGCACCCGCAGTTCGAG	/	Oligo assembly: *bamhI-SP-HA-Strep-xbaI* (f)
SR344	AAGGCCTCGCCCTACCCCTACGACGTGCCCGACTACGCCT	/	Oligo assembly: *bamhI-SP-HA-Strep-xbaI* (f)
SR345	CGAGCAGCTTGGTCATGTTGAGCGAGAGCACGGCTCTCATG	/	Oligo assembly: *bamhI-SP-HA-Strep-xbaI* (r)
SR346	TGAACGGCGACAAGTATCGGCAGGATGACCAGCAACAAGG	/	Oligo assembly: *bamhI-SP-HA-Strep-xbaI* (r)
SR347	GTAGGGCGAGGCCTTCTCGAACTGCGGGTGCGACCAGGCC	/	Oligo assembly: *bamhI-SP-HA-Strep-xbaI* (r)
SR348	CTAGAGGCGTAGTCGGGCACGTCGTAGGG	/	Oligo assembly: *bamhI -SP-HA-Strep-xbaI* (r)
SR387	ACGACCACTCAGTCTAGACTTGTACAGCTCGTCCATGC	*xbaI*	Amplification of *gfp/mcherry* (f)

SR388	TGCACGTTCGTATCTAGAATGGTGAG CAAGGGCGAGG	*xbaI*	Amplification of *gfp/mcherry* (r)
SR390	GATCCATGAGAGCCGTGCTCTCGCTC AACATGACCAAGCTGCTCG	*bamhI*	Oligo assembly: *bamhI-SP-bamhI* (f)
SR391	CCTTGTTGCTGGTCATCCTGCCGATAC TTGTCGCCGTTCAGGCCG	/	Oligo assembly: *bamhI-SP-bamhI* (f)
SR392	TGACCAGCAACAAGGCGAGCAGCTT GGTCATGTTGAGCGAGAGCACGGCTC TCATG	/	Oligo assembly: *bamhI-SP-bamhI* (r)
SR393	GATCCGGCCTGAACGGCGACAAGTAT CGGCAGGA	*bamhI*	Oligo assembly: *bamhI-SP-bamhI* (r)
SR435	CATATG**TGGAGCCACCCGCAGTTCG AAAAA**TCGGGCTCTGACTTCAAGTCC AAGG	*ndeI*	Amplification of *scp2*, inserts N-terminal **Strep-tag** (f)
SR436	GGATCCTTAGAGCTTGGCCTTCTGGG	*bamhI*	Amplification of *scp2* (r)
SR457	TACTTTCTCGAGAATAGGAACTTCTG GCCATCTAGGCCGGTGCGTAGGTGAT CAAGG	*sfiI*	Amplification of the *um11277* left border (r) (Drag&Drop)
SR458	GTAACGCCAGGGTTTTCCCAGTCACG ACGAATATTCCTGTCTCGGTATCATG AAC	*sspI*	Amplification of the *um11277* left border (f) (Drag&Drop)
SR459	TTCTCGAGAAAGTATAGGAACTTCTG GCCTGAGTGGCCGTTCGGCATGCTGT CTGCTGC	*sfiI*	Amplification of the *um11277* right border (f) (Drag&Drop)
SR460	GCGGATAACAATTTCACACAGGAAAC AGCAATATTGGTTCTAACTCGACCGA CAG	*sspI*	Amplification of the *um11277* right border (r) (Drag&Drop)
SR461	GTAACGCCAGGGTTTTCCCAGTCACG ACGAATATTAACTAAAGCGGGCACA AAGC	*sspI*	Amplification of the *um01850* left border (r) (Drag&Drop)
SR462	GCGGCCGCAATTGTCACGCCATGGTG GCCATCTAGGCCCGTGATGGGTTAAG CTCC	*sfiI*	Amplification of the *um01850* left border (f) (Drag&Drop)
SR463	GCGGATAACAATTTCACACAGGAAAC AGCAATATTATCGTCTCAAGTGCGTT AGG	*sspI*	Amplification of the *um01850* right border (r) (Drag&Drop)
SR464	CTGTAGGAGTGCGGCCGCATTAATAG GCCTGAGTGGCCTTGGCGTAGTTGGC GTATCG	*sfiI*	Amplification of the *um01850* right border (f) (Drag&Drop)
SR507	AACGACGACGCGGCCGCTTAGGCCG AGCCGAGCTTGGCCTTCTGG	*notI*	Amplification of *scp2*, adds the amino acids GSA to the Scp2 C-terminus (r)
SR510	AACGACGACGCGGCCGCTTAGAGCTT GGCGAGCTTGGCCTTCTGG	*notI*	Amplification of *scp2*, adds the amino acids AKL to the Scp2 C-terminus (r)
SR526	GTCGTCGTTGGTACCCCTGTCTCGGT ATCATGAAC	*kpnI*	Amplification of the *um11277* gene and promoter sequence (f)
SR527	AACGACGACGCGGCCGCTCAAAGCCT TGCGCGATCG	*notI*	Amplification of the *um11277* gene and promoter sequence (r)
SR528	GTCGTCGTTGGTACCAGCTGAGCAGT GATGGTTTG	*kpnI*	Amplification of the *um01850* gene and promoter sequence (f)
SR529	AACGACGACGCGGCCGCCTAGAGCTT TGCAACCCTGG	*notI*	Amplification of the *um01850* gene and promoter sequence (r)
SR530	GGCGACCTTGATCACTCTAGACTACG CACCATGTCC	*xbaI*	Mutagenic primer that inserts restriction sites into the *um11277* promoter sequence (f)

SR574	TCCATCCGGATGGCTCGAGTTTTTCAGCAAAATATTTTGAGCTATCGAGCAGTAGG	*sspI*	Amplification of the *um01892* left border (f) (Gibson cloning)
SR575	TACTTTCTAGAGAATAGGAACTTCTGGCCATCTAGGCCGATGATGCTCGATCAGTAGAGG	*sfiI*	Amplification of the *um01892* left border (r) (Gibson cloning)
SR576	TCTAGAAAGTATAGGAACTTCTGGCCTGAGTGGCCATGTTTGTTGCGAATCAGAATAC	*sfiI*	Amplification of the *um01892* right border (f) (Gibson cloning)
SR577	CTGAGAATATTGTAGGAGATCTTCTAGAAACCGGGACAGTCGATGAGGTTGAGTAG	*sspI*	Amplification of the *um01892* right border (r) (Gibson cloning)
SR594	GCTTAACCCATCACGGGATCCAAATCTAGAATGGCTAAAAACGAAGAACACG	*bamhI*, *xbaI*	Mutagenic primer that inserts restriction sites into the *um01850* promoter sequence (f)
SR715	GATCGGATCCATGTGGTCGCACCCGCAG	*bamhI*	Amplifies the sequence *Strep-HA-gfp-AKL* (f)
SR716	GATCGCGGCCGCCTAGAGCTTGGCCTTGTACAGCTCGTCCATGC	*notI*	Amplifies the sequence *Strep-HA-gfp-AKL* (r)
SR717	GTGCTTAGTTCTAGAATGGTGAGCAAGGGCGAGG	*xbaI*	Amplifies the sequence *mcherry-AKL* (f)
SR718	ACTAAGCACGCGGCCGCTTAGAGCTTGGCCTTGTACAGCTCGTCC	*notI*	Amplifies the sequence *mcherry-AKL* (r)
SR743	TGCTTAGTGGTACCCCTCGAGCCTCGTCCCTG	*kpnI*	Amplification of the *um01779* promoter (f)
SR744	ACTAAGCACCATGGCTTGAGCGAAGGTTTACC	*ncoI*	Amplification of the *um01779* promoter (r)
SR745	TGCTTAGTGATATCTATGTATGTGCAGAACAG	*ecoRV*	Amplifies the construct P_{rsp3}-*mcherry-HA* (f)
SR746	ACTAAGCAGATATCCTCATGTTTGACAGCTTATC	*ecoRV*	Amplifies the construct P_{rsp3}-*mcherry-HA* (r)

[1] Restriction sites encoded within the primer sequence are underlined
[2] The oligo nucleotide either hybridizes with the sense-strand (r) or the antisense strand (f) of the respective gene.

4.3.4 Plasmids

In the following chapter the progenitor plasmids used in this study and plasmids constructed for this study are described. All plasmids were verified via enzymatic restriction prior to use. After the insertion of PCR amplified fragments the nucleotide sequences were analyzed by sequencing (Eurofins Genomics, Ebersberg/Munich, Germany). Primers used for sequencing are not listed separately. Sequencing always covered parts of the backbone, the transition sites as well as the inserts. All plasmids carry a resistance cassette mediating resistance to ampicillin.

4.3.4.1 Plasmids for the expression in *E. coli*

pET21a(+) (Novagen, Darmstadt, Germany):
The plasmid allows the IPTG-induced expression of genes in *E. coli*. The vector contains the *lac* operator downstream of the *T7* promoter. The pET21a(+) vector carries an N-terminal T7-tag sequence and an optional C-terminal His-tag sequence. The gene of interest can be inserted into the multiple cloning side between the two tags. The transcription is terminated by the *T7* terminator. pET21a(+) confers ampicillin resistance.

pSR226 (*P_{T7}-Strep-scp2*):
The pET21a(+) derivative was used for the expression of N-terminal Strep affinity tagged Scp2 in *E. coli*. The plasmid contains the *scp2* sequence excluding introns under the control of the *T7* promoter and the *T7* terminator. The plasmid was generated by amplifying the *scp2* sequence from *U. maydis* cDNA using the primer pair SR435/SR436. The resulting 0.4 kb fragment was inserted by blunt-end cloning into the intermediate vector pJET-stuffer. From there the fragment was extracted using NdeI/BamHI and inserted into the vector pET21a(+). pSR226 confers ampicillin resistance.

pPR-IBA102 (IBA, Goettingen, Germany):
The plasmid allows the IPTG-induced expression of genes in *E. coli*. The vector can be utilized for the expression of N-terminal Twin-Strep affinity tagged fusion proteins. The expression cassette is under transcriptional control of the strong bacteriophage T7 promoter. pPR-IBA102 confers ampicillin resistance.

pPR-IBA102-Tin2dSP (S. Tanaka, unpublished):
The pPR-IBA102 derivative was used for the expression of N-terminal Twin-Strep affinity tagged Tin2 in *E. coli*. The plasmid contains the *tin2* (*um05302*) sequence, excluding the first 75 nucleotides encoding for the Tin2 signal peptide, under the control of the *T7* promoter and the *T7* terminator. pPR-IBA102-Tin2dSP confers ampicillin resistance.

4.3.4.2 Plasmids for the generation of stable *U. maydis* mutants

Progenitor plasmids:

p123 (Aichinger *et al.*, 2003):
Used as a progenitor construct. The plasmid contains the *gfp* gene under the control of the *otef* promoter and the *nos* terminator. For stable integration, the plasmid was cut using SspI and integrated into the *U. maydis ip* locus.

p123-mCherry-HA #4 (T. Brefort, unpublished):
The p123 derivative allows the expression of *mcherry* with a C-terminal HA affinity tag under the control of the *otef* promoter and the *nos* terminator. For stable integration, the plasmid was cut using SspI and integrated into the *U. maydis ip* locus.

pCRII-TOPO (Invitrogen, Karlsruhe):
The topoisomerase I-activated pCRII-TOPO vector was used as a progenitor construct for the cloning of PCR products. The vector can be used for blue-white screenings.

pHwtFRT (Y. Khrunyk *et al.*, 2010):
The plasmid pHwtFRT contains the *hph* gene (hygromycin resistance) under the control of the *U. maydis hsp70* promoter and the *nos* terminator flanked by directly repeated FRT sites and *sfi*I sites at both ends.

pJET-stuffer (K. O. Schink and M. Bölker, personal communication):
The pJET1 derivative (Fermentas, St. Leon-Rot) is a linearized plasmid for the cloning of blunt-end DNA-fragments. Re-circularized pJET1 expresses a lethal restriction enzyme (Eco47IR) after transformation into *E. coli*. pJET-stuffer contains a 0.6 kb protective sequence within the orf of *eco47IR* which allows the amplification in *E. coli*. For the cloning of DNA fragments, the protective sequence can be excised with EcoRV and replaced by the sequence of interest.

pLW174 (*P_{rsp3}-gfp*) (L. Wang, unpublished):
The p123 derivative allows the expression of *gfp* under control of the native *rsp3* promoter and the *nos* terminator. For stable integration, the plasmid can be linearized using AgeI and integrated into the *U. maydis ip* locus.

pMF1-n (Brachmann *et al.*, 2004):
Used as a progenitor construct. The plasmid contains a nourseothricin resistence cassette. The *nat1* gene from *Streptomyces noursei (Krügel et al., 1988)* is expressed under the control of the *gapdh* promoter (from *U. maydis*) and the *cyc1* terminator (from *S. cerevisiae*). The 1.4 kb resistance cassette can be extracted using SfiI.

pMM001 (pHwtFRT-G) (M. Moretti, unpublished):
The plasmid pMM001 contains the *neo* resistance gene (geneticin resistance) under the control of the *otef* promoter and the *cyc1* terminator. The resistance cassette can be extracted by using SfiI.

pSI14 (*P_{otef}-gfp-HA-Strep*)
(S. Krombach, unpublished):
The p123 derivative allows the expression of *gfp* as a C-terminal Strep-HA affinity tagged fusion under the control of the *otef* promoter and the *nos* terminator. The plasmid was generated by amplifying the *gfp* gene from the plasmid p123 by using the primer pair SI34/SI35. The resulting 0.7 kb fragment was cut using SfiI and inserted into the vector pSR60. For stable integration, the plasmid was cut using SspI and integrated into the *U. maydis ip* locus.

pRS426 (Christianson *et al.*, 1992):
The plasmid was used as an intermediate vector for "Drag&Drop cloning in yeast" (Jansen *et al.*, 2005). pRS426 is a yeast high-copy-number (20 copies per

cell) shuttle vector based on the backbone of the phagemid vector pBluescript II SK (+). The plasmid contains an URA3 selection marker for yeast and the ampicillin resistance marker for the amplification in *E. coli*.

pSR57 (*P_{otef}-Strep-HA-sfiI*)
(S. Reißmann, unpublished):
The p123 derivative was used as a progenitor plasmid for N-terminal Strep-HA tagged gene fusions. The plasmid allows the expression of the respective genes under the control of the *otef* promoter and the *nos* terminator. The *Strep-HA* sequence is followed by two *sfiI* restriction sites that can be used for inserting the respective gene of interest. pSR57 was generated by *de novo* synthesis (oligo assembly) of a di-codon optimized *Strep-HA-sfiI-sfiI* construct using the primers SR91-SR94. The resulting fragment was integrated into the plasmid p123 (NcoI/NotI).

pSR60 (*P_{otef}-sfiI-HA-Strep*)
(S. Reißmann, unpublished):
The p123 derivative was used as a progenitor plasmid for C-terminal Strep-HA tagged gene fusions. The plasmid allows the expression of the respective genes under the control of the *otef* promoter and the *nos* terminator. Upstream of the *Strep-HA* sequence are two *sfiI* restriction sites that can be used for inserting the respective gene of interest. pSR60 was generated by *de novo* synthesis (oligo assembly) of a di-codon optimized *SfiI-SfiI-HA-Strep* construct using the primers SR95-SR98. The resulting fragment was integrated into the plasmid p123 (NcoI/NotI).

pSR67 (*P_{otef}-Strep-HA-scp2*)
(S. Reißmann, unpublished):
The p123 derivative was used as a progenitor plasmid for the generation of pSR115. The plasmid allows the expression of *scp2* (*um11938*) with an N-terminal Strep-HA affinity tag under the control of the *otef* promoter and the *nos* terminator. pSR67 was generated by amplifying the *scp2* gene sequence including introns from *U. maydis* gDNA using the primer pair SR116/SR117. The 1.0 kb PCR product was cut using SfiI and inserted into the plasmid pSR57. For stable integration, the plasmid was cut using SspI and integrated into the *U. maydis ip* locus.

pSR115 (*P_{scp2}-Strep-HA-scp2*)
(S. Reißmann, unpublished):
The p123 derivative was used as a progenitor plasmid for the generation of pSR162. The plasmid allows the expression of *scp2* as an N-terminal Strep-HA affinity tagged fusion under the control of the native *scp2* promoter and the *nos* terminator. The plasmid was generated by amplifying the 1.0 kb promoter sequence of *scp2* from *U. maydis* gDNA using the primer pair SR281/SR300. The PCR product was cut using Acc65I/NcoI and integrated into the plasmid pSR67. For stable integration, the plasmid was cut using SspI and integrated into the *U. maydis ip* locus.

pSR141 (*P_{scp2}-(xbaI-bamhI)-scp2*)
(S. Krombach, unpublished):
The p123 derivative was used as a progenitor plasmid for the generation of pSR140. The plasmid allows the expression of the *scp2* gene under the control of the native *scp2* promoter and the *nos* terminator. pSR141 was generated by performing a QuikChange™ PCR with the mutagenic primer SR334 on the progenitor plasmid pSR110. SR334 integrates an *xbaI* and a *bamhI* restriction site into the plasmid sequence between the *scp2* promoter and *scp2*. For stable integration, the plasmid was cut using SspI and integrated into the *U. maydis ip* locus.

pSR146 (*P_{scp2}-scp2(AKL/AAA)*)
(S. Krombach, unpublished):
The p123 derivative was used as a progenitor plasmid for the generation of pSR162. The plasmid allows the expression of cytoplasmic Scp2. The *scp2* gene is expressed under the control of the native *scp2* promoter and the *nos* terminator. The C-terminal *scp2* PTS1 sequence was mutated from the amino acids AKL to AAA by QuikChange™ PCR using the mutagenic primer SR338 on the template plasmid pSR110. For stable integration, the plasmid was cut using SspI and integrated into the *U. maydis ip* locus.

pSR149 (*p123 P_{scp2}-gfp-scp2*)
(S. Krombach, unpublished):
The p123 derivative allows the expression of Scp2 as an N-terminal GFP fusion under the control of the native *scp2* promoter and the *nos* terminator. The plasmid was generated by amplifying *gfp* from the plasmid pSI14 using the primer pair SR335/SR336. The PCR product was cut using XbaI/BamHI and inserted into the vector pSR141. For stable integration, the plasmid was cut using SspI and integrated into the *U. maydis ip* locus.

pSR175 (*P_{scp2}-SP-Strep-HA-gfp-scp2*)
(S. Krombach, unpublished):
The p123 derivative was used to express a fluorescently labeled Scp2 fusion protein that is targeted to the secretory pathway. The plasmid contains an N-terminal Strep-HA affinity tagged *gfp-scp2* construct under the control of the native *scp2* promoter and the *nos* terminator. The fusion protein Strep-HA-GFP-Scp2 further contains the signal peptide from the effector protein Stp1 at its N-terminus which targets the protein to the secretory pathway. pSR175 was generated by amplifying the *gfp* gene from the vector p123 by using the primer pair SR387/SR388. The PCR product was cut using XbaI and subsequently inserted into the plasmid pSR140.

pSR176 (*P_{scp2}-SP-Strep-HA-mcherry-scp2*) (S. Krombach, unpublished):
The p123 derivative resembles the vector pSR175 but contains a *mcherry* gene instead of a *gfp* gene. pSR176 was generated by amplifying the *mcherry* gene from the plasmid p123-mCherry-HA #4 using the primer pair SR387/SR388 which insert *xbaI* restriction sites. The PCR product was cut using XbaI and subsequently inserted into the plasmid pSR140. For stable integration, the plasmid was cut using SspI and integrated into the *U. maydis ip* locus.

pSR262 (*P_{scp2}-scp2-GSA)* (this thesis):
The p123 derivative was used as a progenitor plasmid for the generation of pSR261. The plasmid contains the *scp2* gene under the control of the native *scp2* promoter and the *nos* terminator and allows the cytoplasmic expression of Scp2. pSR262 was generated by performing a PCR with the primer pair SR281/SR507 on the plasmid pSR141 to achieve the primer based insertion of the three additional amino acids GSA at the Scp2 C-terminus. The 2.0 kb PCR product was cut using Acc65I7/NotI and reintegrated into the plasmid pSR141. For stable integration, the plasmid was cut using SspI and integrated into the *U. maydis ip* locus.

pSR285 (*$P_{um11277}$-um11277*) (this thesis):
The p123 derivative was used as a progenitor plasmid for the generation of pSR288. The plasmid allows the expression of *um11277* under control of the native *um11277* promoter and the *nos* terminator. The plasmid was generated by amplifying the *um11277* promoter and gene sequence from *U. maydis* gDNA using the primer pair SR526/SR527. The 1.9 kb PCR product was cut using KpnI/NotI and integrated into the plasmid p123. For stable integration, the plasmid was cut using AgeI and integrated into the *U. maydis ip* locus.

pSR286 (*$P_{um01850}$-um01850*) (this thesis):
The p123 derivative was used as a progenitor plasmid for the generation of pSR336. The plasmid allows the expression of *um01850* under control of the native *um01850* promoter and the *nos* terminator. pSR286 was generated by amplifying the *um01850* promoter and gene sequence from *U. maydis* gDNA using the primer pair SR528/SR529. The 1.6 kb PCR product was cut using KpnI/NotI and inserted into the plasmid p123. For stable integration, the plasmid was cut using SspI and integrated into the *U. maydis ip* locus.

pSR288 (*$P_{um11277}$-(xbaI)-um11277*) (this thesis):
The p123 derivative was used as a progenitor plasmid for the generation of pSR291. The plasmid allows the expression of *um11277* under control of the native *um11277* promoter and the *nos* terminator. The C-terminal part of the *um11277* promoter sequence contains an *xbaI* restriction site for the generation of mCherry or GFP fusion constructs. The plasmid was generated by performing a QuikChange™ PCR with the mutagenic primer SR530 on the plasmid pSR285. For stable integration, the plasmid was cut using AgeI and integrated into the *U. maydis ip* locus.

pSR291 (*$P_{um11277}$-gfp-um11277*) (this thesis):
The p123 derivative allows the expression of *um11277* as an N-terminal GFP fusion under the control of the native *um11277* promoter and the *nos* terminator. The plasmid was generated by extracting the sequence encoding *gfp* from pSR175 using XbaI and inserting it into pSR288. For stable integration, the plasmid was cut using AgeI and integrated into the *U. maydis ip* locus.

pSR336 (*$P_{um01850}$-(bamhI-xbaI)-um01850*) (this thesis):
The p123 derivative was used as a progenitor plasmid for the generation of pSR337. The plasmid allows the expression of *um01850* under control of the native *um01850* promoter and the *nos* terminator. pSR336 was generated by performing a QuikChange™ PCR on the plasmid pSR286 using the mutagenic primer SR594 which inserts a *bamhI* and *xbaI* restriction site in the C-terminus of the *um01850* promoter sequence. For stable integration, the plasmid was cut using SspI and integrated into the *U. maydis ip* locus.

pSR337 (*$P_{um01850}$-gfp-um01850*) (this thesis):
The p123 derivative was used for the visualization of the Scp2 paralog Um01850. The plasmid allows the expression of *um01850* as an N-terminal GFP fusion under the control of the native *um01850* promoter and the *nos* terminator. The plasmid was generated by excising the *gfp* encoding sequence from pSR149 using BamHI/XbaI and inserting it into the plasmid pSR336. For stable integration, the plasmid was cut using SspI and integrated into the *U. maydis ip* locus.

pSR393 (*P_{rsp3}-mcherry-HA*) (this thesis):
The p123 derivative was used for the expression of cytoplasmic mCherry upon penetration. The plasmid allows the expression of *mcherry* as a C-terminal HA affinity tagged fusion under the control of the penetration specific *rsp3* (*um03274*) promoter and the *nos* terminator. pSR393 was generated by extracting the *mcherry-HA* construct from p123-mCherry-HA #4 using BamHI/NotI and inserting the 0.8 kb fragment into the vector pLW174. For stable integration, the plasmid was linearized using AgeI and integrated into the *U. maydis ip* locus.

pSR398 (*P_{scp2}-gfp-um11277*) (this thesis):
The p123 derivative was used for the localization of the Scp2 paralog Um11277 in *U. maydis*. The plasmid contains a *gfp-um11277* fusion construct under the control of the native *scp2* promoter and the *nos* terminator. pSR398 was generated by excising *um11277* from the plasmid pSR291 using XbaI/NotI and inserting it into the vector pSR149. For stable

integration, the plasmid was cut using SalI and integrated into the *U. maydis ip* locus.

pSR421 (P_{am1}-*gfp*) (this thesis):
The p123 derivative was used as a marker construct for appressorium formation. The plasmid contains a single *gfp* under the control of the *um01779* (*am1*) gene promoter and the *nos* terminator (Mendoza-Mendoza *et al*., 2009). pSR421 was generated by amplifying the 1.2 kb *um01779* promoter sequence from *U. maydis* gDNA by using the primer pair SR743/SR744. The PCR product was cut using KpnI/NcoI and inserted into the vector p123.

Plasmids used in this thesis:

JF1742 (J. Freitag, AG M. Bölker):
The plasmid was used to visualize peroxisomes. The plasmid contains the gene *gfp* under control of the *etef* promoter and the *nos* terminator. The *gfp* gene was C-terminally fused with the peroxisomal targeting sequence 1 from the gene *gapdh*. The targeting sequence consists of the 36 nucleotides at the C-terminus of *gapdh* and encode for the 12 amino acid PTS1 sequence: MAQKDSAGASRL. For stable integration, the plasmid was cut using SspI and integrated into the *U. maydis ip* locus.

pMM69 (M. Moretti, unpublished):
The plasmid was used for the appressorium specific expression of cytoplasmic mCherry. It contains the gene *mcherry* under control of the *am1* (*um01799*) promoter (Mendoza-Mendoza et al., 2009) and the *nos* terminator. pMM69, further, encodes for a neomycin resistance gene (*neo*) under the control of the *otef* promoter and the *cyc1* terminator. The *mig2-6* locus encoded in the vector was used for the integration of the plasmid into the *U. maydis* genome. For stable integration, the plasmid was linearized in the *mig2-6* locus using EcoNI and integrated into the *U. maydis mig2-6* locus.

pomChrab5a (Schuster *et al*., 2011):
The plasmid was used to visualize early endosomes. The p123 derivative contains a *mcherry-rab5a* fusion construct under control of the *otef* promoter and the native *rab5a* terminator. The plasmid, further, encodes for a nourseothricin resistance cassette upstream of the *otef* promoter. For stable integration, the plasmid was cut using HpaI and SspI, the resulting 5.3 kb fragment was extracted and integrated ectopically into the *U. maydis* genome.

pSR110 (P_{scp2}-*scp2*) (F. Ahrens, unpublished):
The p123 derivative served as a complementation construct for *um11938* (*scp2*) deletion strains. The plasmid contains the gene *scp2* under the control of the native *scp2* promoter and the *nos* terminator. pSR110 was generated by amplifying the promoter and gene sequence of *scp2* from *U. maydis* gDNA using the primer pair SR281/SR282. The resulting 1.9 kb PCR product was cut using Acc65I/NotI and integrated into the plasmid p123. For stable integration, the plasmid was cut using SspI and integrated into the *U. maydis ip* locus.

pSR140 (P_{scp2}-*SP-Strep-HA-scp2*)
(S. Krombach, unpublished):
The p123 derivative was used for the signal peptide (SP) mediated secretion of Scp2 via the classical secretory pathway. The plasmid allows the expression of *scp2* as an N-terminal Strep-HA affinity tagged fusion under the control of the native *scp2* promoter and the *nos* terminator. The *scp2* gene is N-terminally fused to the signal peptide sequence of the effector Stp1. The *SP-HA-Strep* construct was generated *de novo* (oligo assembly) with the primers SR341-SR348 and integrated into the plasmid pSR141 (BamHI/XbaI). For stable integration, the plasmid was cut using SspI and integrated into the *U. maydis ip* locus.

pSR162 (P_{scp2}-*Strep-HA-scp2 (AKL/AAA)*)
(S. Krombach, unpublished):
The p123 derivative was used for the expression of cytoplasmic Scp2. The plasmid allows the expression of *scp2* as an N-terminal Strep-HA affinity tagged fusion under the control of the native *scp2* promoter and the *nos* terminator. The C-terminal *scp2* PTS1 sequence AKL was replaced by the mutant version AAA to prohibit peroxisomal targeting. pSR162 was generated by extracting the 0.8 kb mutated version of the *scp2* C-terminus from the plasmid pSR146 by using the restriction enzymes MluI and NotI. The mutated *scp2* C-terminus extracted from pSR146 subsequently replaced the non-mutated C-terminus of *scp2* in the progenitor plasmid pSR115. For stable integration, the plasmid was cut using SspI and integrated into the *U. maydis ip* locus.

pSR209 (TOPOΔ*um11938*-Hyg) (this thesis):
The construct was generated for the deletion of the gene *um11938* (*scp2*). The plasmid contains the *hph* gene (hygromycin resistance) under the control of the *U. maydis hsp70* promoter and the *nos* terminator flanked by the 1.0 kb left border and 1.1 kb right border of the gene *um11938* (*scp2*). The left and right border of *scp2* were amplified using the primer pairs SK109/SK110 and SR322/SR323, respectively. In an intermediate cloning step both flanks were integrated into the pCRII-TOPO vector. The hygromycin resistance cassette was extracted from the plasmid pHwtFRT using SfiI. The right *scp2* border was extracted from its intermediate vector by using the restriction enzymes SfiI and NotI. The intermediate vector harboring the left *scp2*

border linearized with SfiI and NotI served as the backbone vector. A three fragment ligation was performed to assemble the deletion construct pSR209. For stable integration, the plasmid was cut using EcoRI and the resulting 4.9 kb fragment was extracted and transformed into the *U. maydis* genome.

pSR239 (Δ*um11277*-Neo)
(S. Reißmann, unpublished):
Generated for the deletion of the gene *um11277*. The plasmid contains the geneticin resistance cassette under the *otef* promoter and the *cyc1* terminator flanked by the 1.1 kb left border and the 1.1 kb right border of the gene *um11277*. The left and right border of *um11277* were amplified using the primer pairs SR457/SR458 and SR459/SR460, respectively. The geneticin resistance cassette was extracted from the plasmid pMM001 using SfiI. The yeast vector pRS426 linearized using BamHI/KpnI served as a backbone. pSR239 was assembled using "Drag&Drop cloning in yeast" (Jansen *et al*., 2005). For stable integration, the plasmid was cut using SspI and the resulting 4.2 kb fragment was extracted and transformed into the *U. maydis* genome.

pSR241 (Δ*um01850*-Nat)
(S. Reißmann, unpublished):
The construct was generated for the deletion of the gene *um01850.* The plasmid contains the *nat* gene (nourseothricin resistance (ClonNat)) under the control of the *gapdh* promoter and the *cyc1* terminator flanked by the 1.1 kb left border and 1.1 kb right border of the gene *um01850*. The left and right border of *um01850* were amplified using the primer pairs SR461/SR462 and SR463/SR464, respectively. The nourseothricin resistance cassette was extracted from the plasmid pMF1-n using SfiI. The yeast vector pRS426 linearized using BamHI/KpnI served as a backbone. pSR241 was assembled using "Drag&Drop cloning in yeast" (Jansen *et al*., 2005). For stable integration, the plasmid was cut using PvuII and the resulting 3.7 kb fragment was extracted and transformed into the *U. maydis* genome.

pSR261 (P_{scp2}-*SP-scp2-GSA*) (this thesis):
The p123 derivative was used for the signal peptide (SP) mediated secretion of Scp2 via the classical secretory pathway. The plasmid contains the *scp2* gene under the control of the native *scp2* promoter and the *nos* terminator. The *scp2* gene is N-terminally fused to the signal peptide sequence of the effector Stp1. The C-terminal *scp2* PTS1 sequence AKL is masked by the addition of the three amino acids GSA. The Stp1 signal peptide was generated by *de novo* synthesis (oligo assembly) using the primers SR390-SR393 and integrated into the vector pSR262 (BamHI). For stable integration, the plasmid was cut using SspI and integrated into the *U. maydis ip* locus.

pSR263 (P_{scp2}-*scp2-AKL)* (this thesis)*:*
The p123 derivative contains the *scp2* gene under the control of the native *scp2* promoter and the *nos* terminator and allows the cytoplasmic expression of Scp2. pSR263 was generated by performing a PCR with the primer pair SR281/SR510 on the plasmid pSR141 to achieve the primer based insertion of the three additional amino acids AKL at the Scp2 C-terminus. The 2.0 kb PCR product was cut using Acc65I7/NotI and reintegrated into the plasmid pSR141. For stable integration, the plasmid was cut using SspI and integrated into the *U. maydis ip* locus.

pSR319 (P_{scp2}-*gfp-scp2-GSA*) (this thesis):
The p123 derivative was used to analyze the localization of GFP-Scp2 with a masked peroxisomal targeting sequence. The plasmid contains a *gfp-scp2* fusion construct under the control of the native *scp2* promoter and the *nos* terminator. The peroxisomal targeting sequence of *scp2* is thereby masked by the addition of the three amino acids GSA at the C-terminus of the protein. The plasmid was generated by amplifying the *gfp* gene from the plasmid pSI14 using the primer pair SR387/SR388. After restriction of the 0.8 kb PCR product with XbaI the fragment was integrated into the plasmid pSR261. For stable integration, the plasmid was cut using SspI and integrated into the *U. maydis ip* locus.

pSR324 (Δ*um01892*-Neo)
(S. Reißmann, unpublished)
The pJET derivative was generated for the deletion of the mitochondrial *U. maydis* isocitrate lyase *um01892*. The plasmid contains the *neo* gene (geneticin resistance) under the control of the *otef* promoter and the *cyc1* terminator flanked by the 0.7 kb left border and 0.9 kb right border of the gene *um01892*. The left and right border of *um01892* were amplified using the primer pairs SR574/SR575 and SR576/SR577, respectively. The geneticin resistance cassette was extracted from the plasmid pMM001 using SfiI. pSR324 was assembled using the DNA assembly method described in Gibson *et al.*, 2009 . For stable integration, the plasmid was cut using SspI and the resulting 4.0 kb fragment was integrated into the *U. maydis* genome.

pSR395 (P_{scp2}-*hscp2*) (this thesis):
The p123 derivative was used for the expression of human *scp2* (*hscp2*). The plasmid allows the expression of *hscp2* under control of the native *U. maydis scp2* promoter and the *nos* terminator. The synthesized codon optimized version of *hscp2* contained *xbaI*/*notI* restriction sites that were used to insert the sequence into the vector pSR141. For stable integration, the plasmid was cut using SspI and integrated into the *U. maydis ip* locus.

pSR396 (P_{scp2}-*YLscp2*) (this thesis):
The p123 derivative was used for the expression of *Yarrowia lipolytica* Scp2 (*YLscp2*). The plasmid

allows the expression of *YLscp2* under control of the native *U. maydis scp2* promoter and the *nos* terminator. The synthesized codon optimized version of *YLscp2* contained *xbaI*/*notI* restriction sites that were used to insert the sequence into the vector pSR141. For stable integration, the plasmid was cut using SspI and integrated into the *U. maydis ip* locus.

pSR397 (P_{scp2}-*Strep-HA-gfp-AKL*) (this thesis):
The p123 derivative was used to express peroxisomal GFP. The plasmid allows the expression of *gfp* as an N-terminal Strep-HA affinity tagged fusion under the control of the native *scp2* promoter and the *nos* terminator. In addition, the peroxisomal targeting sequence 1 (AKL) was fused to the C-terminus of *gfp*. The plasmid was generated by amplifying a *Strep-HA-gfp* fusion construct from the plasmid pSR175 using the primer pair SR715/SR716. The PCR product was cut using BamHI/NotI and subsequently inserted into the plasmid pSR141. For stable integration, the plasmid was cut using SspI and integrated into the *U. maydis ip* locus.

pSR399 (P_{scp2}-*gfp-um01850*) (this thesis):
The p123 derivative was used for the localization of the Scp2 paralog Um01850 in *U. maydis*. The plasmid contains a *gfp-um01850* fusion construct under the control of the native *scp2* promoter and the *nos* terminator. pSR399 was generated by excising *um01850* from the plasmid pSR337 using XbaI/NotI and inserting it into the vector pSR149. For stable integration, the plasmid was cut using SspI and integrated into the *U. maydis ip* locus.

pSR404 (P_{cmu1}-*scp2*) (this thesis):
The p123 derivative was used for the overexpression of the gene *scp2* during plant infections. The plasmid contains the gene *scp2* under the control of the *cmu1* (*um05731*) promoter and the *nos* terminator. pSR404 was generated by amplifying the 0.9 kb *cmu1* promoter sequence from *U. maydis* gDNA using the primer pair OLL248/OLL294. The PCR product was cut using KpnI/BamHI and integrated into the vector pSR141. For stable integration, the plasmid was cut using SspI and integrated into the *U. maydis ip* locus.

pSR405 (P_{cmu1}-*mcherry-AKL*) (this thesis):
The p123 derivative was used for the overexpression of peroxisomal mCherry during plant infections. The plasmid contains *mcherry* with a C-terminal peroxisomal targeting sequence 1 (AKL). The fusion construct is under the control of the *cmu1* (*um05731*) promoter and the *nos* terminator. pSR405 was generated by amplifying *mcherry-AKL* from the plasmid pSR176 by using the primer pair SR717/SR718. The PCR product was cut using XbaI/NotI and integrated into the vector pSR404. For stable integration, the plasmid was cut using SspI and integrated into the *U. maydis ip* locus.

pSR422 ($P_{um01779}$-*gfp* P_{rsp3}-*mcherry-HA*) (this thesis):
The p123 derivative was used as a marker construct for appressorium formation and penetration of the plant cuticle, simultaneously. The plasmid allows the appressorium specific expression of a single *gfp* under the control of the *um01779* (*am1*) gene promoter and the *nos* terminator (Mendoza-Mendoza *et al.*, 2009). In addition pSR422 expresses a *mcherry* gene under the control of the native *rsp3* (*um03274*) promoter and the *nos* terminator that contains a C-terminal HA-affinity tag. *Rsp3* is upregulated upon penetration and therefore allows the visualization of successful penetration events. pSR422 was generated by amplifying the P_{rsp3}-*mcherry-HA* construct from the plasmid pSR393 using the primer pair SR745/SR746. The 2.7 kb PCR product was cut using EcoRV and inserted into the vector pSR421. For stable integration, the plasmid was cut using AgeI and integrated into the *U. maydis ip* locus.

pSR429 (P_{scp2}-*scp2*-Nat) (this thesis):
The p123 derivative served as a complementation construct for *scp2* deletion strains. The plasmid contains the gene *scp2* under the control of the native *scp2* promoter and the *nos* terminator. The plasmid further contains a *nat* resistance gene that confers resistance to nourseothricin. The plasmid was generated by extracting the resistance cassette from the plasmid pMF1-n (Brachmann *et al.*, 2004) by using PvuII and the subsequent insertion into the vector pSR110. For stable integration, the plasmid was cut using SspI and integrated into the *U. maydis ip* locus.

4.4 Microbiological and cell biology methods

4.4.1 Competent cell preparation and transformation of *E. coli*

Competent cell preparation and chemical transformation of *E. coli* were modified from Cohen *et al*. (1972). *E. coli* TOP10 cells were grown in 20 ml dYT medium at 37 °C and 200 rpm overnight. Cultures were diluted 1:50 in 100 ml dYT medium supplemented with $MgCl_2$ and $MgSO_4$ to a final concentration of 10 mM, respectively. Cultures were grown to a cell density OD_{600} of about 0.6 at 37 °C and 200 rpm for 2-2.5 hours. The culture was transferred to a microcentrifuge tube, incubated on ice for 30 min and centrifuged at 4 °C for 8 min at 3,000 rpm. The supernatant was discarded and cells were resuspended in 33 ml (1/3 of the initial volume) of pre-chilled RF1-solution and incubated for 30 min on ice at 4 °C. The suspension was centrifuged at 4 °C for 8 min at 3,000 rpm and the supernatant was discarded. *E. coli* cells were resuspended in 1/20 culture volume (5 ml) of pre-chilled RF2-solution and incubated for 30 min on ice. Finally, 50 µl aliquots of competent cell suspension in pre-chilled 1.5-ml microcentrifuge tubes were kept on ice for direct use or stored at - 80 °C for later use.

RF1-solution

100 mM Rubidium chloride
50 mM Manganese(II) chloride x $4H_2O$
30 mM Kaliumacetate*
10 mM Calcium chloride x $2H_2O$
15 % (w/v) Glycerol
pH was adjusted to 5.8 (glacial acetic acid) and sterile filtered (Store at 4 °C)

* Use 1 M Kaliumacetate solution adjusted to pH=7.5 using glacial acetic acid.

RF2-solution

10 mM MOPS*
10 mM Rubidium chloride
75 mM Calcium chloride x $2H_2O$
15 % (w/v) Glycerol
pH was adjusted to 5.8 (NaOH) and sterile filtered (Store at 4 °C)

* Use 0.5 M MOPS adjusted to pH=6.8 using NaOH

To transform *E. coli*, 50 µl aliquots of competent *E. coli* cells were thawed on ice for 2 min. Subsequently, up to 10 µl DNA solution was added (re-transformation of plasmids: 1 µl of a plasmid miniprep; ligation: 1 µl of ligation product), gently mixed and incubated on ice for 20 min. *E. coli* cells were then heat shocked at 42 °C for 30 sec and immediately cooled on ice. For the recovery of the cells, 600 µl dYT medium (without antibiotics) was added and cells were incubated on a heating block (Eppendorf, Wesseling-Berzdorf) at 850 rpm for 15 min (for transformations using ampicillin) at 37 °C. The *E. coli* cell suspension was centrifuged at 6,000 rpm. Half of the supernatant was discarded and the cells were resuspended in the remaining

supernatant. Finally, the entire cell suspension was plated on YT-agar containing the appropriate selective antibiotic and incubated at 37 °C overnight.

4.4.2 Protoplast preparation and transformation of *U. maydis*

Protoplast preparation and transformation of *U. maydis* strains was performed as described in Schulz *et al*. (1990). *U. maydis* cells were incubated overnight in 50 ml $YEPS_{light}$ medium at 28° C and 200 rpm. In the morning, cell cultures were diluted to a cell density of OD_{600} 0.1-0.2 and grown to a cell density of OD_{600} 0.8-1.0. Cells were harvested by centrifugation at 4 °C for 5 min at 3,000 rpm, washed in 25 ml SCS and resuspended in 2 ml SCS containing 3.5 mg/ml Novozyme. Cells were incubated for about 5 min at room temperature to digest the cell wall, which was monitored under the microscope. Afterwards, *U. maydis* cells were washed three times with 10 ml ice cold SCS and centrifuged at 2,400 rpm for 5 min at 4 °C. This was followed by an additional wash with ice cold STC and centrifugation step. Finally, protoplast pellets were carefully resuspended in 0.5 ml of ice cold STC, and 60 µl of protoplasts were aliquoted into pre-chilled 1.5 ml microcentrifuge tubes for immediate use, or stored at -80 °C for later use.
For transformation of protoplasts, 1 µl heparin (stock solution 15 mg/ml) and up to 10 µl of DNA (3-5 µg) was added to the protoplast aliquot and incubated for 10 min on ice. Afterwards, 500 µl STC/PEG were added to the protoplasts, mixed gently, and incubated for another 15 min on ice. The transformation mix was plated on regeneration agar plates. Transformed colonies appeared after 4-6 days and were singled out on PD-agar plates containing the appropriate antibiotic. Single colonies were picked and saved on PD-plates. The regeneration agar plates were prepared by first pouring a bottom phase with 10 ml regeneration agar containing the appropriate concentration of antibiotic (twice the amount as indicated for solid medium plates, chapter 4.2.2). Subsequently, 10 ml of regeneration agar without antibiotics was poured on top and solidified.

SCS solution

Solution 1
0.6 % (w/v) Sodium citrate * $2H_2O$ (f. c. 20 mM)
18.2 % (w/v) Sorbitol (Sigma S-1876) (f. c. 1 M)

Solution 2
0.4 % (w/v) Citric acid * H_2O (f. c. 20 mM)
18.2 % (w/v) Sorbitol (Sigma S-1876) (f. c. 1 M)

Dissolve each in H_2O_{bid}. Add enough solution 2 to solution 1 to reach pH 5.8 (The ratio between solution 1 to solution 2 is approximately 5:1) and autoclave.

STC solution	10 mM Tris-Cl, pH 7.5 100 mM $CaCl_2$ 1 M Sorbitol Dissolve in H_2O_{bid} and sterile filtrate
STC/PEG solution	60.0 % (v/v) STC-buffer 40.0 % (w/v) PEG (Sigma P-3640) Mix and sterile filtrate
Regeneration agar *U. maydis*	1.0 % (w/v) Yeast-Extract (Bacto) 0.4 % (w/v) Peptone (Bacto) 0.4 % (w/v) Sucrose (Roth) 18.22 % (w/v) Sorbitol (Sigma S-1876) (f.c. 1 M) 1,5 % (w/v) Agar (Bacto) Dissolve in H_2O_{bid} and autoclave.

4.4.3 Induction of filaments and appressoria *in vitro*

The *in vitro* induction of *b*-filaments and appressoria was accomplished as described in Mendoza-Mendoza (2009) with slight changes. Parafilm M (Pechiney Plastic Packaging, Chicago/USA) was used as an artificial hydrophobic surface. Respective strains were grown until reaching OD_{600} 0.6 and subsequently harvested by centrifugation at 3,500 g for 5 min at room temperature. The supernatant was discarded and the cell pellet diluted in 2 % $YEPS_{light}$ (in H_2O_{bid}) to an OD_{600} of 0.1. The cell suspension was supplemented with 100 µM 16-hydroxy hexadecanoic acid (HFA) (Sigma-Aldrich, Munich, Germany). For this a 10 mM stock solution (in ethanol) was diluted to a ratio of 1:100 with the cell suspension. Subsequently, the cell suspensions were sprayed on parafilm (EcoSpray, Roth, Karlsruhe) with a drops size of not more than 1 mm. The microscope slide was transferred to a petri dish containing moist filter paper, sealed with parafilm and incubated at 28 °C for 16 h.

Prior to the microscopic analysis sporidia that remained on the parafilm surface were washed off with water. For the microscopic quantification of filaments expressing the appressorial AM1-marker (Mendoza-Menodza *et al*., 2009), the percentage of AM1-positive hyphae was determined relative to the total number of filaments. For the microscopic quantification of appressoria, the percentage of AM1-positive filaments displaying a thickening of the hyphal tip was determined relative to the total number of AM1-positive filaments.

For the induction of SG200 *b*-filaments in liquid culture using HFA the cells were cultivated as described earlier for applying cells on parafilm. One milliliter of the cell suspension was filled into a 2 ml reaction tube and supplemented with 500 µM 16-hydroxyhexadecanoic acid (HFA). The cells were incubated on a rotating incubator for 16 hours and forming filaments were analyzed by microscopy.

For the induction of *b*-filaments in AB33 derivatives the strains were cultivated to an OD_{600} of 0.6 in $YEPS_{light}$ and harvested by centrifugation at 3,500 g for 5 min at RT. Subsequently, the cells were washed twice with pre-warmed (28 °C) H_2O_{bid} to remove residual medium. The cell pellet was dissolved in pre-warmed (28 °C) NM-glc. The formation of *b*-filaments was observed microscopically after approximately 6 hours of incubation at 28 °C.

4.5 Molecular biological methods

4.5.1 *In vitro* modification of nucleic acids

Standard molecular biology methods, such as purification, precipitation, electrophoresis of DNA or molecular cloning techniques were performed following the protocols described in Ausubel *et al.* (1987) and Sambrook *et al.* (1989). The concentration of nucleic acids was determined by photometry. Photometric measurements were performed using a NanoDrop 2000 spectrophotometer (Life Technologies GmbH, Darmstadt, Germany). The purity of nucleic acids was determined by the ratio of A260 to A280. For purified DNA and RNA samples, the A260 to A280 ratios were about 1.8 and 2.0, respectively.

4.5.1.1 Restriction of DNA

The restriction of DNA fragments was accomplished by type II restriction endonucleases (NEB, Frankfurt, Germany) for 2-16 hours at enzyme specific temperatures. The amount of utilized DNA ranged from 0.5 µg to 5 µg.

Restriction reaction:

0.5 - 5 µg	plasmid DNA
2 µl	enzyme specific 10x NEB-Puffer 1-4
2 µl	10x BSA
0.5 U	restriction endonuclease

20 µl vol. with H_2O_{bid}

4.5.1.2 Dephosphorylation of linear DNA

Dephosphorylation was done whenever necessary in the cloning procedure such as blunt-end ligations. Dephosphorylation using the Antarctic phosphatase (NEB, Frankfurt, Germany) was utilized to remove phosphate groups from the 5´-ends of DNA fragments.

Dephosphorylation reaction:

20 µl	restriction reaction
10 µl	Antarctic phosphatase buffer
25 U	Antarctic phosphatase

100 µl vol. with $H_2O_{bid.}$

4.5.1.3 Ligation of DNA fragments

For the ligation of DNA fragments the T4 DNA ligase (NEB, Frankfurt, Germany) was used. In ligation reactions in which a linearized vector was ligated with an insert the corresponding DNA was used in a molar ratio of 1:3. For three-fragment-ligations a molar ratio of 1:1:1 was used. Commonly 20 µl reactions contained one U of T4 DNA ligase and were incubated for at least 2 hours at room temperature or overnight in a 16 °C circulating water bath. The amount of utilized DNA ranged from 50 ng to 2 µg.

4.5.1.4 Self-assembly reaction of oligonucleotides (Oligo assembly)

For the *de novo* synthesis of small DNA fragments a self-assembly reaction was performed. Overlapping primers were designed that covered the whole length of the desired construct. The primers positioned at the 3´and 5´ end of the assembled construct were designed to generate cohesive ends allowing the immediate ligation of the construct into the target vector without previous restriction enzyme treatment. For the oligo assembly reaction all oligos were phosphorylated in separate reactions using the Polynucleotide kinase (PNK) (NEB, Frankfurt, Germany) for 30 min at 37 °C. The PNK was subsequently inactivated for 20 min at 65 °C.

Phosphorylation reaction (oligo assembly):

5 µl	oligo (100 pmol/µl)
5 µl	T4 DNA ligase buffer (10x)
39 µl	H_2O_{bid}
1 µl	Polynucleotide kinase (NEB, Frankfurt, Germany)

The phosphorylated oligos were combined in a single reaction tube and denatured at 99 °C for 15 min on a heating block. Subsequently, the heating block was turned off and the reaction was slowly cooled down to room temperature. The following annealing reaction combined the phosphorylated oligos and simultaneously mediated the insertion into the respective vector backbone. The backbone vector was linearized with restriction enzymes beforehand and dephosphorylated to prevent self-ligation (chapter 4.5.1.2). The ligation reaction was incubated overnight in a 16 °C circulating water bath.

Ligation reaction (Oligo assembly):

5 µl	linearized vector backbone
1 µl	denatured oligo mix
1 µl	T4 DNA ligase buffer (10x)
39 µl	H_2O_{bid}
1 µl	T4 DNA ligase

4.5.1.5 *De novo* synthesis of genes

The sequence of the human Scp2 precursor protein (GenBank: M55421.1), the protein sequence of the mature human 13 kDa Scp2 protein (PDB: 1QND_A) and the *Yarrowia lipolytica* Scp2 sequence (accession number P80547.4) were derived from the "National Center of Biotechnology Information" (NCBI; http://www.ncbi.nlm.nih.gov/). The synthetic genes of *hscp2* and *YLscp2* were purchased from Eurofins Genomics (Ebersberg/Munich, Germany). The respective gene sequences were ordered as optimized versions for *U. maydis* codon usage and contained an *xbaI* restriction site at the 5` and a *notI* restriction site at the 3` end for further cloning. The following restriction sites were determined to be excluded from the synthesized sequences: *bamhI*, *notI* (except at the 3` end), *pvuII*, *sspI* and *xbaI* except at the 5` end). The *de novo* synthesized genes were subcloned and delivered in a standard vector from which they were excised using XbaI and NotI.

4.5.1.6 Site-directed mutagenesis

The site-specific mutation of plasmids was performed using the "QuikChange Lightning Site-Directed Mutagenesis Kit" (Agilent Technologies, Santa Clara, CA, USA) which allows the insertion of site-specific mutations in double-stranded plasmids. The mutagenesis was performed according to the manufacturers' specifications.

4.5.1.7 Polymerase Chain Reaction (PCR)

To amplify DNA fragments for cloning or for analytical purposes, the polymerase chain reaction (PCR) was used (Mullis *et al.*, 1986). Depending on the application, different polymerases were used. For amplification of DNA for cloning purposes Phusion DNA polymerase was used (Thermo Fisher Scientific, Dreieich, Germany). For Colony-PCR/Screens on a large scale the RedMix premix (Bioline, Luckenwalde, Germany) was used which contained the Taq polymerase. Typical approaches for the individual polymerases are described below. The respective PCR program used is represented by the following scheme: Initial denaturation - [denaturation - annealing - elongation] x number of cycles - final elongation. The elongation time was chosen based on the expected fragment size and rate of synthesis by the polymerase used. The annealing and melting temperatures of the oligonucleotides were calculated by the Clone Manager 9.0 software (Sci-Ed Software, Cary / USA) *in silico*. All PCR reactions were performed in a TProfessional Standard Gradient Thermocycler (Biometra, Goettingen, Germany).

PCR approach with Phusion DNA polymerase:

50 ng	template DNA
250 µM	dNTPS (1:1:1:1 ratio)
1 µM	primer 1 (binds on 5´Strand)
1 µM	primer 2 (binds on 3´Strand)
0.5 U	Phusion DNA polymerase

1x concentrated HF buffer (Thermo Fisher Scientific, Dreieich, Germany)
Program: 98 °C/1 m - [98 °C/10 s - 55-74 °C/20 s - 72 °C/20 s/kb] x 35 cycles - 72 °C/7 m

PCR approach with RedMix:

1.25 µM	primer 1 (binds on 5´Strand)
1.25 µM	primer 2 (binds on 3´Strand)
1 µl	cell culture or 1 colony (fungi or bacteria)

1x concentrated RedMix (Bioline)
Program: 94 °C/2 m - [94 °C/10 s -50-65 °C/30 s - 72 °C/30 s/kb] x 35 cycles - 72 °C/8 m

4.5.1.8 TOPO TA cloning

TOPO TA cloning of DNA fragments containing blunt ends or A-overhangs into the pCRII-TOPO vector was performed using the TOPO® TA Cloning® Kit (Invitrogen, Karlsruhe, Germany) according to the manufacturers' specifications.

4.5.1.9 Sequencing of nucleic acids

All generated plasmids and constructs were checked by sequencing for unwanted mutations. Sequencing was carried out by Eurofins MWG Synthesis (Ebersberg/Munich, Germany) using the cycle sequencing method (dideoxy chain termination/cycle sequencing) on ABI370XL sequencing machines.

4.5.2 Isolation of nucleic acids

4.5.2.1 Isolation of plasmid DNA from *E. coli*

E. coli plasmid preparation was performed using the Qiaprep® Spin Miniprep Kit (250) (Qiagen GmbH, Hilden, Germany) according to the manufacturers' specifications.

4.5.2.2 Isolation of genomic DNA from *U. maydis*

U. maydis cultures were grown in $YEPS_{light}$ at 28 °C and 200 rpm for 24 hours. Individual clones were saved by dropping 6 µl of each culture on PD plates. *U. maydis* cultures were then transferred to 2 ml microcentrifuge tubes containing 300 mg glass beads, and centrifuged for 1 min at 13,000 rpm. The supernatant was discarded and 400 µl of *Ustilago*-lysis buffer and 500 µl of TE-phenol/chloroform was added. The cells were lysed on a Vibrax-VXR shaker (IKA) at 1,600 rpm for 15-20 min. Next, samples were centrifuged for 15 min at

13,000 rpm and 400 µl of the aqueous phase was transferred to a new 1.5-ml microcentrifuge tube. Afterwards, 1 ml of ethanol was added and mixed by inverting 2-3 times. Subsequently the mixtures were centrifuged for 5 min at 13,000 rpm. The DNA pellets were washed once with 75 % ethanol as described above. Then, the pellets were centrifuged for an additional minute at 13,000 rpm and leftover ethanol was removed using a pipette. Finally, DNA pellets were dissolved in 50 µl TE buffer containing 50 µg/ml RNase A, and incubated in a heating block at 55 °C with gentle shaking for 15 min. Genomic DNA was stored at 4 °C.

***Ustilago*-lysis buffer**	2% (v/v) Triton X-100 1% (w/v) SDS 100 mM NaCl 10 mM Tris-Cl, pH 8.0 1 mM EDTA dissolve in H_2O_{bid}
TE-phenol/chloroform	Mixture of phenol (in TE-buffer) and chloroform in a 1:1 ratio

4.5.2.3 Isolation of genomic DNA from infected plant material

For the isolation of total gDNA from *U. maydis* infected plant tissue, *U. maydis* strains were injected into the corn variety Early Golden Bantam as described in chapter 4.7.2 (Pathogenicity assays). Infected leaf tissue was harvested at 20 hours post infection (hpi), 2 and 4 days post infection (dpi) in three independently conducted experiments (biological replicates). Approximately 2.0 cm of the third leaf (below the injection holes) of the infected plants was dissected, washed in 0.1 % Tween-20 (to remove sporidia remaining on the leaf surface) and rinsed in H_2O_{bid}. The 20 hpi leaf samples were excluded from the washing step. Subsequently, infected leaf tissue was patted dry with a paper towel. The samples were stored in 50 ml Falcon™ tubes, flash frozen in liquid nitrogen, and directly used for gDNA isolation or stored at -80 °C for later use. Genomic plant and fungal DNA was extracted from approximately 300 µl grinded leaf material following the protocol in chapter 4.5.2.2 (Isolation of genomic DNA from *U. maydis*) starting with the *Ustilago*-lysis buffer and TE-phenol/chloroform step (without glass beads). gDNA samples were stored at +4 °C until use.

4.5.2.4 Isolation of *U. maydis* RNA from axenic culture

TRIzol® Reagent (Thermo Scientific, Darmstadt, Germany) was used for total RNA isolation according to the manufacturers' specifications. 4 ml of *U. maydis* overnight culture with a cell density of OD_{600} 1.0 was harvested in a 2 ml microcentrifuge tube by centrifugation at 3,500 g for 5 min. The pellet was dissolved in 1.0 ml Trizol reagent, 300 mg of glass beads were added to the pellet and homogenized by shaking for 30 min on a Vibrax-VXR shaker (IKA) set to

1,600. Afterwards, tubes were centrifuged for 10 min at 12,000 g and 4 °C and the supernatant was transferred to an RNase free tube. 200 µl of chloroform were added to the samples before inverting them several times followed by an incubation step for 5 min at room temperature. Samples were centrifuged for 15 min at 12,000 g and 4 °C. The upper aqueous phase (500 µl) was transferred to a new 1.5 ml RNase free microcentrifuge tube. RNA was precipitated by addition of 500 µl isopropanol and incubated for 10 min at room temperature. After centrifugation for 10 min at 12,000 g and 4 °C the pellets were washed once with 1 ml of 75 % ethanol (freshly prepared using nuclease-free water), centrifuged for 5 min at 7,500 g and air dried. Finally, the RNA pellet was dissolved in 45 µl RNase free water and incubated with its lid open in a heating block for 10 min at 55 °C with gentle shaking. To remove traces of DNA, RNA samples were treated with Turbo DNase (Ambion/Applied Biosystems, Darmstadt, Germany). 5 µl of 10x Turbo DNase buffer and 0.5 µl of Turbo DNase were added to 45 µl of total RNA. Samples were incubated for 30 min at 37 °C. Another 0.5 µl of Turbo DNase was added followed by another 30 min of incubation at 37 °C. 5 µl of DNase inactivation reagent was added to the samples with subsequent incubation at room temperature for 5 min (mix in between). Samples were centrifuged for 90 sec at 10,000 rpm. The supernatant was transferred into a new RNase-free PCR-tube and the samples were stored at -80 °C until further use.

4.5.2.5 Isolation of RNA from infected plant material

Infected leaf tissue was harvested as described in chapter 4.5.2.3 (Isolation of genomic DNA from infected plant material). Samples were taken at 20 hours post infection, 2, 4 and 12 days post infection. Plants infected with water ("mock") served as control. Total RNA was extracted from frozen homogenized infected plant tissue using Trizol reagent (Invitrogen, Karlsruhe, Germany) as described in the previous section 4.5.2.4 (Isolation of *U. maydis* RNA from axenic culture). For plant samples a 1.5 ml reaction tube filled up to 0.3-0.5 ml with grinded plant material was used starting the protocol by adding 1 ml TRIzol® Reagent without using glass beads.

4.5.3 Separation and detection of nucleic acids

4.5.3.1 Agarose gel electrophoresis

For a size-specific separation of nucleic acids, agarose gel electrophoresis was performed. Due to its negative charge, DNA migrates towards the anode if an electric field is applied. Concentrations of agarose gels varied between 0.8 and 2 %, depending on the size of the fragments to be separated. The respective amount of agarose was dissolved in 1x TAE or 0.5x TBE buffer by boiling. After the solution was cooled down to 60 °C ethidium bromide (f. c.

0.25 µg/ml) was added. The gel was poured into an appropriate gel casting tray. After solidifying, the gel was transferred into a running gel chamber and covered with 1x TAE or 0.5x TBE buffer, respectively. Samples were mixed with non-denaturing loading dye, loaded on the gel at the side of the cathode, and separated by applying a constant voltage of 90-120 V. DNA was visualized by UV irradiation at 254 nm on a UV table (2UV™ Transilluminator, UVP, Upland, CA, USA) and documented using the UV solo TS Imaging system (Biometra GmbH, Goettingen, Germany).

50x TAE buffer	2 M Tris base 2 M acetic acid 50 mM EDTA, pH 8.0 dissolve in H_2O_{bid}
5x TBE buffer	440 mM Tris base 440 mM boric acid 10 mM EDTA, pH 8.0 dissolve in H_2O_{bid}
6x DNA loading dye	50 % (w/v) sucrose 0.1 % (v/v) bromophenol blue dissolve in 1x TE buffer, sterile filtrate and store at 4 °C
1x TE buffer	10 mM Trizma® base (Sigma T6066) 1 mM Na_2-EDTA $*2H_2O$ dissolve in H_2O_{bid}, adjust pH to 8.0 with HCl and autoclave

4.5.3.2 DNA blotting and hybridization (Southern analysis)

For southern analysis (Southern, 1975) 10 µl of genomic DNA, isolated as described in chapter 4.5.2.2 (Isolation of genomic DNA from *U. maydis*), was treated with the respective restriction enzyme overnight. Digestions were separated on a 1x TAE 0.8 % agarose gel for 3 h at 90 V. After depurination with 0.25 M HCl for 15 min, which is a prerequisite for transfer of large DNA fragments, and subsequent neutralization with 0.4 M NaOH for 15 min, the DNA was transferred from the gel to a nylon membrane (Hybond-N+, GE Healthcare Munich, Germany). The transfer was facilitated by a capillary blot with 0.4 M NaOH as transfer solution. Afterwards the membrane was placed into a hybridization tube, in which all subsequent steps were carried out. The membrane was pre-hybridized with 20 ml Southern hybridization buffer in a hybridization oven (HB-1000 Hybridizer, UVP) at 68 °C for 30 min. Immobilized DNA was detected by DIG-labeled probes. To generate such probes, DNA fragments were labeled with PCR-based DIG-High Prime labeling mix (Roche Diagnostics, Mannheim, Germany) according to the manufacturers' specifications. Probes were denatured at 95 °C for 10 min and added to 20 ml pre-warmed Southern hybridization buffer (68 °C). After prehybridization of

the membrane with Southern hybridization buffer, the buffer was removed and the prepared probe solution was added. Hybridization was performed at 68 °C for at least 6 h. Afterwards the membrane was washed twice with Southern wash buffer at 68 °C for 15 min. All subsequent steps were performed at room temperature. The membrane was washed once with DIG wash buffer for 5 min followed by a 30 min blocking step with DIG2 buffer. After blocking, 20 ml of the DIG antibody solution was added. Membrane and antibody solution were incubated for 30 min followed by three 15 min washing steps in DIG wash buffer to remove residual antibody. The membrane was equilibrated in DIG3 buffer for 5 min. Subsequently, the membrane was incubated in CDP star solution for 5 min. After an incubation of 15 min at 37 °C, to activate the light emitting reaction, DNA fragments were visualized using X-ray films (AGFA HealthCare, Mortsel, Belgium) and a developer machine (Fuji Medical Film Processor, Fujifilm).

Southern hybridization buffer	50 % (v/v) Na-phosphate buffer, pH 7.0 (f. c. 0.5 M) 35 % (v/v) 20 % SDS dissolve in H_2O_{bid}
Southern wash buffer	10.0 % (v/v) 1 M Na-phosphate buffer, pH 7.0 (f. c. 0.1 M) 5.0 % (v/v) 20 % SDS (f. c. 1 %) dissolve in H_2O_{bid}
1 M Na-phosphate buffer, pH 7.0	Solution 1: 1 M Na_2HPO_4 Solution 2: 1 M $NaH_2PO_4xH_2O$ Add Solution 2 to Solution 1 until pH reaches 7.0 in H_2O_{bid}
DIG wash buffer	0.3 % (v/v) Tween-20 in DIG1
Anti-DIG antibody solution	Anti-DIG AB 1:10,000 in DIG2
DIG1 (1x)	0.1 M maleic acid 0.15 M NaCl dissolve in H_2O_{bid}, adjust pH to 7.5 (NaOH)
DIG2 (1x)	1 % (w/v) milk powder in DIG1
DIG3 (1x)	0.1 M Tris-HCl (pH 9.5) 0.1 M NaCl 50 mM $MgCl_2$ dissolve in H_2O_{bid}, adjust pH to 9.5 (Tris-HCl) and sterile filtrate
CDP-Star Solution	CDP-Star (Roche) 1:100 in 10 ml DIG3

4.5.3.3 Quantitative Real-Time-PCR (qPCR)

For expression analysis of genes total RNA was obtained from axenic culture samples (chapter 4.5.2.4) as well as from infected leaf material (chapter 4.5.2.5). Removal of DNA contaminations from RNA samples was performed with the Turbo DNA-*free* Kit (Thermo Fisher Scientific) according to the manufacturers' specifications. The purity of RNA samples was accessed by determining the ratio of absorbance at 260 nm and 280 nm using the NanoDrop 2000 Spectrophotometer (Life Technologies GmbH, Darmstadt, Germany). A sample ratio of 2.0 is generally accepted as pure RNA. The approximate total amount of RNA was visualized by gel electrophoreses. After removal, the pure RNA was subjected to reverse transcription to generate cDNA from mRNA. mRNA was transcribed into cDNA employing the Super III First Strand Synthesis Super Mix Kit (Invitrogen, Karlsruhe, Germany). Reverse transcription was performed according to the manufacturers' specifications. Each reaction contained 1-3 µg DNase-treated total RNA. Reverse transcription was performed using oligo-d(T)-primers. The synthesized cDNA was diluted with a ration of 1:10 in RNase free water and stored at -80 °C until use.

Quantitative Real-Time-PCR was performed on a Bio-Rad iCycler using the Platinum® SYBR® Green qPCR SuperMix-UDG (Invitrogen, Karlsruhe, Germany) and 1 µl of the diluted cDNA. As a reference dye Fluorescein isothiocyanate (FITC) Sigma-Aldrich (Munich, Germany) was used.

FITC stock solution 1 mM in H_2O_{bid} (Sigma F4274)

FITC working solution 1 µM in H_2O_{bid}

qPCR reaction:

12.5 µl SYBR green
1 µl FIT-C (internal standard)
1 µl cDNA (diluted as described above)
1µl primers (1:1 mixture of the respective primers (10 µM each))
9.5 µl H_2O_{bid}

The Bio-Rad iCycler was run with the following settings: 95 °C/2min - [95 °C/30 s - 62 °C/30 s - 72 °C/30 s] x 45 cycles. The specificity of the reaction was ensured by melting curve calculations after the qPCR run. The determination of threshold cycles was performed with the Bio-Rad Software. Relative expression values were calculated with the $2^{-\Delta\Delta Ct}$ method (Livak and Schmittgen, 2001). The oligonucleotides utilized for the qPCR are listed in chapter 4.3.3.

4.5.3.4 Determination of fungal biomass during plant colonization (Biomass assay)

A biomass assay was performed to analyze the plant colonization process of SG200Δscp2 (SR336) in comparison to SG200. SG200 and SG200Δscp2 infected plant material was harvested as described in chapter 4.5.2.3 (Isolation of genomic DNA from infected plant material). The isolated gDNA was diluted in H_2O_{bid} in two steps. First gDNA concentration was measured using a NanoDrop 2000 Spectrophotometer (Life Technologies GmbH, Darmstadt, Germany) and adjusted to 500 ng in 30 µl. Concentrations were measured once more and adjusted to 25 ng/µl. For the quantification of plant colonization the reference genes *ppi* (fungus) (SR135/SR136) and *gapdh* (plant) (SR137/SR138) were used. The Biomass assay was run on a Bio-Rad iCycler system as described in chapter 4.5.3.3 (Quantitative Real-Time PCR (qPCR)).

qPCR reaction (determination of biomass):

2 µl	gDNA (25 ng/µl)
12.5 µl	SYBRgreen
1.0 µl	FITC
1.0 µl	primer mix (1:1 ratio of forward and reverse primer (10 pmol) for one gene)
8.5 µl	H_2O_{bid}

4.6 Protein and biochemical methods

4.6.1 Purification of proteins expressed in *E. coli*

Recombinant *E. coli* Rosetta™(DE3)pLysS cells (Merck Chemicals GmbH, Darmstadt, Germany) containing plasmids encoding Strep-Scp2 (pSR226) or TwinStrep-Tin2 (pPR-IBA102-Tin2dSP) were grown overnight in a 250 ml baffled flask containing 25 ml dYT medium supplemented with 55 µg/ml chloramphenicol and 100 µg/ml ampicillin at 200 rpm at 37 °C. 10 ml of pre-culture was inoculated into 1 L of pre-warmed fresh medium and grown until OD_{600} absorption reached 0.6-0.8. After addition of 1 mM (f. c.) IPTG the cells were incubated for four hours and subsequently centrifuged for 20 min at 8,000 rpm and 4 °C. All following steps were carried out on ice. The pellet was resuspended in 5 ml 1x PBS per gram of cells and incubated with 1.5 mg lysozyme per gram cells (SIGMA 62970-5G-F) for 30 min on ice. Subsequently, the cells were ruptured by sonication for 9 x 30 sec (40 % duty cycle, output control 4, Branson Sonifier 250; Danbury, USA). Cell debris and intact cells were removed by centrifugation for 20 min at 30,000 g and 4 °C.The supernatant was transferred to a fresh tube and kept on ice until use. Protein samples were sterile filtrated prior to affinity chromatography using a 0.2 µm filter unit (GE Healthcare, Munich, Germany). Protein purification via Strep-affinity chromatography was performed according to the manufacturers`

specifications using a 400 µl Strep-Tactin® Sepharose resin (IBA, GmbH Goettingen, Germany). The final elution step was conducted using six times 100 µl of the elution buffer described in the IBA Strep-tag® Purification Protocol (100 mM Tris-HCl pH 8, 150 mM NaCl, 1 mM EDTA, 2.5 mM desthiobiotin). For subsequent gel filtration chromatography the purified protein was mixed with 6 ml sterile filtrated Buffer W as described in the Strep-tag® Purification Protocol (100 mM Tris-HCl pH 8, 150 mM NaCl, 1 mM EDTA). Gel filtration chromatography was perfomed using a Superdex 75 prep grade column with the dimension 1.6 x 60 cm (EMBL, Heidelberg, Germany) and an ÄKTA FPLC system (GE Healthcare, Munich, Germany). The column was washed with 10 ml Buffer W before loading of the protein sample. 1 ml gel filtration elution fractions were collected separately, peak fractions pooled and concentrated using an Amicon® Ultra-4 Centrifugal Filter Unit (3 K cut-off) (Merck, Darmstadt, Germany) following the user manual. The protein concentration was determined by Bradford assay using Roti®-Quant solution (Carl Roth GmbH, Karlsruhe, Germany) (chapter 4.6.4).

4.6.2 Protein-lipid overlay assay

Membrane Lipid Strips (P-6002) were purchased from Echelon Biosciences (Salt Lake City, USA). The membrane was blocked in PBST-BSA (3 % (w/v) fatty acid-free BSA (Sigma A-7030) in PBST) overnight at 4 °C. The blocking buffer was discarded. The membrane was then incubated in 10 ml PBST-BSA containing 0.5 µg/ml of the indicated protein for 1 hour under gentle agitation. The membrane was washed three times. For antibody treatment the membrane was incubated with a 1:10,000 dilution of primary anti-Scp2 polyclonal antibody (Eurogentec, Seraing, Belgium) or anti-Strep antibody (Strep-Tactin®-HRP, IBA GmbH, Goettingen, Germany) for 1 h. The membrane was washed three times as before, and then incubated with a 1:10,000 dilution of anti-mouse or anti-rabbit secondary antibody (Cell Signaling Technology (NEB), Frankfurt, Germany) for 1 h. Finally, the membrane was washed again three times for 10 min in PBST, and membrane bound protein was detected by enhanced chemiluminescence using the ECL chemiluminescent detection reagent (GE Healthcare, Munich, Germany).

PBS (10x)	0.89 % (w/v) Na_2HPO_4 (f. c. 79 mM) 1.97 % (w/v) KH_2PO_4 (f. c. 145 mM) 0.09 % (w/v) $MgCl_2$ x 6 H_2O (f. c. 5 mM) 0.2 % (w/v) KCl (f. c. 27 mM) 8.0 % (w/v) NaCl (f. c. 1.37 M) Dissolve in H_2O_{bid}, adjust pH to 7.2 (HCl) and autoclave
PBST	0.1 % (v/v) Tween-20 in 1x PBS buffer

4.6.3 Protein isolation from *U. maydis* cultures

For the analysis of protein expression in *U. maydis* cells the respective strains were grown in 50 ml $YEPS_{light}$ to an OD_{600} of 0.6-0.8. The cells were harvested by centrifugation at 3,500 g for 5 min at RT. The cell pellet was transferred into a 2 ml screw cap reaction tube. 300 µl Buffer W (chapter 4.6.1, Purification of proteins expressed in *E. coli*) containing protease inhibitor and approximately 200 µl of silica spheres (Lysing Matrix B Bulk, MP Biomedicals, Irvine, Californien, USA) were added to the cells. The cells were disrupted mechanically using the Fast-Prep®-24 sample preparation system (MP Biomedicals, Irvine, Californien, USA) for 3 times at 6 m/s for 1 min and cooled on ice in between the steps. Cell debris was removed by centrifugation at 300 g for 15 min at 4 °C. The supernatant was transferred into a new reaction tube and the protein concentration was determined by Bradford protein assay as described in chapter 4.6.4 (Protein quantitation assay according to Bradford).

4.6.4 Protein quantitation assay according to Bradford

The quantitation of protein levels was carried out following the method of Bradford (Bradford, 1976) using Roti®-Quant Bradford solution (Carl Roth GmbH, Karlsruhe Germany). To create a calibration curve bovine serum albumin (BSA) was used as standard.

4.6.5 SDS polyacrylamide gel electrophoresis

The separation of proteins was performed by SDS polyacrylamide gel electrophoresis (SDS-PAGE) according to Laemmli (1970). During SDS-PAGE proteins are separated in an electric field according to their size. To achieve separation, proteins were denatured by addition of 1x SDS loading dye and incubation for 10 min at 98 °C. Negatively charged SDS molecules bind to proteins, which leads to a negative charge that correlates with the molecular mass of each protein. After denaturation, samples were loaded on a vertical SDS polyacrylamide gel composed of stacking and separation gel (Mini Protean System, Bio-Rad). The stacking gel facilitates protein concentration before the proteins enter the separation gel. In the separation gel proteins are separated according to their molecular weight, smaller proteins migrate faster than bigger proteins. The higher the concentration of acrylamide, the higher is the density of the meshed molecular network. While gels with high acrylamide concentrations are used for separation of the small proteins, low percentage gels are preferred for the separation of large proteins. As reference for the molecular weight of the separated proteins the PageRuler Prestained Protein ladder (ThermoFisher Scientific) was used. The separation of proteins was performed with a current of 20 mA until proteins were concentrated in the stacking gel followed by 25 mA for separation.

1 SDS gel (10.5 x 11.5 x 1 cm):

Stacking gel (5 %)	0.5 ml 0.5 M Tris-HCl pH 6.8 0.333 ml 30 % Polyacrylamide (PAA) 20 µl 10 % SDS 1.125 ml H_2O_{bid} For the initiation of polymerization: 20 µl 10 % Ammonium persulfate (APS) 2 µl Tetramethylethylenediamine (TEMED)
Stacking gel (15 %)	1.25 ml 1.5 M Tris-HCl pH 8.8 2.49 ml 30 % Polyacrylamide (PAA) 50 µl 10 % SDS 1.17 ml H_2O_{bid} For the initiation of polymerization: 50 µl 10 % Ammonium persulfate (APS) 5 µl Tetramethylethylenediamine (TEMED)
4x SDS-gel loading buffer	10 ml 1.5 M Tris-HCl pH 6.8 30 ml glycerin 6 ml 20 % SDS 5 mg bromophenol blue 3 g DTT (f. c. 400 mM) Fill up to 50 ml with H_2O_{bid}
SDS running buffer	25 mM Tris-HCl, pH 8.0 192 mM glycin 4 mM SDS

4.6.6 Immunological protein detection by chemiluminescence (Western blot)

Proteins separated by SDS-PAGE were transferred to a PVDF nitrocellulose membrane by using the semi-dry Trans-Blot Turbo Transfer System (BioRad, Munich, Germany). The blotting procedure was performed according to the manufacturers' specifications using the Trans-Blot Turbo blotting apparatus as well as the membranes and protein blotting consumables provided for the system. The Bio-Rad preprogrammed protocol “Mixed MW (Turbo) for proteins with a molecular weight ranging from 5-150 kDa (7 min) was used by default. The Transfer was performed at 1.3 A; up to 25 V (one Mini format gel) or at 2.5 A; up to 25 V (two Mini format gels). After the transfer, the membrane was incubated in blocking solution for 1 hour at RT. The blocking solution was replaced with antibody solution containing the primary antibody. The membrane was incubated for approximately 16 hours at 4 °C. Thereafter, the membrane was washed three times for 10 min with TBS-T buffer followed by incubation for 1 hour at RT in TBS-T buffer containing the secondary antibody. The antibodies used in this

study are listed in Table 5. After three more washes with TBS-T buffer for 10 min each, the membrane was incubated for 5 min with ECL chemiluminescent detection reagent (GE Healthcare, Munich, Germany). The blots were sealed in a plastic bag and developed using X-ray films (CEA, Hamburg, Germany) and the Agfa CP 1000 film processor (AGFA HealthCare, Mortsel, Belgium). The exposure time ranged from 1-60 min, depending on the intensity of the signal observed.

TBS-T	50 mM Tris-HCl, pH 7.5 150 mM NaCl 0.1 % (v/v) Tween 20
Blocking solution	5 % (w/v) milk powder in TBS-T
Antibody solution	antibody diluted in 2.5 % (w/v) milk powder in TBS-T

4.6.7 Antibodies

The primary and secondary antibodies used in this study are summarized in table 5. The peptide specific antibody for Scp2 was ordered and generated by Eurogentec (Seraing, Belgium). For the generation of the polyclonal antibody the rabbit "Speedy Mini program" with a 28-day immunisation was selected. The peptide specific antibody was generated against the Scp2 peptide: DLKKNAEAYEGKAKG.

Table 5: Utilized antibodies with the respective dilution and manufacturer information

Antibody	Usage	Manufacturer
Mouse anti-HA	Monoclonal primary antibody derived from mouse for detection of HA-fusion proteins (1:10,000 dilution)	Sigma-Aldrich (Munich, Germany)
Anti-mouse IgG	Horse anti-mouse HRP-linked secondary antibody for detection of primary antibodies derived from mouse (1:10,000 dilution)	Cell Signaling Technology (Leiden, Netherlands)
Rabbit anti-Scp2	Custom anti-peptide specific (DLKKNAEAYEGKAKG) polyclonal primary antibody derived from rabbit for detection of the Scp2 protein (1:10,000 dilution)	Eurogentec (Seraing, Belgium)
Anti-rabbit IgG	Goat anti-rabbit HRP-linked secondary antibody for detection of primary antibodies derived from rabbit (1:10,000 dilution)	Cell Signaling Technology (Leiden, Netherlands)
Anti-Strep	Strep-Tactin® HRP conjugate (Strep-Tactin® labeled with horseradish peroxidase) for detection of Strep-tag® II fusion proteins. (1:4,000 dilution)	IBA GmbH (Goettingen, Germany)

4.6.8 Colony secretion analysis

To assay the secretion of affinity-tagged fusion proteins in *U. maydis* colony secretion assays were performed. To assay secretion, an ECL-nitrocellulose membrane (GE Healthcare, Munich, Germany) was activated in sterile water and placed on CM-glc or NM-glc solid medium. The respective *U. maydis* strains were cultivated in $YEPS_{light}$ to an OD_{600} of 0.6-0.8. To attain equal cell densities for the secretion analysis the OD_{600} was adjusted to 0.6. The sporidia were washed twice in pre-warmed (28 °C) H_2O_{bid} (3,500 g, 5 min, RT) before dissolving the cell pellet in the respective CM-glc or NM-glc liquid medium. The cultures were incubated for one hours at 28 °C to allow the adaption to the new medium. Following this, the cells were concentrated to a cell density of 1.2 before spotting 10 µl of each strain on the nitrocellulose membrane. The plates were sealed with parafilm and incubated at 28 °C overnight. In the morning, the cells were removed from the nitrocellulose under running tap water using a silicone brush. Secreted proteins were detected following the protocol for Western analysis (chapter 4.6.6) starting with the incubation of the membrane in blocking solution.

4.6.9 Recovery of nitrocellulose-bound proteins

The method is based on the protocol from Anderson (Anderson, 1985). To isolate proteins from a nitrocellulose membrane a colony secretion assay was performed as described in chapter 4.6.8. To attain sufficing protein levels for the analysis 500 µl of cell culture were spotted on the nitrocellulose membrane. After incubation overnight the cells were removed as described in chapter 4.6.8 and a 1 cm x 1 cm piece of the membrane previously covered with cells was excised using a scalpel. The membrane was cut into small pieces and transferred into a 2 ml reaction tube. To disintegrate the membrane 1 ml of 100 % acetone was added to the membrane fragments (don´t use cold acetone since this disturbs the disintegration process) and vortexed until the membrane completely dissolved. 13 % of H_2O_{bid} was added and the reaction was inverted several times. After centrifugation at 13,000 rpm for 15 min at RT the supernatant was discarded and the forming pellet was dried at 50 °C for approximately 5 min. Subsequently, the precipitated proteins were dissolved in 50 µl 4x SDS sample buffer, denatured at 98 °C for 10 min and analyzed by SDS-PAGE and Western analysis.

4.6.10 Instant blue staining

For the visualization of proteins after SDS-PAGE gels were stained using the ready to use Coomassie protein stain InstantBlue™ (Expedeon Inc., San Diego, CA, USA) in accordance to the manufacturers' specifications.

4.7 Plant methods

4.7.1 Cultivation of *Z. mays*

For the conducted infection assays of this thesis the maize variant Early Golden Bantam (EGB) (UrbanFarmers, New York City, USA) was used. All corn plants were cultivated in a temperature controlled greenhouse with a light-dark cycle of 28 °C for 14 hours and 20 °C for 10 hours. During the day phase, the illumination intensity was at least 25 kLux - 30 kLux (with additional sunlight up to 90 kLux). For qPCR and biomass experiments, maize plants were grown in a phytochamber (Vötsch Industrietechnik GmbH, Balingen-Frommern, Germany) with the same conditions as described above whereas phytochamber daytime phases included a one hour simulation of sunrise (13 hours +1 hour sunrise) and nighttime phases one hour for the simulation of the sunset (9 hours +1 hour sunset) (ramping). Humidity was set to 60 % during daytime phases and to 40 % during nighttime phases. Four corn grains were sowed per pot. EGB was grown in Fruhstorfer soil type "T" and watered once a day.

4.7.2 Pathogenicity assays

Pathogenicity assays were performed as described in Kämper *et al.*, 2006. For maize (*Zea mays*) infections, cultures of *U. maydis* strains were grown to an OD_{600} of 0.8-1.0 in $YEPS_{light}$, harvested by centrifugation at 3,500 g, 5 min, RT (Heraeus Multifuge 4 KR) and the OD_{600} of each culture was adjusted in H_2O_{bid} to 1.0. Compatible strains were mixed in the ration 1:1. By default, 500 µl of cell suspension was injected into 7-day-old maize seedlings using a syringe. The injection site was chosen to be approximately 0.5 cm above the soil. Disease symptoms were scored according to severity 12 days after plant infection (Kämper *et al.*, 2006).

Table 6: Classification of symptoms of infected maize seedlings

Symptoms	Description
no symptoms	No infection symptoms are visible
chlorosis	The plant displays yellowish discoloration on infected leaves
swelling of the ligula	The plant displays a slight swelling of the ligula
small tumors (< 1 mm)	Only few and/or little tumors (< 1 mm) are visible
normal tumors (> 1 mm)	The biggest tumors visible are > 1 mm
heavy tumors/ stunted growth	The plant displays a change of growth axis as a result of tumor formation
dead plants	The plant died due to the infection with *U. maydis*

4.8 Staining and microscopy

4.8.1 Staining methods

4.8.1.1 Preparation of cells for microscopy

For the analysis of *U. maydis* sporidia and filaments in liquid culture a 2 % agarose pad was placed on a microscope slide (2 % agarose in H_2O_{bid}) to prevent the floating of cells during microscopy.

4.8.1.2 WGA Alexa fluor/Propidium iodide staining

Infected leaf tissue was harvested from maize plants 2 and 4 dpi and discolored in ethanol overnight. The next day, the samples were washed in water before treatment with 10 % KOH at 85 °C for 3-4 h. The leaves were subsequently washed twice with 1 ml 1x PBS (pH 7.4). For visualizing hyphae in the plant vasculature, fungal hyphae were stained with Alexafluor 488, WGA (Invitrogen, Karlsruhe, Germany). Plant cell walls were visualized using Propidium Iodide (Sigma-Aldrich, Munich, Germany). The samples were incubated in WGA/PI staining solution for 30 min. During the incubation the leaves were vacuum infiltrated 3 times 2 min with 2 min break in-between. Following this, the leaves were washed in 1x PBS and analyzed by confocal microscopy using a Leica TCS SP5 confocal microscope.

Propidium iodide stock solution	10 mg/ml PI (Sigma 81845) in 1x PBS (store at 4 °C)
WGA-AF488 stock solution	1mg/ml in H_2O (store at 4 °C in the dark)
WGA/PI staining solution	20 µg/ml Propidium iodide 10 µg/ml WGA-AF488 0.02 % Tween20 in PBS (pH 7.4) (store at 4 °C in the dark)

4.8.1.3 Calcofluor white staining

Calcofluor white binds to chitin, cellulose and other b-1,4-linked carbohydrates and is used for the visualization of plant and fungal cell walls. For staining of leaf samples with calcofluor white, seven days old maize plants were infected with respective *U. maydis* strains. After 16 hours the most inner leave of the plant was isolated and incubated in calcofluor staining solution for 30 sec.

Calcofluor stock solution	10 mg/ml (Sigma F3543) in DMSO (store at -20 °C, protect from light)
Calcofluor staining solution	Calcofluor stock solution was diluted 1:1,000 in H_2O_{bid} (or 0.2 M Tris pH 8)

4.8.1.4 Nile red staining

For the visualization of lipid droplets of *in vitro* induced filaments on parafilm (chapter 4.4.3) the objective slides were washed in water and subsequently placed up-side-down in calcofluor staining solution (chapter 4.8.1.3) for one minute. Following this, the objective slide was dipped in water and placed up-side-down in nile red staining solution for 10 min.

Nile red stock solution	500 µg/ml in acetone (store at -20 °C, protect from light)
Nile red staining solution	Dilute nile red stock solution in a ratio 1:1,000 in 75 % glycerin

4.8.1.5 Filipin staining

For filipin stains the Filipin III from *Streptomyces filipinensis* (Sigma, Munich, Germany) was used. *U. maydis* strains were cultivated to an OD_{600} of 0.6 and harvested by centrifugation at 3,500 g for 5 min at RT. The cell pellet was dissolved in 1x PBS and 1 µl of 5 mg/ml filipin stock solution was added (f. c. 5 µg/ml). The cells were incubated for 5 min in the dark at RT. Subsequently, the cells were centrifuged at 3,500 g for 5 min at RT, the supernatant was discarded and the cell pellet was dissolved to an OD_{600} of 1.2 in fresh 1x PBS.
For visualizing the sterol distribution of *in vitro* induced filaments on parafilm (chapter 4.4.3) the objective slides were washed in water and placed up-side-down in filipin staining solution. After 5 min incubation in the dark the objective slides were dipped in water and analyzed. Filipin fluorescence was visualized using fluorescence microscopy (DAPI channel).

Filipin stock solution	5 mg/ml (Sigma F4767) in DMSO*
Filipin staining solution	5 µg/ml in 1 x PBS

* Filipin is light and oxygen sensitive, therefore the generation and the partition of the stock solution was performed in an oxygen-free environment and under red light conditions. Aliquots of the stock solution were stored at -80 °C and only thawed prior to use.

4.8.1.6 Propidium iodide (PI) /fluorescein diacetate (FDA) staining

For assaying the mortality rate of *U. maydis* filaments on parafilm a PI/FDA stain was performed (Kwolek-Mirek and Zadrag-Tecza, 2014). *In vitro* filaments were induced as described in chapter 4.4.3. The parafilm slides were subsequently washed in water to remove remaining sporidia and placed upside-down in PI/FDA staining solution for 20 min in the dark. To prevent the crushing of cells, the microscope slide was propped up on thin roles of parafilm. PI/FDA fluorescence was examined under a fluorescence microscope. Viable cells displayed green fluorescent while dead cells displayed red fluorescent.

PI stock solution	10 mg/ml PI (Sigma 81845) in 1x PBS (store at 4 °C)

PI staining solution	5 µg/ml PI stock solution 1x PBS
FDA stock solution	1 mg/ml FDA (Sigma F7378) in acetone
FDA staining solution	10 µg/ml FDA stock solution 1x PBS

4.8.2 Microscopy methods

4.8.2.1 Confocal microscopy

For confocal microscopy the Leica TCS SP5 confocal microscope was used and for the processing of images, the Leica Application Suite Advanced Fluorescence (LAS AF) software.

Table 7: Laser and emission wave lengths for confocal microscopy

Fluorecent protein/Fluorophore	Laser	Emission
mCherry	561 (DPSS laser)	610 (600-620) nm
GFP (eGFP)	488 (Argon laser)	507 (497-517) nm
Nile red	488 (Argon laser)	580 (570-590) nm
Fluorescent brightner (Calcofluor white)	405 diode	435 (425-445) nm
AF488	488 (Argon laser)	500-540 nm
PI	561 (DPSS laser)	580-660 nm

4.8.2.2 Epifluorescence and binocular microscopy

Epifluorescence microscopy was performed with a Zeiss Axioplan 2 imaging microscope (Carl Zeiss AG, Oberkochen, Germany). All microscopic observations were done using a CoolSNAP-HQ charge-coupled device camera (Photometrics, Tucson, AZ, USA) controlled by the imaging software MetaMorph (Universal Imaging, Downingtown, PA, USA). Binocular images were taken using a Leica M165FC binocular microscope (Leica Microsystems, Wetzlar, Germany).

4.9 Bioinformatic analyses

4.9.1 Databases, servers and softwares

U. maydis gene and protein sequences were derived from the PEDANT 3 database (http://pedant.gsf.de/). The prediction of non-classical secreted proteins was performed using the SecretomeP 2.0 Server (http://www.cbs.dtu.dk/services/SecretomeP/). Amino acid sequence alignments were performed using the "T-Coffee multiple sequence alignment program" (http://www.ebi.ac.uk/Tools/msa/tcoffee/). Homologous amino acid sequences were compared with "CLC Main Workbench v7.0.2" (Qiagen). Protein domains were identified

using the Simple Modular Architecture Research Tool "SMART" (http://smart.embl-heidelberg.de/). Signal sequences were predicted using the "SignalP 4.1 Server" (http://www.cbs.dtu.dk/services/SignalP/). The generation of the structural model for the *U. maydis* Scp2 was performed using the "Phyre2" web portal for protein modeling, prediction and analysis (http://www.sbg.bio.ic.ac.uk/phyre2/html/page.cgi?id=index). The virtual cloning of plasmids was performed using the "Clone Manager 9" software (Scientific & Educational Software, Denver, CO, USA).

4.9.2 Quantification of peroxisomal and lipid droplet misdistribution

To visualize the misdistribution of lipid droplets and peroxisomes confocal Z-stacks of peroxisomes (GFP-PTS1) or lipid droplets (nile red) were taken in AM1-marker expressing filaments and converted to maximum projections using the Leica Application Suite Advanced Fluorescence (LAS AF) software. The filament length was determined starting from the hyphal tip until the first septum (cytoplasm filled tip compartment) using the ImageJ software (https://imagej.nih.gov/ij/). Fluorescence signal intensity plots of peroxisomes or lipid droplets were generated along a line drawn througout the entire cytoplasm filled tip compartment of the respective filaments. The signal intensity from the generated intensity plots was normalized to intensities ranging from 0 to 100 % with the highest value determined for each individual filament equaling 100 %. The length of the tip compartments differed between filaments and was therefore normalized to values between 1 and 100 to allow a direct comparison between filaments with different length. Average values of fluorescence intensities within each of the 100 sections was plotted. Average values of 15 filaments per strain were calculated and visualized in a bar diagram.

5. References

Ahn, N., Kim, S., Choi, W., Im, K. H., Lee, Y. H. (2004). Extracellular matrix protein gene, EMP1, is required for appressorium formation and pathogenicity of the rice blast fungus, *Magnaporthe grisea*. *Mol Cells,* **17**, 166-173.

Aichinger, C., Hansson, K., Eichhorn, H., Lessing, F., Mannhaupt, G., Mewes, W., Kahmann, R. (2003). Identification of plant-regulated genes in *Ustilago maydis* by enhancer-trapping mutagenesis. *Mol Genet Genomics,* **270**, 303-314.

Alsteens, D., Van Dijck, P., Lipke, P. N., Dufrene, Y. F. (2013). Quantifying the forces driving cell-cell adhesion in a fungal pathogen. *Langmuir,* **29**, 13473-13480.

Alvarez, F. J., Douglas, L. M., Konopka, J. B. (2007). Sterol-Rich Plasma Membrane Domains in Fungi. *Eukaryotic Cell,* **6**, 755-763.

Anderson, P. J. (1985). The recovery of nitrocellulose-bound protein. *Anal Biochem,* **148**, 105-110.

Anjard, C., Loomis, W. F. (2005). Peptide signaling during terminal differentiation of *Dictyostelium*. *Proc Natl Acad Sci U S A,* **102**, 7607-7611.

Asakura, M., Ninomiya, S., Sugimoto, M., Oku, M., Yamashita, S., Okuno, T., Sakai, Y., Takano, Y. (2009). Atg26-mediated pexophagy is required for host invasion by the plant pathogenic fungus *Colletotrichum orbiculare*. *Plant Cell,* **21**, 1291-1304.

Asakura, M., Yoshino, K., Hill, A. M., Kubo, Y., Sakai, Y., Takano, Y. (2012). Primary and secondary metabolism regulates lipolysis in appressoria of *Colletotrichum orbiculare*. *Fungal Genet Biol,* **49**, 967-975.

Ast, J., Stiebler, A. C., Freitag, J., Bölker, M. (2013). Dual targeting of peroxisomal proteins. *Front Physiol,* **4**, 297.

Atshaves, B. P., Storey, S. M., McIntosh, A. L., Petrescu, A. D., Lyuksyutova, O. I., Greenberg, A. S., Schroeder, F. (2001). Sterol carrier protein-2 expression modulates protein and lipid composition of lipid droplets. *J Biol Chem,* **276**, 25324-25335.

Ausubel, F. M., Brent, R., Kingston, R. E., Moore, D. D., Seidman, J. G., Smith, J. A., and Struhl, K. (1987). Current Protocols in Molecular Biology, *Greene Publishing Associates/Wiley Interscience*.

Baes, M., Huyghe, S., Carmeliet, P., Declercq, P. E., Collen, D., Mannaerts, G. P., Van Veldhoven, P. P. (2000). Inactivation of the peroxisomal multifunctional protein-2 in mice impedes the degradation of not only 2-methyl-branched fatty acids and bile acid intermediates but also of very long chain fatty acids. *J Biol Chem,* **275**, 16329-16336.

Banuett, F., Herskowitz, I. (1989). Different a alleles of *Ustilago maydis* are necessary for maintenance of filamentous growth but not for meiosis. *Proc Natl Acad Sci U S A,* **86**, 5878-5882.

Banuett, F., Herskowitz, I. (1996). Discrete developmental stages during teliospore formation in the corn smut fungus, *Ustilago maydis*. *Development,* **122**, 2965-2976.

Basse, C. W., Steinberg, G. (2004). *Ustilago maydis*, model system for analysis of the molecular basis of fungal pathogenicity. *Mol Plant Pathol,* **5**, 83-92.

Bebber, D. P., Ramotowski, M. A. T., Gurr, S. J. (2013). Crop pests and pathogens move polewards in a warming world. *Nature Climate Change,* **3**, 985-988.

Bendtsen, J. D., Jensen, L. J., Blom, N., Von Heijne, G., Brunak, S. (2004). Feature-based prediction of non-classical and leaderless protein secretion. *Protein Eng Des Sel,* **17**, 349-356.

Berger, A. C., Vanderford, T. H., Gernert, K. M., Nichols, J. W., Faundez, V., Corbett, A. H. (2005). *Saccharomyces cerevisiae* Npc2p is a functionally conserved homologue of the human Niemann-Pick disease type C 2 protein, hNPC2. *Eukaryot Cell,* **4**, 1851-1862.

Binns, D., Januszewski, T., Chen, Y., Hill, J., Markin, V. S., Zhao, Y., Gilpin, C., Chapman, K. D., Anderson, R. G., Goodman, J. M. (2006). An intimate collaboration between peroxisomes and lipid bodies. *J Cell Biol,* **173**, 719-731.

Blitzer, E. J., Vyazunova, I., Lan, Q. (2005). Functional analysis of AeSCP-2 using gene expression knockdown in the yellow fever mosquito, *Aedes aegypti*. *Insect Mol Biol,* **14**, 301-307.

Bohlmann, R. (1996). Isolierung und Charakterisierung von filamentspezifisch exprimierten Genen aus *Ustilago maydis*. Dissertation der Fakultät für Biologie, Ludwig-Maximilians-Universität München.

Bölker, M., Urban, M., Kahmann, R. (1992). The a mating type locus of *U. maydis* specifies cell signaling components. *Cell,* **68**, 441-450.

Brachmann, A., König, J., Julius, C., Feldbrügge, M. (2004). A reverse genetic approach for generating gene replacement mutants in *Ustilago maydis*. *Mol Genet Genomics,* **272**, 216-226.

Brachmann, A., Weinzierl, G., Kämper, J., Kahmann, R. (2001). Identification of genes in the bW/bE regulatory cascade in *Ustilago maydis*. *Mol Microbiol,* **42**, 1047-1063.

Bradford, M. M. (1976). A rapid and sensitive method for the quantitation of microgram quantities of protein utilizing the principle of protein-dye binding. *Anal Biochem,* **72**, 248-254.

Brefeld, O. (1883). Untersuchungen aus dem Gesamtgebiet der Mykologie. , Heft 5,67-75

Brefort, T., Döhlemann, G., Mendoza-Mendoza, A., Reissmann, S., Djamei, A., Kahmann, R. (2009). *Ustilago maydis* as a Pathogen. *Annual Review of Phytopathology,* **47**, 423-445.

Brefort, T., Tanaka, S., Neidig, N., Döhlemann, G., Vincon, V., Kahmann, R. (2014). Characterization of the largest effector gene cluster of *Ustilago maydis*. *PLoS Pathog,* **10**, e1003866.

Broomfield, P. L., Hargreaves, J. A. (1992). A single amino-acid change in the iron-sulphur protein subunit of succinate dehydrogenase confers resistance to carboxin in *Ustilago maydis*. *Curr Genet,* **22**, 117-121.

Brown, L. A., Baker, A. (2008). Shuttles and cycles: transport of proteins into the peroxisome matrix (review). *Mol Membr Biol,* **25**, 363-375.

Bruns, C., McCaffery, J. M., Curwin, A. J., Duran, J. M., Malhotra, V. (2011). Biogenesis of a novel compartment for autophagosome-mediated unconventional protein secretion. *J Cell Biol,* **195**, 979-992.

Campbell, M. T., Proctor, C. A., Dou, Y., Schmitz, A. J., Phansak, P., Kruger, G. R., Zhang, C., Walia, H. (2015). Genetic and molecular characterization of submergence response identifies Subtol6 as a major submergence tolerance locus in maize. *PLoS One,* **10**, e0120385.

Cánovas, D., Pérez-Martín, J. (2009). Sphingolipid biosynthesis is required for polar growth in the dimorphic phytopathogen *Ustilago maydis*. *Fungal Genet Biol,* **46**, 190-200.

Christianson, T. W., Sikorski, R. S., Dante, M., Shero, J. H., Hieter, P. (1992). Multifunctional yeast high-copy-number shuttle vectors. *Gene*, **110**, 119-122.

Chua, C. E., Lim, Y. S., Lee, M. G., Tang, B. L. (2012). Non-classical membrane trafficking processes galore. *J Cell Physiol,* **227**, 3722-3730.

Cohen, S. N., Chang, A. C., Hsu L. (1972). Nonchromosomal antibiotic resistance in bacteria: Genetic transformation of *Escherichia coli* by R-factor DNA. *PNAS*, USA, **69**, 2110-2114.

Corpas, F. J., Barroso, J. B., del Río, L. A. (2001). Peroxisomes as a source of reactive oxygen species and nitric oxide signal molecules in plant cells. *Trends Plant Sci,* **6**, 145-150.

Curwin, A. J., Brouwers, N. (2016). ESCRT-III drives the final stages of CUPS maturation for unconventional protein secretion. **5**.

Day, P. R., Anagnostakis, S. L. (1971). Corn smut dikaryon in culture. *Nat New Biol*, **231**, 19-20.

De Berti, F. P., Capaldi, S., Ferreyra, R., Burgardt, N., Acierno, J. P., Klinke, S., Monaco, H. L., Ermácora, M. R. (2013). The crystal structure of sterol carrier protein 2 from *Yarrowia lipolytica* and the evolutionary conservation of a large, non-specific lipid-binding cavity. *Journal of Structural and Functional Genomics,* **14**, 145-153.

de Duve, C. (1969). The peroxisome: a new cytoplasmic organelle. *Proc R Soc Lond B Biol Sci,* **173**, 71-83.

del Río, L. A. (2011). Peroxisomes as a cellular source of reactive nitrogen species signal molecules. *Arch Biochem Biophys,* **506**, 1-11.

Ding Y., Robinson D. G., Jiang L. (2014). Unconventional protein secretion (UPS) pathways in plants. *Curr Opin Cell Biol,* **29**, 107-115.

Djamei, A., Kahmann, R. (2012). *Ustilago maydis*: dissecting the molecular interface between pathogen and plant. *PLoS Pathog,* **8**, e1002955.

Djamei, A., Schipper, K., Rabe, F., Ghosh, A., Vincon, V., Kahnt, J., Osorio, S., Tohge, T., Fernie, A. R., Feussner, I., Feussner, K., Meinicke, P., Stierhof, Y. D., Schwarz, H., Macek, B., Mann, M., Kahmann, R. (2011). Metabolic priming by a secreted fungal effector. *Nature,* **478**, 395-398.

Döhlemann, G., van der Linde, K., Assmann, D., Schwammbach, D., Hof, A., Mohanty, A., Jackson, D., Kahmann, R. (2009). Pep1, a secreted effector protein of *Ustilago maydis*, is required for successful invasion of plant cells. *PLoS Pathog,* **5**, e1000290.

Donaldson, M. E., Meng, S., Gagarinova, A., Babu, M., Lambie, S. C., Swiadek, A. A., Saville, B. J. (2013). Investigating the *Ustilago maydis*/*Zea mays* pathosystem: transcriptional responses and novel functional aspects of a fungal calcineurin regulatory B subunit. *Fungal Genet Biol,* **58-59**, 91-104.

Dunn, M. F., Ramirez-Trujillo, J. A., Hernandez-Lucas, I. (2009). Major roles of isocitrate lyase and malate synthase in bacterial and fungal pathogenesis. *Microbiology,* **155**, 3166-3175.

Edqvist, J., Blomqvist, K. (2006). Fusion and Fission, the Evolution of Sterol Carrier Protein-2. *Journal of Molecular Evolution,* **62**, 292-306.

Erdmann, R. (2016). Assembly, maintenance and dynamics of peroxisomes. *Biochim Biophys Acta,* **1863**, 787-789.

Falomir Lockhart, L. J., Burgardt, N. I., Ferreyra, R. G., Ceolin, M., Ermacora, M. R., Corsico, B. (2009). Fatty acid transfer from *Yarrowia lipolytica* sterol carrier protein 2 to phospholipid membranes. *Biophys J,* **97**, 248-256.

Fisher, M. C., Henk, D. A., Briggs, C. J., Brownstein, J. S., Madoff, L. C., McCraw, S. L., Gurr, S. J. (2012). Emerging fungal threats to animal, plant and ecosystem health. *Nature,* **484**, 186-194.

Flis, V. V., Fankl, A., Ramprecht, C., Zellnig, G., Leitner, E., Hermetter, A., Daum, G. (2015). Phosphatidylcholine Supply to Peroxisomes of the Yeast *Saccharomyces cerevisiae*. *PLoS One,* **10**, e0135084.

Freitag, J., Ast J., Bölker, M. (2012). Cryptic peroxisomal targeting via alternative splicing and stop codon read-through in fungi. *Nature,* **485**, 522-525.

Freitag, J., Ast, J., Linne, U., Stehlik, T., Martorana, D., Bölker, M., Sandrock, B. (2014). Peroxisomes contribute to biosynthesis of extracellular glycolipids in fungi. *Mol Microbiol,* **93**, 24-36.

Frolov, A., Miller, K., Billheimer, J. T., Cho, T. H., Schroeder, F. (1997). Lipid specificity and location of the sterol carrier protein-2 fatty acid-binding site: a fluorescence displacement and energy transfer study. *Lipids,* **32**, 1201-1209.

Fukunaga, K., Hill, J., Vigouroux, Y., Matsuoka, Y., Sanchez, G. J., Liu, K., Buckler, E. S., Doebley, J. (2005). Genetic diversity and population structure of teosinte. *Genetics,* **169**, 2241-2254.

Gabaldón, T. (2010). Peroxisome diversity and evolution. *Philos Trans R Soc Lond B Biol Sci,* **365**, 765-773.

Gallegos, A. M., Atshaves, B. P., Storey, S. M., Starodub, O., Petrescu, A. D., Huang, H., McIntosh, A. L., Martin, G. G., Chao, H., Kier, A. B., Schroeder, F. (2001). Gene structure, intracellular localization, and functional roles of sterol carrier protein-2. *Prog Lipid Res,* **40**, 498-563.

Gao, Q., Goodman, J. M. (2015). The lipid droplet-a well-connected organelle. *Front Cell Dev Biol,* **3**, 49.

García-Muse, T., Steinberg, G., Pérez-Martin, J. (2003). Pheromone-induced G2 arrest in the phytopathogenic fungus *Ustilago maydis*. *Eukaryot Cell,* **2**, 494-500.

García, F. L., Szyperski, T., Dyer, J. H., Choinowski, T., Seedorf, U., Hauser, H., Wuthrich, K. (2000). NMR structure of the sterol carrier protein-2: implications for the biological role. *J Mol Biol,* **295**, 595-603.

Gee, H. Y., Noh, S. H., Tang, B. L., Kim, K. H., Lee, M. G. (2011). Rescue of DeltaF508-CFTR trafficking via a GRASP-dependent unconventional secretion pathway. *Cell,* **146**, 746-760.

Gibson, D. G., Young, L., Chuang, R. Y., Venter, J. C., Hutchison, C. A., 3rd, Smith, H. O. (2009). Enzymatic assembly of DNA molecules up to several hundred kilobases. *Nat Methods,* **6**, 343-345.

Giraldo, M. C., Dagdas, Y. F., Gupta, Y. K., Mentlak, T. A., Yi M., Martinez-Rocha, A. L., Saitoh, H., Terauchi, R., Talbot, N. J., Valent, B. (2013). Two distinct secretion systems facilitate tissue invasion by the rice blast fungus *Magnaporthe oryzae*. *Nat Commun,* **4**, 1996.

Girzalsky, W., Saffian, D., Erdmann, R. (2010). Peroxisomal protein translocation. *Biochim Biophys Acta,* **1803**, 724-731.

Glazebrook, J. (2005). Contrasting mechanisms of defense against biotrophic and necrotrophic pathogens. *Annu Rev Phytopathol,* **43**, 205-227.

Goroncy, A. K., Murayama, K., Shirouzu, M., Kuramitsu, S., Kigawa, T., Yokoyama, S. (2010). NMR and X-ray structures of the putative sterol carrier protein 2 from *Thermus thermophilus* HB8 show conformational changes. *J Struct Funct Genomics,* **11**, 247-256.

Greenspan, P., Mayer, E. P., Fowler, S. D. (1985). Nile red: a selective fluorescent stain for intracellular lipid droplets. *J Cell Biol,* **100**, 965-973.

Grieve, A. G., Rabouille, C. (2011). Golgi bypass: skirting around the heart of classical secretion. *Cold Spring Harb Perspect Biol,* **3**.

Guimaraes, S. C., Schuster, M., Bielska, E., Dagdas, G., Kilaru, S., Meadows, B. R., Schrader, M., Steinberg, G. (2015). Peroxisomes, lipid droplets, and endoplasmic reticulum "hitchhike" on motile early endosomes. *J Cell Biol,* **211**, 945-954.

Hammond, G. R., Machner, M. P., Balla, T. (2014). A novel probe for phosphatidylinositol 4-phosphate reveals multiple pools beyond the Golgi. *J Cell Biol,* **205**, 113-126.

Heimel, K., Freitag, J., Hampel, M., Ast, J., Bölker, M., Kämper, J. (2013). Crosstalk between the unfolded protein response and pathways that regulate pathogenic development in *Ustilago maydis*. *Plant Cell,* **25**, 4262-4277.

Hemetsberger, C., Herrberger, C., Zechmann, B., Hillmer, M., Döhlemann, G. (2012). The *Ustilago maydis* effector Pep1 suppresses plant immunity by inhibition of host peroxidase activity. *PLoS Pathog,* **8**, e1002684.

Hewald, S. (2005). Identifizierung und Charakterisierung zweier für die Produktion extrazellulärer Glykolipide verantwortlichen Gencluster in *Ustilago maydis*. Dissertation der Fakultät für Biologie, Philipps-Universität Marburg.

Holliday, R. (1974). *Ustilago maydis*. In King, R.C. (ed.) *Handbook of Genetics* 1, *Plenum Press,* New York/USA: 575-595.

Inoue, K., Suzuki, T., Ikeda, K., Jiang, S., Hosogi, N., Hyon, G. S., Hida, S., Yamada, T., Park, P. (2008). Extracellular matrix of *Magnaporthe oryzae* may have a role in host adhesion during fungal penetration and is digested by matrix metalloproteinases (vol 73, pg 388, 2007). *Journal of General Plant Pathology,* **74**, 96-96.

Jansen, G., Wu, C., Schade, B., Thomas, D. Y., Whiteway, M. (2005). Drag&Drop cloning in yeast. *Gene,* **344**, 43-51.

Kahmann, R., Steinberg, G., Basse, C., Feldbrügge, M., Kämper, J. (2000). *Ustilago maydis*, the Causative Agent of Corn Smut Disease. *In: Fungal Pathology*, pp. 347-371 Ed J. W. Kronstad. Dordrecht: Springer Netherlands.

Kämper, J. (2004). A PCR-based system for highly efficient generation of gene replacement mutants in *Ustilago maydis*. *Molecular Genetics and Genomics,* **271**, 103-110.

Kämper, J., Kahmann, R., Bölker, M., Ma, L. J., Brefort, T., Saville, B. J., Banuett, F., Kronstad, J. W., Gold, S. E., Müller, O., Perlin, M. H., Wösten, H. A., de Vries, R., Ruiz-Herrera, J., Reynaga-Pena, C. G., Snetselaar, K., McCann, M., Perez-Martin, J., Feldbrügge, M., Basse, C. W., Steinberg, G., Ibeas, J. I., Holloman, W., Guzman, P., Farman, M., Stajich, J. E., Sentandreu, R., Gonzalez-Prieto, J. M., Kennell, J. C., Molina, L., Schirawski, J., Mendoza-Mendoza, A., Greilinger, D.,

Münch, K., Rössel, N., Scherer, M., Vranes, M., Ladendorf, O., Vincon, V., Fuchs, U., Sandrock, B., Meng, S., Ho, E. C., Cahill, M. J., Boyce, K. J., Klose, J., Klosterman, S. J., Deelstra, H. J., Ortiz-Castellanos, L., Li W., Sanchez-Alonso, P., Schreier, P. H., Hauser-Hahn, I., Vaupel, M., Koopmann, E., Friedrich, G., Voss, H., Schluter, T., Margolis, J., Platt, D., Swimmer, C., Gnirke, A., Chen, F., Vysotskaia, V., Mannhaupt, G., Guldener, U., Munsterkotter, M., Haase, D., Oesterheld, M., Mewes, H. W., Mauceli, E. W., DeCaprio, D., Wade, C. M., Butler, J., Young, S., Jaffe, D. B., Calvo, S., Nusbaum, C., Galagan, J., Birren, B. W. (2006). Insights from the genome of the biotrophic fungal plant pathogen *Ustilago maydis*. *Nature,* **444**, 97-101.

Kämper, J., Reichmann, M., Romeis, T., Bölker, M., Kahmann, R. (1995). Multiallelic recognition: nonself-dependent dimerization of the bE and bW homeodomain proteins in *Ustilago maydis*. *Cell,* **81**, 73-83.

Karkowska-Kuleta, J., Kozik, A. (2014). Moonlighting proteins as virulence factors of pathogenic fungi, parasitic protozoa and multicellular parasites. *Mol Oral Microbiol,* **29**, 270-283.

Kelley, L. A., Mezulis, S., Yates, C. M., Wass, M. N., Sternberg, M. J. (2015). The Phyre2 web portal for protein modeling, prediction and analysis. *Nat Protoc,* **10**, 845-858.

Khrunyk, Y. (2010). The use of FLP-mediated recombination for the functional analysis of an effector gene family in the biotrophic smut fungus *Ustilago maydis*. Dissertation der Fakultät für Biologie, Philipps-Universität Marburg.

Klose, J., Kronstad, J. W. (2006). The Multifunctional β-Oxidation Enzyme Is Required for Full Symptom Development by the Biotrophic Maize Pathogen *Ustilago maydis*. *Eukaryotic Cell,* **5**, 2047-2061.

Krahmer, N., Guo, Y., Wilfling, F., Hilger, M., Lingrell, S., Heger, K., Newman, H. W., Schmidt-Supprian, M., Vance, D. E., Mann, M., Farese, R. V., Jr., Walther, T. C. (2011). Phosphatidylcholine synthesis for lipid droplet expansion is mediated by localized activation of CTP:phosphocholine cytidylyltransferase. *Cell Metab,* **14**, 504-515.

Krügel, H., Fiedler, G., Haupt, I., Sarfert, E., Simon, H. (1988). Analysis of the nourseothricin-resistance gene (nat) of *Streptomyces noursei*. *Gene,* **62**, 209-217.

Kunze, M., Pracharoenwattana, I., Smith, S. M., Hartig, A. (2006). A central role for the peroxisomal membrane in glyoxylate cycle function. *Biochim Biophys Acta,* **1763**, 1441-1452.

Kwolek-Mirek, M., Zadrag-Tecza, R. (2014). Comparison of methods used for assessing the viability and vitality of yeast cells. *Fems Yeast Research,* **14**, 1068-1079.

Laemmli, U. K. (1970). Cleavage of structural proteins during the assembly of the head of bacteriophage T4. *Nature,* **227**, 680-685.

Lan, Q., Massey, R. J. (2004). Subcellular localization of the mosquito sterol carrier protein-2 and sterol carrier protein-x. *J Lipid Res,* **45**, 1468-1474.

Lanver, D. (2011). Appressorienbildung von *Ustilago maydis* auf hydrophoben Oberflächen: Regulation durch Membranproteine. Dissertation der Fakultät für Biologie, Philipps-Universität Marburg.

Lanver, D., Berndt, P., Tollot, M., Naik, V., Vranes, M., Warmann, T., Münch, K., Rössel, N., Kahmann, R. (2014). Plant surface cues prime *Ustilago maydis* for biotrophic development. *PLoS Pathog,* **10**, e1004272.

Lanver, D., Mendoza-Mendoza, A., Brachmann, A., Kahmann, R. (2010). Sho1 and Msb2-related proteins regulate appressorium development in the smut fungus *Ustilago maydis*. *Plant Cell,* **22**, 2085-2101.

Leenders, F., Tesdorpf, J. G., Markus, M., Engel, T., Seedorf, U., Adamski, J. (1996). Porcine 80-kDa protein reveals intrinsic 17 beta-hydroxysteroid dehydrogenase, fatty acyl-CoA-hydratase/dehydrogenase, and sterol transfer activities. *J Biol Chem,* **271**, 5438-5442.

Lensink, M. F., Haapalainen, A. M., Hiltunen, J. K., Glumoff, T., Juffer, A. H. (2002). Response of SCP-2L domain of human MFE-2 to ligand removal: binding site closure and burial of peroxisomal targeting signal. *J Mol Biol,* **323**, 99-113.

Liu, F., Zhang, X., Lu, C., Zeng, X., Li, Y., Fu, D., Wu, G. (2015). Non-specific lipid transfer proteins in plants: presenting new advances and an integrated functional analysis. *J Exp Bot,* **66**, 5663-5681.

Liu, T., Song, T., Zhang, X., Yuan, H., Su, L., Li, W., Xu, J., Liu, S., Chen, L., Chen, T., Zhang, M., Gu, L., Zhang, B., Dou, D. (2014). Unconventionally secreted effectors of two filamentous pathogens target plant salicylate biosynthesis. *Nat Commun,* **5**, 4686.

Livak, K. J., Schmittgen, T. D. (2001). Analysis of relative gene expression data using real-time quantitative PCR and the 2(-Delta Delta C(T)) Method. *Methods,* **25**, 402-408.

Lo Presti, L., Zechmann, B., Kumlehn, J., Liang, L., Lanver, D., Tanaka, S., Bock, R., Kahmann, R. (2016). An assay for entry of secreted fungal effectors into plant cells. *New Phytol*.

Malhotra, V. (2013). Unconventional protein secretion: an evolving mechanism. *Embo j,* **32**, 1660-1664.

Manjithaya, R., Anjard, C., Loomis, W. F., Subramani, S. (2010). Unconventional secretion of *Pichia pastoris* Acb1 is dependent on GRASP protein, peroxisomal functions, and autophagosome formation. *J Cell Biol,* **188**, 537-546.

Marie, M., Dale, H. A., Sannerud, R., Saraste, J. (2009). The function of the intermediate compartment in pre-Golgi trafficking involves its stable connection with the centrosome. *Mol Biol Cell,* **20**, 4458-4470.

Maruyama, J., Kitamoto, K. (2013). Expanding functional repertoires of fungal peroxisomes: contribution to growth and survival processes. *Front Physiol,* **4**, 177.

McGrath, J. P., Varshavsky, A. (1989). The yeast STE6 gene encodes a homologue of the mammalian multidrug resistance P-glycoprotein. *Nature,* **340**, 400-404.

Meinecke, M., Bartsch, P., Wagner, R. (2016). Peroxisomal protein import pores. *Biochim Biophys Acta,* **1863**, 821-827.

Mendoza-Mendoza, A., Berndt, P., Djamei, A., Weise, C., Linne, U., Marahiel, M., Vranes, M., Kämper, J., Kahmann, R. (2009). Physical-chemical plant-derived signals induce differentiation in *Ustilago maydis*. *Mol Microbiol,* **71**, 895-911.

Michels, P. A., Bringaud, F., Herman, M., Hannaert, V. (2006). Metabolic functions of glycosomes in trypanosomatids. *Biochim Biophys Acta,* **1763**, 1463-1477.

Mortimer, C. E., Müller, U. (2003). Chemie: Das Basiswissen der Chemie, 8th ed. , Thieme

Müller, A. N., Ziemann, S., Treitschke, S., Assmann, D., Döhlemann, G. (2013). Compatibility in the *Ustilago maydis*-maize interaction requires inhibition of host cysteine proteases by the fungal effector Pit2. *PLoS Pathog,* **9**, e1003177.

Müller, O., Schreier, P. H., Uhrig, J. F. (2008). Identification and characterization of secreted and pathogenesis-related proteins in *Ustilago maydis*. *Mol Genet Genomics*, **279**, 27-39.

Mullis, K., Faloona, F., Scharf, S., Saiki, R., Horn, G., Erlich, H. (1986). Specific enzymatic amplification of DNA in vitro: the polymerase chain reaction. *Cold Spring Harb Symp Quant Biol,* **51 Pt 1**, 263-273.

Murphy, E. J., Stiles, T., Schroeder, F. (2000). Sterol carrier protein-2 expression alters phospholipid content and fatty acyl composition in L-cell fibroblasts. *J Lipid Res*, **41**, 788-796.

Neuberger, G., Maurer-Stroh, S., Eisenhaber, B., Hartig, A., Eisenhaber, F. (2003). Prediction of peroxisomal targeting signal 1 containing proteins from amino acid sequence. *J Mol Biol,* **328**, 581-592.

Nickel, W. (2011). The unconventional secretory machinery of fibroblast growth factor 2. *Traffic,* **12**, 799-805.

Nickel, W., Rabouille, C. (2009). Mechanisms of regulated unconventional protein secretion. *Nat Rev Mol Cell Biol,* **10**, 148-155.

Oku, M., Sakai, Y. (2016). Pexophagy in yeasts. *Biochim Biophys Acta,* **1863**, 992-998.

Park, S. Y., Jauh, G. Y., Mollet, J. C., Eckard, K. J., Nothnagel, E. A., Walling, L. L., Lord, E. M. (2000). A lipid transfer-like protein is necessary for lily pollen tube adhesion to an in vitro stylar matrix. *Plant Cell,* **12**, 151-164.

Patkar, R. N., Suresh, A., Naqvi, N. I. (2010). MoTea4-mediated polarized growth is essential for proper asexual development and pathogenesis in *Magnaporthe oryzae*. *Eukaryot Cell,* **9**, 1029-1038.

Petre, B., Kamoun, S. (2014). How do filamentous pathogens deliver effector proteins into plant cells? *PLoS Biol,* **12**, e1001801.

Pol, A., Gross, S. P., Parton, R. G. (2014). Review: biogenesis of the multifunctional lipid droplet: lipids, proteins, and sites. *J Cell Biol*, **204**, 635-646.

Prydz, K., Tveit, H., Vedeler, A., Saraste, J. (2013). Arrivals and departures at the plasma membrane: direct and indirect transport routes. *Cell Tissue Res*, **352**, 5-20.

Rabouille, C., Malhotra, V., Nickel, W. (2012). Diversity in unconventional protein secretion. *Journal of Cell Science,* **125**, 5251-5255.

Ramos-Pamplona, M., Naqvi, N. I. (2006). Host invasion during rice-blast disease requires carnitine-dependent transport of peroxisomal acetyl-CoA. *Mol Microbiol,* **61**, 61-75.

Raposo, G., Stoorvogel, W. (2013). Extracellular vesicles: exosomes, microvesicles, and friends. *J Cell Biol,* **200**, 373-383.

Redkar, A., Hoser, R., Schilling, L., Zechmann, B., Krzymowska, M., Walbot, V., Döhlemann, G. (2015). A Secreted effector protein of *Ustilago maydis* guides maize leaf cells to form tumors. *Plant Cell,* **27**, 1332-1351.

Reina-Pinto, J. J., Yephremov, A. (2009). Surface lipids and plant defenses. *Plant Physiol Biochem,* **47**, 540-549.

Robin, J. B., Arffa, R. C., Avni, I., Rao, N. A. (1986). Rapid visualization of three common fungi using fluorescein-conjugated lectins. *Invest Ophthalmol Vis Sci.,* **Vol.27**, 500-506.

Rodriguez-Serrano, M., Romero-Puertas, M. C., Sparkes, I., Hawes, C., del Río, L. A., Sandalio, L. M. (2009). Peroxisome dynamics in Arabidopsis plants under oxidative stress induced by cadmium. *Free Radic Biol Med,* **47**, 1632-1639.

Salogiannis, J., Egan, M. J., Reck-Peterson, S. L. (2016). Peroxisomes move by hitchhiking on early endosomes using the novel linker protein PxdA. *Journal of Cell Biology,* **212**, 289-296.

Sambrook, J., Frisch, E. F.,Maniatis, T. (1989). Molecular Cloning: A laboratory manual. *Cold Spring Harbour*, New York.

Scherer, M., Heimel, K., Starke, V., Kämper, J. (2006). The Clp1 protein is required for clamp formation and pathogenic development of *Ustilago maydis*. *Plant Cell,* **18**, 2388-2401.

Schipper, K. (2009). Charakterisierung eines *Ustilago maydis* Genclusters, das für drei neuartige sekretierte Effektoren kodiert. Dissertation der Fakultät für Biologie, Philipps-Universität Marburg.

Schirawski, J., Böhnert, H. U., Steinberg, G., Snetselaar, K., Adamikowa, L., Kahmann, R. (2005). Endoplasmic reticulum glucosidase II is required for pathogenicity of *Ustilago maydis*. *Plant Cell,* **17**, 3532-3543.

Schrader, M., Costello, J. L., Godinho, L. F., Azadi, A. S., Islinger, M. (2016). Proliferation and fission of peroxisomes - An update. *Biochim Biophys Acta,* **1863**, 971-983.

Schroeder, F., Atshaves, B. P., McIntosh, A. L., Gallegos, A. M., Storey, S. M., Parr, R. D., Jefferson, J. R., Ball, J. M., Kier, A. B. (2007). Sterol carrier protein-2: new roles in regulating lipid rafts and signaling. *Biochim Biophys Acta,* **1771**, 700-718.

Schulz, B., Banuett, F., Dahl, M., Schlesinger, R., Schäfer, W., Martin, T., Herskowitz, I., Kahmann, R. (1990). The *b* alleles of *Ustilago maydis*, whose combinations program pathogenic development, code for polypeptides containing a homeodomain-related motif. *Cell,* **60,** 295-306.

Schuster, M., Lipowsky, R., Assmann, M. A., Lenz, P., Steinberg, G. (2011). Transient binding of dynein controls bidirectional long-range motility of early endosomes. *Proc Natl Acad Sci U S A,* **108**, 3618-3623.

Schuster, M., Schweizer, G., Reissmann, S., Kahmann, R. (2016). Genome editing in *Ustilago maydis* using the CRISPR-Cas system. *Fungal Genet Biol,* **89**, 3-9.

Shai, N., Schuldiner, M., Zalckvar, E. (2016). No peroxisome is an island - Peroxisome contact sites. *Biochim Biophys Acta,* **1863**, 1061-1069.

Shoji, J. Y., Kikuma, T., Kitamoto, K. (2014). Vesicle trafficking, organelle functions, and unconventional secretion in fungal physiology and pathogenicity. *Curr Opin Microbiol,* **20**, 1-9.

Silva, B. M., Prados-Rosales, R., Espadas-Moreno, J., Wolf, J. M., Luque-Garcia, J. L., Goncalves, T., Casadevall, A. (2014). Characterization of *Alternaria infectoria* extracellular vesicles. *Med Mycol,* **52**, 202-210.

Skibbe, D. S., Döhlemann, G., Fernandes, J., Walbot, V. (2010). Maize tumors caused by *Ustilago maydis* require organ-specific genes in host and pathogen. *Science,* **328**, 89-92.

Snetselaar, K. M. M., C.W. (1993). Infection of maize stigmas by *Ustilago maydis*: Light and electron microscopy. *Phytopathology,* **83**, 843-850.

Snetselaar, K. M. M., C.W. (1994). Light and electron microscopy of *Ustilago maydis* hyphae in maize. *Mycol. Res.*, **98**, 347-355.

Soundararajan, S., Jedd, G., Li, X., Ramos-Pamplona, M., Chua, N. H., Naqvi, N. I. (2004). Woronin body function in *Magnaporthe grisea* is essential for efficient pathogenesis and for survival during nitrogen starvation stress. *Plant Cell*, **16**, 1564-1574.

Southern, E. M. (1975). Detection of specific sequences among DNA fragments separated by gel electrophoresis. *J Mol Biol*, **98**, 503-517.

Starodub, O., Jolly, C. A., Atshaves, B. P., Roths, J. B., Murphy, E. J., Kier, A. B., Schroeder, F. (2000). Sterol carrier protein-2 localization in endoplasmic reticulum and role in phospholipid formation. *Am J Physiol Cell Physiol*, **279**, C1259-1269.

Steinberg, G., Perez-Martin, J. (2008). *Ustilago maydis*, a new fungal model system for cell biology. *Trends Cell Biol*, **18**, 61-67.

Steinberg, G., Schliwa, M., Lehmler, C., Bölker, M., Kahmann, R., McIntosh, J. R. (1998). Kinesin from the plant pathogenic fungus *Ustilago maydis* is involved in vacuole formation and cytoplasmic migration. *Journal of Cell Science*, **111**, 2235-2246.

Steinberg, S. J., Dodt, G., Raymond, G. V., Braverman, N. E., Moser, A. B., Moser, H. W. (2006). Peroxisome biogenesis disorders. *Biochim Biophys Acta*, **1763**, 1733-1748.

Steringer, J. P., Bleicken, S., Andreas, H., Zacherl, S., Laussmann, M., Temmerman, K., Contreras, F. X., Bharat, T. A., Lechner, J., Muller, H. M., Briggs, J. A., Garcia-Saez, A. J., Nickel, W. (2012). Phosphatidylinositol 4,5-bisphosphate (PI(4,5)P2)-dependent oligomerization of fibroblast growth factor 2 (FGF2) triggers the formation of a lipidic membrane pore implicated in unconventional secretion. *J Biol Chem*, **287**, 27659-27669.

Stock, J., Sarkari, P., Kreibich, S., Brefort, T., Feldbrügge, M., Schipper, K. (2012). Applying unconventional secretion of the endochitinase Cts1 to export heterologous proteins in *Ustilago maydis*. *J Biotechnol*, **161**, 80-91.

Stolowich, N. J., Petrescu, A. D., Huang, H., Martin, G. G., Scott, A. I., Schroeder, F. (2002). Sterol carrier protein-2: structure reveals function. *Cellular and Molecular Life Sciences CMLS*, **59**, 193-212.

Strable, J., Scanlon, M. J. (2009). Maize (*Zea mays*): a model organism for basic and applied research in plant biology. *Cold Spring Harb Protoc*, **2009**, pdb emo132.

Takenouchi, T., Tsukimoto, M., Iwamaru, Y., Sugama, S., Sekiyama, K., Sato, M., Kojima, S., Hashimoto, M., Kitani, H. (2015). Extracellular ATP induces unconventional release of glyceraldehyde-3-phosphate dehydrogenase from microglial cells. *Immunol Lett*, **167**, 116-124.

Tanaka, S., Brefort, T., Neidig, N., Djamei, A., Kahnt, J., Vermerris, W., Koenig, S., Feussner, K., Feussner, I., Kahmann, R. (2014). A secreted *Ustilago maydis* effector promotes virulence by targeting anthocyanin biosynthesis in maize. *Elife*, **3**, e01355.

Tatsuta, T., Langer, T. (2016). Intramitochondrial phospholipid trafficking. *Biochim Biophys Acta*.

Thines, E., Weber, R. W., Talbot, N. J. (2000). MAP kinase and protein kinase A-dependent mobilization of triacylglycerol and glycogen during appressorium turgor generation by *Magnaporthe grisea*. *Plant Cell*, **12**, 1703-1718.

Titorenko, V. I., Rachubinski, R. A. (2001). The life cycle of the peroxisome. *Nat Rev Mol Cell Biol*, **2**, 357-368.

Tollot, M., Assmann, D., Becker, C., Altmuller, J., Dutheil, J. Y., Wegner, C. E., Kahmann, R. (2016). The WOPR Protein Ros1 Is a Master Regulator of Sporogenesis and Late Effector Gene Expression in the Maize Pathogen *Ustilago maydis*. *PLoS Pathog*, **12**, e1005697.

Tucker, S. L., Talbot, N. J. (2001). Surface attachment and pre-penetration stage development by plant pathogenic fungi. *Annu Rev Phytopathol*, **39**, 385-417.

Voet, D. and Voet, J. G. (2004). Biochemie, 3rd ed., John Wiley & Sons

Wanders, R. J. (2014). Metabolic functions of peroxisomes in health and disease. *Biochimie*, **98**, 36-44.

Wanders, R. J. A., Waterham, H. R., Ferdinandusse, S. (2016). Metabolic interplay between peroxisomes and other subcellular organelles including mitochondria and the endoplasmic reticulum. *Frontiers in Cell and Developmental Biology*, **3**.

Wang, Z. Y., Soanes, D. M., Kershaw, M. J., Talbot, N. J. (2007). Functional analysis of lipid metabolism in *Magnaporthe grisea* reveals a requirement for peroxisomal fatty acid beta-oxidation during appressorium-mediated plant infection. *Mol Plant Microbe Interact*, **20**, 475-491.

Wang, Z. Y., Thornton, C. R., Kershaw, M. J., Li, D. B., Talbot, N. J. (2003). The glyoxylate cycle is required for temporal regulation of virulence by the plant pathogenic fungus *Magnaporthe grisea*. *Mol Microbiol*, **47**, 1601-1612.

Wegehingel, S., Zehe, C., Nickel, W. (2008). Rerouting of fibroblast growth factor 2 to the classical secretory pathway results in post-translational modifications that block binding to heparan sulfate proteoglycans. *FEBS Lett*, **582**, 2387-2392.

Wei, W., Zhu, W., Cheng, J., Xie, J., Li, B., Jiang, D., Li, G., Yi, X., Fu, Y. (2013). CmPEX6, a gene involved in peroxisome biogenesis, is essential for parasitism and conidiation by the sclerotial parasite *Coniothyrium minitans*. *Appl Environ Microbiol*, **79**, 3658-3666.

Wriessnegger, T., Gubitz, G., Leitner, E., Ingolic, E., Cregg, J., de la Cruz, B. J., Daum, G. (2007). Lipid composition of peroxisomes from the yeast *Pichia pastoris* grown on different carbon sources. *Biochim Biophys Acta*, **1771**, 455-461.

Zechner, R., Madeo, F. (2009). Cell biology: Another way to get rid of fat. *Nature*, **458**, 1118-1119.

Zelinger, E., Hawes, C. R., Gurr, S. J., Dewey, F. M. (2006). Attachment and adhesion of conidia of *Stagonospora nodorum* to natural and artificial surfaces. *Physiological and Molecular Plant Pathology*, **68**, 209-215.

Zemskov, E. A., Mikhailenko, I., Hsia, R. C., Zaritskaya, L., Belkin, A. M. (2011). Unconventional secretion of tissue transglutaminase involves phospholipid-dependent delivery into recycling endosomes. *PLoS One*, **6**, e19414.

Zhao, H., Xu, C., Lu, H. L., Chen, X., St Leger, R. J., Fang, W. (2014). Host-to-pathogen gene transfer facilitated infection of insects by a pathogenic fungus. *PLoS Pathog*, **10**, e1004009.

Zheng, B. S., Ronnberg, E., Viitanen, L., Salminen, T. A., Lundgren, K., Moritz, T., Edqvist, J. (2008). Arabidopsis sterol carrier protein-2 is required for normal development of seeds and seedlings. *J Exp Bot*, **59**, 3485-3499.

Zinser, E., Sperka-Gottlieb, C. D., Fasch, E. V., Kohlwein, S. D., Paltauf, F., Daum, G. (1991). Phospholipid synthesis and lipid composition of subcellular membranes in the unicellular eukaryote *Saccharomyces cerevisiae*. *J Bacteriol,* **173**, 2026-2034.